

Chemical Modification of Polypropylene with Organo-functional Silanes

by

Fahad Al-Mutairi

A thesis
presented to the University of Waterloo
in fulfillment of the
thesis requirement for the degree of
Master of Applied Science
in
Chemical Engineering

Waterloo, Ontario, Canada, 2014

© Fahad Al-Mutairi 2014

AUTHOR'S DECLARATION

I hereby declare that I am the sole author of this thesis. This is a true copy of the thesis, including any required final revisions, as accepted by my examiners.

I understand that my thesis may be made electronically available to the public.

Fahad Al-Mutairi

Abstract

Conventional polypropylene (PP) suffers at higher service temperatures and its poor melt strength limits its application in some processes. PP also lacks functional groups necessary for good adhesion to synthetic or natural fillers. However, the thermal resistance of PP could potentially be improved by chemical crosslinking and its melt strength is known to be enhanced by light crosslinking and introducing long chain branches onto its backbone. Moreover, PP adhesion to polar fillers is proven to be significantly improved by using coupling agents.

Organo-functional silanes can be used to achieve these goals because of their bi-functional chemical nature. Their grafting onto polymeric chains helps in crosslinking these chains as well as forming stable covalent bonds with polar fillers. The objectives of this study were to compare the grafting efficiencies of nine different organo-functional silanes, to study their effect on the crystallization temperature of crosslinked PP and its soluble materials, to study the influence of two selected silanes, with different grafting efficiencies, on melt properties of PP with light crosslinking, and finally to study the impact of the PP grafted with two selected silanes, with the highest grafting efficiencies, on the mechanical properties of the wood-fiber/PP composites.

The grafting process was performed in a co-rotating twin-screw mini-extruder Haake Minilab Microcompounder (Minilab) using a recirculating mode (batch). The grafted products were purified and then studied by Fourier Transform Infrared Spectroscopy (FT-IR) to verify the grafting and compare the grafting efficiencies of those silanes. Gel content test was performed after crosslinking the grafted products in a hot water bath to confirm the FTIR results. Results showed that 6-azidosulfonylhexyltriethoxysilane (Azido-silane) had the highest grafting efficiency. The order of grafting efficiency of the other silanes is as follows: (3-acryloxypropyl)trimethoxysilane (APTMS) > 3-methacryloxypropyltrimethoxysilane (VMMS) > Vinyltrimethoxysilane (VTMS), 7-octenyltrimethoxysilane (ONTMS), Ureidopropyltrimethoxysilane (UPTMS), (3-glycidoxypropyl)trimethoxysilane (GPTMS), 3-aminopropyltrimethoxysilane (AMPTMS), Bis(3-trimethoxysilylpropyl)amine (BTMSPA).

Differential Scanning Calorimetry (DSC) was used to obtain the crystallization temperatures (T_c) of the crosslinked PP and its soluble materials. Crosslinking was found to significantly increase the T_c of PP except with UPTMS, GPTMS, AMPTMS, and BTMSPA. The soluble materials of highly crosslinked samples (with APTMS and VMMS) exhibited T_c close to that of the pure PP except with Azido-silane while the soluble materials of lightly crosslinked samples (with VTMS and ONTMS) exhibited high T_c compared to that of the pure PP.

The melt properties were studied by oscillatory shear rheology experiments and MFI test. Light crosslinking (gel content ≤ 5 wt.%) was found to decrease MFI, increase complex viscosity (η^*) and storage modulus (G') at low frequency, and decrease $\tan \delta$ at low frequency. APTMS-crosslinked PP (gel content ~ 5 wt.%) had greater influence compared to ONTMS-crosslinked PP (gel content 2 wt.%).

In general, the addition of the PP grafted with silanes (PP-g-APTMS and PP-g-Azidosilane) improved the mechanical properties of wood-fiber/PP composites. PP-g-APTMS had better effect compared to PP-g-Azidosilane.

Acknowledgements

In the name of Allah, the Most Gracious, the Most Merciful

First and foremost, all praises to Allah Almighty for the strengths and His blessing in completing this work.

I would like to express my deep gratitude to my supervisor, Professor Leonardo Simon, for his great support and encouragement to me throughout this project. I was so fortunate to work under his supervision and to learn a lot from him.

I would also like to thank my thesis committee members Professor. Ali Elkamel and Professor Aiping Yu for the time and effort they spent in reading and reviewing my thesis.

I am also very grateful to all my colleagues in Professor Simon's research group, Chong Meng, Mariana Silva Beauvalet, Charles Dal Castel, and Ryan Park for their support and very constructive discussions.

I would like to express my great thanks to my co-op students Mahyar Hallaj and Sayantan Sengupta for their valuable help and assistance during my lab work.

I would like also to acknowledge the financial and technical support from Saudi Basic Industries Corporation (SABIC).

The last but not the least, my deep and grateful thanks go to my parents and my wife for their support and encouragement.

Dedication

I would like to dedicate this thesis to my parents and my wife for their support and understanding throughout my studies.

Table of Contents

AUTHOR'S DECLARATION	ii
Abstract	iii
Acknowledgements	v
Dedication	vi
Table of Contents	vii
List of Figures	x
List of Schemes	xiv
List of Tables	xv
List of Abbreviations	xvi
Chapter 1 Introduction	1
1.1 Objectives and Motivation	2
1.2 Outline of the Thesis	3
1.3 Experimental Plan	4
Chapter 2 Literature Review	5
2.1 Polypropylene	5
2.2 Polypropylene Limitations	7
2.3 Chemical Modification of PP by Organo-functional Silanes using Reactive Extrusion	8
2.3.1 Ways to Minimize Molecular Weight Loss during Chemical Modification of PP with Silane	10
2.3.2 Effect of Silane Type and Concentration on PP Properties	14
2.3.3 Effect of Co-agents	22
2.3.4 Effect of Peroxides	26
2.3.5 Effect of Processing Conditions	34
2.4 Introduction of Long Chain Branching onto PP through Silane	36
2.5 Use of Polypropylene-g-silane as a Coupling Agent in Natural-fiber/Polypropylene Composites	39
Chapter 3 Materials and Methods.....	44
3.1 Materials.....	44
3.2 Sample Preparations	46
2.3.1 Grinding	46
2.3.2 Preparation of PP-g-silane Samples.....	47

2.3.3 Preparation of Silane-crosslinked PP Samples.....	49
2.3.4 Preparation of Wood-fiber/PP Composites	49
3.3 Characterization.....	50
3.3.1 Fourier Transform Infrared Spectroscopy (FTIR) Analysis	50
3.3.2 Gel Content Determination	52
3.3.3 Differential Scanning Calorimetry (DSC).....	53
3.3.4 Melt Flow Index (MFI).....	53
3.3.5 Oscillatory Shear Rheology Experiments	54
3.3.6 Mechanical Properties	56
3.3.7 Gel Permeation Chromatography (GPC)	58
Chapter 4 Results and Discussions: Chemical Modification of Polypropylene with Organo-functional Silanes and its Impact on Crystallization Temperature and Melt Properties of Polypropylene.....	59
4.1 Grafting Organo-functional Silanes and Chemical Analyses	59
4.2 Gel Contents	76
4.3 Crystallization Peak Temperatures	79
4.3.1 Crosslinked Samples.....	79
4.3.2 Soluble Materials	82
4.4 Melt Properties	86
4.4.1 Melt Flow Index (MFI).....	86
4.4.2 Melt Rheological Properties	87
Chapter 5 Results and Discussions: Influence of PP Grafted with Silane on Mechanical Properties of Wood-fiber/PP Composites	93
5.1 Influence of PP-g-APTMS	93
5.1.1 Tensile Strength.....	94
5.1.2 Tensile Modulus	96
5.1.3 Flexural Strength	98
5.1.4 Flexural Modulus.....	99
5.1.5 Impact Strength	100
5.1.6 Elongation at break	102
5.2 Influence of PP-g-Azidosilane	103
Chapter 6 Conclusions and Recommendations.....	107
Bibliography.....	111

Appendix.....118

List of Figures

Figure 1.1	Experimental Plan	4
Figure 2.1	Chemical structure of polypropylene	6
Figure 2.2	Chemical structure of triallyl trimetate (TATM)	11
Figure 2.3	Chemical structure of mercaptopropyltrimethoxysilane (MPTMS)	12
Figure 2.4	Chemical structure of vinyltrimethoxysilane (VTMS)	12
Figure 2.5	Chemical structure of methacryloxypropyltrimethoxysilane (VMMS)	13
Figure 2.6	Chemical structure of benzoyl peroxide (BPO)	14
Figure 2.7	Chemical structure of vinyltriethoxysilane (VTES)	15
Figure 2.8	Effect of silane type and concentration on the gel content of crosslinked PP	15
Figure 2.9	Effect of DCP concentration on the gel percentage of silane-crosslinked PP	16
Figure 2.10	Effect of silane type and concentration on the MFR of grafted PP	17
Figure 2.11	Effect of silane type and concentration on the equilibrium torque during the grafting reaction	17
Figure 2.12	Effect of VTMS concentration on the gel content of crosslinked PP	18
Figure 2.13	Effect of VTMS concentration on the MFR of crosslinked PP	19
Figure 2.14	Effect of VTES concentration on the grafting degree of grafted PP	20
Figure 2.15	Effect of VTMS concentration on the crystallization curves of crosslinked PP	21
Figure 2.16	Effect of VTMS concentration on thermal stability of crosslinked PP	21
Figure 2.17	WAXD profiles for VTMS-crosslinked PP (HMSPP) and pure PP	22
Figure 2.18	Effect of styrene concentration on the gel content of VMMS-crosslinked PP and the MFR of PP-g-VMMS	23
Figure 2.19	Chemical structure of divinylbenzene (DVB)	24
Figure 2.20	Chemical structure of triallyl isocyanurate (TAIC)	24
Figure 2.21	Chemical structure of trimethylolpropane triacrylate (TMPTA)	24
Figure 2.22	Effect of the co-agent concentration on the gel content of coagent-assisted VTMS-crosslinked PP	25
Figure 2.23	Effect of co-agent concentration on the MFR of co-agent-assisted PP-g-VTMS ...	26
Figure 2.24	Chemical structure of dicumyl peroxide (DCP)	27

Figure 2.25	Effect of DCP concentration on the gel content of VMMS-crosslinked PP and on the MFR of PP-g-VMMS	27
Figure 2.26	Effect of BPO concentration on the gel content of VMMS-crosslinked PP and on the MFR of PP-g-VMMS	28
Figure 2.27	Effect of DCP concentration on the gel content of VMMS-crosslinked PP and on the equilibrium torque during the grafting reaction	29
Figure 2.28	Effect of DCP concentration on the gel content of VTES-crosslinked PP and on the equilibrium torque during the grafting reaction	29
Figure 2.29	Effect of the type of peroxide on the gel content of crosslinked PP	30
Figure 2.30	Effect of the type of peroxide on the equilibrium torque during the grafting reaction	31
Figure 2.31	Effect of DCP concentration on the grafting degree of VTES in PP-g-VTES for different VTES concentrations	32
Figure 2.32	Chemical structure of di-tertbutyl peroxide (TBP)	33
Figure 2.33	Effect of the type of peroxide on the gel content of crosslinked PP	33
Figure 2.34	Effect of processing temperature on the gel content of crosslinked PP and on the MFR of grafted PP	34
Figure 2.35	Effect of screw speed on the gel content of crosslinked PP and on the MFR of grafted PP	35
Figure 2.36	Effect of the processing temperature on the gel content of crosslinked PP and on the equilibrium torque during the grafting reaction	35
Figure 2.37	GPC data for pure PP and long chain branched PP (LCB-PP) prepared by grafting triallyl phosphate (TAP) in the presence of DCP	37
Figure 2.38	Chemical structure of dibutyltin dilaurate (DBTDL)	38
Figure 2.39	GPC data for pure PP, PP-g-VTES and long chain branched PP prepared by grafting VTES (LCB-Si PP) in the presence of DCP	38
Figure 3.1	Retsch Ultra Centrifugal Mill ZM200	47
Figure 3.2	Parts in Haake Minilab extruder	48
Figure 3.3	The view inside Haake Minilab extruder	48
Figure 4.1	FTIR spectra of the pure PP, PP-g-ONTMS, and PP-g-VTMS	62
Figure 4.2	FTIR spectra of the pure PP, PP-g-ONTMS, and PP-g-VTMS	63

Figure 4.3	FTIR spectra of the PP reacted with peroxide, PP-g-BTMSPA, PP-g-AMPTMS, and PP-g-UPTMS (Wavenumber range: 1500-1850 cm ⁻¹)	65
Figure 4.4	FTIR spectra of the PP reacted with peroxide, PP-g-BTMSPA, PP-g-AMPTMS, and PP-g-UPTMS	67
Figure 4.5	FTIR spectra of the PP reacted with peroxide, and PP-g-AMPTMS prepared at different reaction times (Wavenumber range: 1500-1850 cm ⁻¹)	68
Figure 4.6	FTIR spectra of the PP reacted with peroxide, and PP-g-AMPTMS prepared at different reaction times	69
Figure 4.7	FTIR spectra of the PP reacted with peroxide, and PP-g-GPTMS (Wavenumber range: 1500-1850 cm ⁻¹)	70
Figure 4.8	FTIR spectra of the PP reacted with peroxide, and PP-g-GPTMS	71
Figure 4.9	FTIR spectra of the pure PP and PP-g-Azidosilane	73
Figure 4.10	FT-IR absorption ratios of the pure PP, PP-g-ONTMS, PP-g-VTMS, PP-g-VMMS, and PP-g-APTMS	74
Figure 4.11	FT-IR absorption ratios of the PP reacted with peroxide, PP-g-AMPTMS, bPP-g-BTMSPA, and PP-g-UPTMS	75
Figure 4.12	FT-IR absorption ratios of the PP reacted with peroxide, and PP-g-AMPTMS at different reaction times	76
Figure 4.13	Gel contents of APTMS-crosslinked PP, VMMS-crosslinked PP, and Azidosilane-crosslinked PP	78
Figure 4.14	Gel contents of PP crosslinked with VTMS, ONTMS, AMPTMS, BTMSPA, UPTMS, and GPTMS	79
Figure 4.15	The crystallization peak temperatures of the pure PP, PP reacted with peroxide, and PP crosslinked with different silanes	80
Figure 4.16	T _c for APTMS, VMMS, VTMS, ONTMS, and Azido-silane systems before and after gel removal	84
Figure 4.17	Melt flow Index (MFI) of pure PP, PP reacted with two levels of peroxide, ONTMS-crosslinked PP (0.20 wt.% peroxide), and APTMS-crosslinked PP (0.020 wt.% peroxide)	87
Figure 4.18	Complex viscosity (η^*) versus angular frequency of the pure PP, PP reacted with 0.20 wt.% peroxide, ONTMS-crosslinked PP (0.20 wt.% peroxide), and APTMS-crosslinked PP (0.020 wt.% peroxide) at 180°C	89

Figure 4.19	Storage modulus (G') versus angular frequency of the pure PP, PP reacted with 0.20 wt.% peroxide, ONTMS-crosslinked PP (0.20 wt.% peroxide), and APTMS-crosslinked PP (0.020 wt.% peroxide) at 180°C	90
Figure 4.20	Tan δ versus angular frequency of the pure PP, PP reacted with 0.20 wt.% peroxide, ONTMS-crosslinked PP (0.20 wt.% peroxide), and APTMS-crosslinked PP (0.020 wt.% peroxide) at 180°C	91
Figure 4.21	Cole-Cole plot of the pure PP, PP reacted with 0.20 wt.% peroxide, ONTMS-crosslinked PP (0.20 wt.% peroxide), and APTMS-crosslinked PP (0.020 wt.% peroxide) at 180°C	92
Figure 5.1	Tensile strength of PP and wood-fiber/PP composites at different PP-g-APTMS concentrations	96
Figure 5.2	Tensile modulus of PP and wood-fiber/PP composites at different PP-g-APTMS Concentrations	98
Figure 5.3	Flexural strength of PP and wood-fiber/PP composites at different PP-g-APTMS concentrations	99
Figure 5.4	Flexural modulus of PP and wood-fiber/PP composites at different PP-g-APTMS concentrations	100
Figure 5.5	Impact strength of PP and wood-fiber/PP composites at different PP-g-APTMS concentrations	101
Figure 5.6	Elongation at break of PP and wood-fiber/PP composites at different PP-g-APTMS concentrations	102
Figure 5.7	Tensile strength of the non-coupled composite, and composites coupled with PP-g-Azidosilane and PP-g-APTMS (both at 5 wt.%)	104
Figure 5.8	Tensile modulus of the non-coupled composite, and composites coupled with PP-g-Azidosilane and PP-g-APTMS (both at 5 wt.%)	105
Figure 5.9	Flexural strength of the non-coupled composite, and composites coupled with PP-g-Azidosilane and PP-g-APTMS (both at 5 wt.%)	105
Figure 5.10	Flexural modulus of the non-coupled composite, and composites coupled with PP-g-Azidosilane and PP-g-APTMS (both at 5 wt.%)	106
Figure 5.11	Impact strength of the non-coupled composite, and composites coupled with PP-g-Azidosilane and PP-g-APTMS (both at 5 wt.%)	106

List of Schemes

Scheme 2.1	Schematic representation of the reaction mechanism for silane-grafting/crosslinking of PP	10
Scheme 4.1	Schematic representation of VTMS grafting onto PP	61
Scheme 4.2	Schematic representation of AMPTMS grafting onto PP	64
Scheme 4.3	Schematic representation of Azido-silane grafting onto PP	72
Scheme 4.4	Schematic representation of water crosslinking of PP via VTMS grafts	77

List of Tables

Table 3.1	Organo-functional silanes and peroxide used in this study	44
Table 4.1	Samples prepared for FT-IR analysis	60
Table 4.2	Mn, Mw, Mz, and PDI for the PP reacted with peroxide, and the soluble material of ONTMS-crosslinked PP	85
Table 5.1	Wood-fiber/PP composites prepared with different PP-g-APTMS concentrations	93
Table 5.2	Tensile strength and modulus, elongation at break, flexural strength and modulus, and IZOD impact strength of pure PP and wood-fiber/PP composites	94
Table 5.3	Wood-fiber/PP composites prepared without coupling agent, with PP-g-Azidosilane, and with PP-g-APTMS	103
Table 5.4	Tensile strength and modulus, flexural strength and modulus, and IZOD impact strength of different wood-fiber/PP composites	103

List of Abbreviations

%	Percentage
¹ H NMR	Proton NMR
AMPTMS	3-aminopropyltrimethoxysilane
APTMS	(3-acryloxypropyl)trimethoxysilane
Azido-silane	6-Azidosulfonylhexyltriethoxysilane
BHT	Butylated Hydroxytoluene
BPO	Dibenzoylperoxide
BTMSPA	Bis(3-trimethoxysilylpropyl)amine
cm	Centimeter
DBTDL	Dibutyltin dilaurate
DCP	Dicumyl peroxide
DSC	Differential Scanning Calorimetry
DVB	Divinylbenzene
FT-IR	Fourier Transform Infrared Spectroscopy
g	gram
G''	Loss Modulus
G'	Storage Modulus
g/mol	grams per mole
GPC	Gel Permeation Chromatography
GPTMS	(3-glycidoxypropyl)trimethoxysilane
H ₂ O	Water
HMS-PP	High Melt Strength Polypropylene
IR	Infrared Radiation
J	Joule
kg	kilogram
LCB-PP	Long Chain Branched Polypropylene
m	metre
MFI	Melt Flow Index
MFR	Melt Flow Rate
mg	Milligram
mm	Millimetre
M _n	Number-average Molecular Weight
MPa	Megapascal
MPTMS	Mercaptopropyltrimethoxysilane
M _w	Weight-average Molecular Weight
M _z	Z-average Molecular Weight
ONTMS	7-octenyltrimethoxysilane
PDI	Polydispersity

PP	Polypropylene
PP-g-silane	Polypropylene grafted with Silane
PP-g-AMPTMS	Polypropylene grafted with 3-aminopropyltrimethoxysilane
PP-g-APTMS	Polypropylene grafted with (3-acryloxypropyl)trimethoxysilane
PP-g-Azidosilane	Polypropylene grafted with 6-Azidosulfonylhexyltriethoxysilane
PP-g-BTMSPA	Polypropylene grafted with Bis(3-trimethoxysilylpropyl)amine
PP-g-GPTMS	Polypropylene grafted with (3-glycidoxypropyl)trimethoxysilane
PP-g-maleic anhydride	Polypropylene grafted with Maleic Anhydride
PP-g-MAN	Polypropylene grafted with Maleic Anhydride
PP-g-ONTMS	Polypropylene grafted with 7-octenyltrimethoxysilane
PP-g-UPTMS	Polypropylene grafted with Ureidopropyltrimethoxysilane
PP-g-VMMS	Polypropylene grafted with 3-methacryloxypropyltrimethoxysilane
PP-g-VTMS	Polypropylene grafted with Vinyltrimethoxysilane
SEM	Scanning Electron Microscopy
SiAn	3-(triethoxysilyl)propylsuccinic Anhydride
TAIC	Triallyl Isocyanurate
Tan δ	Tangent of the Phase Angle
TAP	Triallyl Phosphate
TATM	Triallyl Trimettitate
TBP	Di-tertbutyl Peroxide
T_c	Crystallization Peak Temperature
TCB	1,2,4-trichlorobenzene
TMPTA	Trimethylolpropane Triacrylate
T_o	Onset Temperature of Crystallization
UPTMS	Ureidopropyltrimethoxysilane
VMMS	3-methacryloxypropyltrimethoxysilane
VTES	Vinyltriethoxysilane
VTMS	Vinyltrimethoxysilane
WAXD	Wide Angle X-ray Diffraction
wt. %	Weight Percent
δ	The Phase Angle
η^*	Complex viscosity
ω	Angular Frequency

Chapter 1

Introduction

Polypropylene (PP) is one of the most widely used commercial thermoplastics due to its many attractive properties such as excellent chemical resistance and good thermal resistance and processability. However, it still suffers at high service temperatures especially when exposed to mechanical stresses. In addition, its poor melt strength creates processing difficulties in processes like blow molding, thermoforming, and extrusion coating. PP also lacks functional groups necessary for the preparation of composites with desirable performance.

Many chemical and physical modification methods were suggested to overcome these limitations and some of them are applied in industry. Chemical modification of PP in the melt state by reactive extrusion is one of the simplest and most common applied methods. It can be used to crosslink PP chains, introduce long chain branches onto PP linear chains, and introduce functional groups onto PP backbone. Crosslinking improves heat resistance while introduction of long chain branching is effective in enhancing PP melt strength. Moreover, compatibility between PP and fillers in PP composites can be greatly improved by introducing functionalities onto PP. Therefore, the above three limitations associated with conventional PP can be avoided using such method of modification.

Among the chemical modification methods that gained considerable attention recently involves the use organo-functional silanes. Due to their bi-functional nature, their grafting onto PP backbone can ultimately crosslink PP chains and improve its thermal resistance. PP with low crosslinking degree and improved melt strength can also be produced using these silanes as revealed by recent works. Their bi-functional nature allows also to improve the compatibility between PP and fillers.

1.1 Objectives and Motivation

The objectives of this study were as follows:

1. To compare the grafting efficiencies of nine different organo-functional silanes onto PP using Fourier transform infrared spectroscopy (FT-IR) analysis and gel content test. Out of these nine silanes, the use of five silanes in the chemical modification of PP has not been reported before.
2. To study the effect of these nine silanes on the crystallization temperature of the silane-crosslinked PP and its soluble materials using Differential Scanning Calorimetry (DSC). It is reported in literature that crosslinking and long chain branching induce a nucleation effect that increases the rate of PP crystallization and its crystallization temperature. Therefore, it is interesting to gain some insight on the effect of crosslinking on the molecular structure of PP before and after removing the insoluble crosslinked material.
3. To study the influence of two selected silanes, with different grafting efficiencies, on the melt properties of PP (with low crosslinking degree) using melt flow index test (MFI) and oscillatory shear rheology measurements. Previous works were carried out only with two different silanes having vinyl organo-functional groups having low grafting efficiencies onto PP.
4. To study the impact of PP grafted with two selected silanes, with the highest grafting efficiencies, on the mechanical properties of wood-fiber/PP composites. Silanes are widely used in surface treatment of fillers applied in PP composite. Few authors have reported the use of PP grafted with silanes in this field. They have shown the performance of PP grafted with silanes having medium and low grafting efficiencies.

1.2 Outline of the Thesis

The thesis is organized as follows:

Chapter 1 – **Introduction**: it provides general information about modification of PP with more emphasis put on chemical modification. It includes the objectives, motivation, outline, and experimental plan.

Chapter 2 – **Literature Review**: it discusses polypropylene, its limitations, and ways to overcome these drawbacks. Chemical modification of PP by organo-functional silanes using reactive extrusion is discussed in more details. It also covers the introduction of long chain branching onto PP through silane and the use of PP-g-silane as a coupling agent in natural-fiber/PP composites.

Chapter 3 – **Materials and Methods**: it introduces the materials used in this work including nine different silanes. It describes the processing methods used to prepare the different samples and the characterization techniques used to evaluate the properties of those samples.

Chapter 4 – **Results and Discussions - Chemical Modification of Polypropylene with Organo-functional Silanes and its Impact on Crystallization Temperature and Melt Properties of Polypropylene**: This chapter presents and discusses the results obtained from FT-IR analysis, gel content test, DSC analysis, MFI test, and oscillatory shear rheology measurements.

Chapter 5 – **Results and Discussions - Mechanical Properties of Wood-fiber/PP Composites**: it includes the discussion of the results obtained from mechanical testing for the different prepared composites.

Chapter 6 – **Conclusions and Recommendations**: it summarizes the project stages and the obtained results. It also gives concluding remarks derived from Chapters 4 and 5 and provides recommendations for future work.

1.3 Experimental Plan

The experimental plane showing materials, processing methods, and characterization techniques is summarized and presented in Figure 1.1.

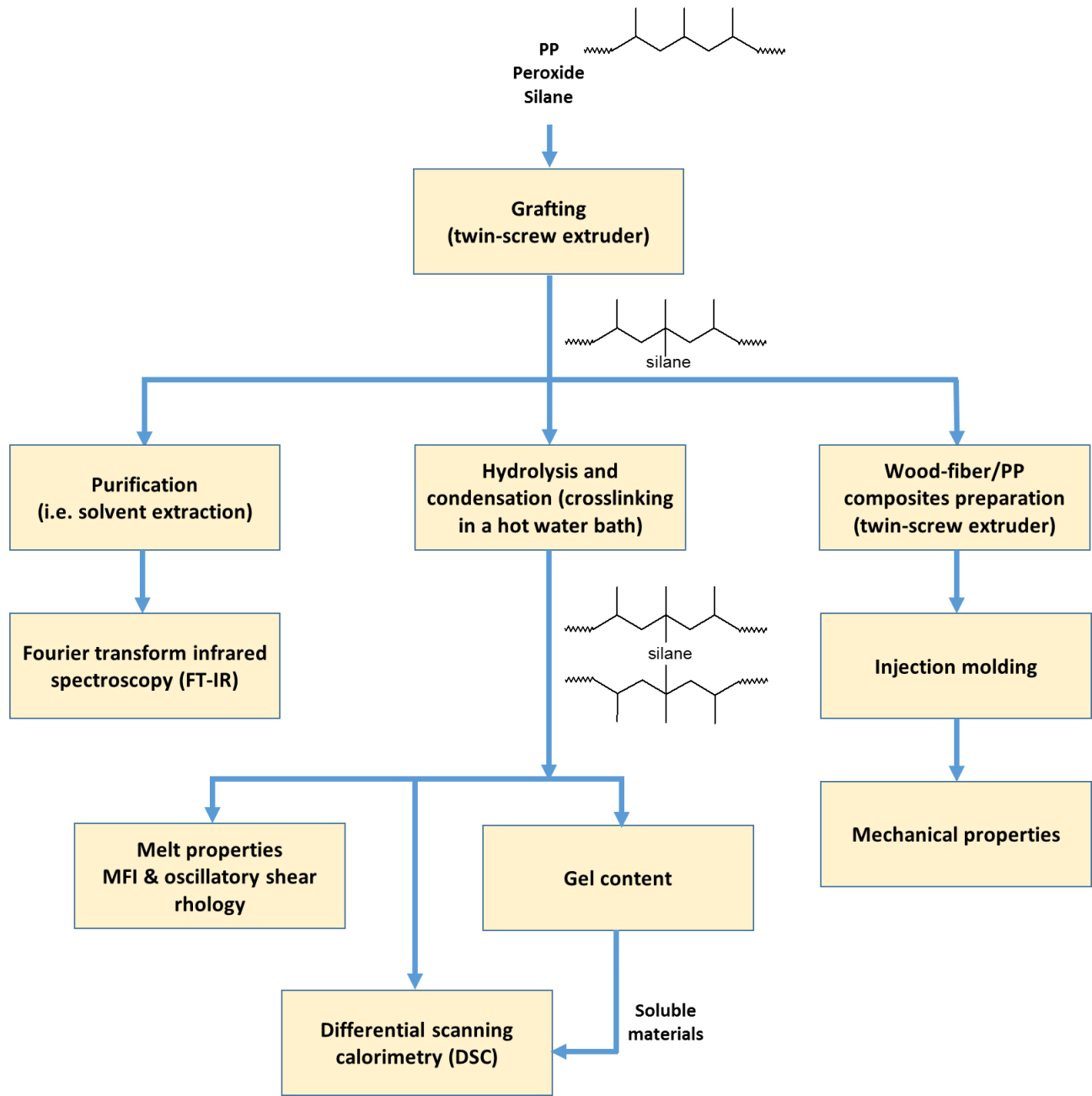


Figure 1.1 Experimental Plan

Chapter 2

Literature Review

2.1 Polypropylene

Isotactic PP is produced commercially in three major forms, depending on the properties desired: PP homopolymers, PP random copolymers, and PP impact copolymers. PP homopolymers, the most widely used form, consist exclusively of propylene monomers and provide rigidity and better thermal resistance in comparison with other forms. On the other hand, its impact resistance at low temperatures and clarity are low. PP random copolymers contain 1.5 wt.% to 6 wt.% of ethylene, 1-butene, or 1-hexene distributed randomly among the propylene units. They exhibit improved clarity and impact resistance and lower melting temperature and rigidity. PP impact copolymers are formed by adding much higher ethylene content (up to 15%) compared with PP random copolymers. The copolymerized portion in PP impact copolymers contains 40%–65% of the ethylene; this rubbery material is evenly distributed throughout the PP homopolymer crystalline matrix in the form of a separate phase. The presence of this rubbery phase (which may comprise up to 25% of the entire polymer) imparts a higher degree of toughness to the polymer and significantly improves the impact resistance at low temperatures (Karian, 2003; Maier, 1998; Tripathi, 2002).

Isotactic Polypropylene (PP) (Figure 2.1) is a thermoplastic resin that is obtained using Ziegler-Natta polymerization technology. The application of such technology allows the production of crystallisable chains containing 10,000 to 20,000 propylene monomers, giving rise to a semi-crystalline solid with many attractive properties. The properties of isotactic PP homopolymer in the melt and solid states are governed by the amount of the isotactic and atactic portions, the molecular weight, and the molecular weight distribution (dispersity). The atactic portion can be as high as 20%, as measured by the level of xylene solubles at room temperature. The molecular weight ranges from $220 \cdot 10^3$ g/mol to $700 \cdot 10^3$ g/mol, and dispersity ranges from 2.1 to 11.0 (Maier, 1998; Tripathi, 2002).

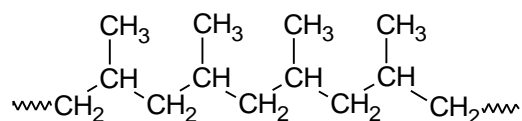


Figure 2.1 Chemical structure of polypropylene

Isotactic PP is classified as a commodity resin due to its numerous uses and applications. It is well suited to various processing techniques, such as injection molding, fiber extrusion, film extrusion, sheet extrusion, and pipe extrusion. Therefore, it is applied in a wide range of commercial applications, including automotive applications, medical applications, appliances, textiles and nonwovens, packaging, consumer products, and construction (Maier, 1998). Approximately 48 million metric tonnes of PP were produced in 2010 worldwide (Malpass, 2012). It is the third most consumed thermoplastic, following low density polyethylene (LDPE) and Poly(vinyl chloride) (PVC) (Maier, 1998). The annual growth rate of PP in the polymer market is high in comparison with other commodity resins. It was 25% until the early 1970s and between 7% and 12% from 1974 to 1999 (Karian, 2003). In recent years, the growth rate has slowed, but it is expected to rise again in the next decade (Malpass, 2012).

Polypropylene exhibits several attractive properties when compared with other thermoplastics. It has excellent mechanical, physical, and thermal properties at room temperature. Its stiffness is relatively high at a lower density than its competitive materials. It exhibits good thermal resistance when it is not exposed to mechanical stresses. Polypropylene has a high melting point and heat deflection temperature. Excellent chemical resistance and good environmental stress crack resistance (ESCR) are additional advantages of PP over other thermoplastics. It can also be easily processed by extrusion, injection molding, and a wide variety of other processing techniques. One of the most desirable merits of PP is its low cost; in fact, it is considered the most economical of the thermoplastics available on the market when a balance of cost and performance is taken into consideration.

2.2 Polypropylene Limitations

Nonetheless, PP still has certain limitations. For example, conventional PP has limitations in its thermal resistance (Zhou, 2009). The crystallization temperature and melting point that arise from its semi-crystalline structure limit the application of PP at higher service temperatures (Chaudhary, 2011). Another limitation of PP is its poor melt strength, which results from the utilization of Ziegler-Natta or metallocene catalysts. Current commercial polymerization processes produce PP with a high linear chain content and narrow molecular weight distribution, causing poor melt strength (Borsig, 2008; Lagendijk, 2001). In addition, its nonpolar characteristics and lack of functionalities limit the application of PP in many technological fields. As a result, the adhesion of PP to synthetic fillers, such as metals and glass, and to natural fillers, such as date palm fibers, is poor. PP is also poorly compatible with other synthetic polymers due to its non-polar nature (Abu-Sharkh, 2004; Munteanu, 1997).

All of the aforementioned disadvantages can be overcome by post-reactor chemical modification of PP, via several techniques such as functionalization or grafting, crosslinking, and branching (Wang et al., 1996).

Converting PP to a thermoset polymer by crosslinking could potentially overcome the limitation in thermal resistance (Chaudhary, 2011). Crosslinking polyolefins is known to be an important technique used to improve thermal resistance (Zhou, 2009). Crosslinking is defined as the process of joining polymer chains by covalent bonds (Munteanu, 1997). Compared with other crosslinking approaches, silane crosslinking of PP via reactive extrusion and water treatment offers numerous advantages, such as low investment costs, easy processing, and improved product properties (An, 2008). Crosslinking of PP with silane is commonly accomplished by means of two sequential steps. The first step involves grafting an unsaturated silane compound onto a PP backbone in the presence of an initiator. The second step involves crosslinking PP chains by curing the PP-g-silane in hot water (Wang, 2005).

Due to its poor melt strength, linear PP presents difficulties in such processes as foaming, extrusion coating, thermoforming, and blow molding where elongational flows are predominant. It is necessary to modify and increase the melt strength of PP in order for it to be utilized in these processes. The most efficient method is to increase elongational viscosity by introducing long-chain branches into linear PP (Borsig, 2008; Lagendijk, 2001). This can be achieved by grafting monomers, such as methyl methacrylate, styrene, or vinyl silanes, onto the PP backbone (Rätzsch, 1999).

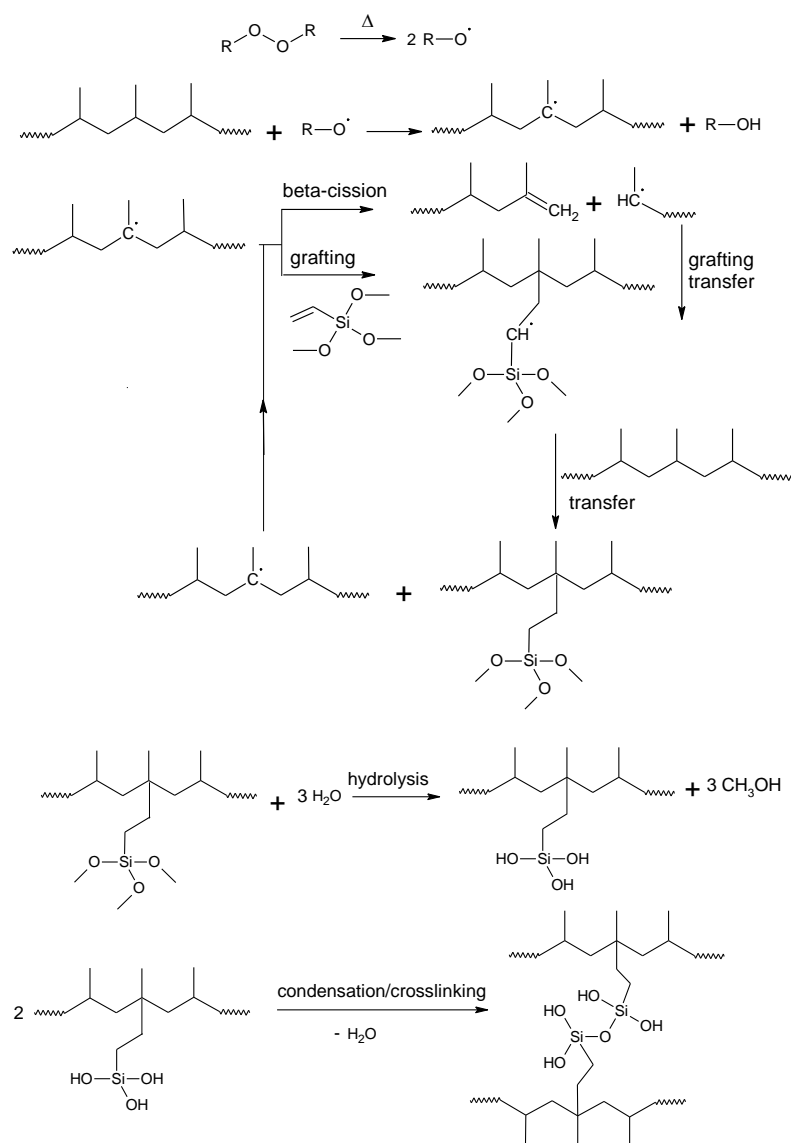
Functionalization of PP by grafting monomers onto its backbone significantly improves the adhesion of PP with synthetic and natural fillers and enhances the compatibility of PP with other polymers. The most widely used monomer for PP functionalization is maleic anhydride. Other reactive monomers are also used, such as vinyl acetate, silanes, and glycidyl methacrylate (Cartier, 1998; Nachtigall 1999; Nachtigall, 2007). One of the common approaches to introduce functional groups into PP is free-radical-induced grafting in the melt state using reactive extruders (Moad, 1999).

2.3 Chemical Modification of PP by Organo-functional Silanes using Reactive Extrusion

Organo-functional silanes are bifunctional molecules with two different functional groups. One functional group is an organic functional group responsible for the reaction with the polymer backbone, while the other is an alkoxy group (R-O-) directly attached to the silicon atom and, after being hydrolyzed and exposed to hot water, is responsible for crosslinking the polymer chains through -Si-O-Si- bridges (Munteanu, 1997). In the case of unsaturated silanes, the grafting step of silane onto PP in the melt state begins by mixing PP, silane, and radical initiator, such as an organic peroxide, and then heating the mixture.

Scheme 2.1 shows the predominant reaction mechanism. As temperature is raised, the peroxide decomposes to form alkoxy radicals. These radicals then react with PP chains and abstract preferentially tertiary hydrogen atoms to create PP macroradicals. The unsaturated silane compound, such as vinyltrimethoxysilane, reacts with the PP macroradicals through

the vinyl group on the silane, forming a stable macroradical. The grafted radical is then stabilized through a radical transfer reaction. The alkoxy groups on the grafted silane can react with water to form silanol groups (-Si-OH) responsible for improving adhesion and compatibility with polar fillers. When crosslinking of PP chains is required, the crosslinking of the PP-g-silane chains is accomplished via the condensation of the silanol groups in the presence of an organometallic catalyst. Water is removed as the condensation reaction product, leaving -Si-O-Si- linkages between the chains. The exposure to water can be carried out at different temperatures (steam can be used), depending on the required crosslinking rate (Rätzsch, 2002; Chaudhary, 2011).



Scheme 2.1 Schematic representation of the reaction mechanism for silane-grafting/crosslinking of PP

2.3.1 Ways to Minimize Molecular Weight Loss during Chemical Modification of PP with Silane

Molecular weight loss is the main disadvantage of this kind of modification and can be significant. The PP macroradicals, initially formed through the reaction with the peroxide, can either react with the monomer for grafting or undergo a β -scission reaction, which is the main side reaction. The process must be optimized to achieve the desired degree of grafting

while reducing the extent of molecular weight loss. Molecular weight loss is undesirable because it weakens many properties and leads to ineffective crosslinking after exposing the product to water (Chaudhary, 2011; Zhou, 2009).

Several researchers have tried different approaches to minimize PP degradation and achieve a higher degree of crosslinking when making silane-crosslinked PP. Note that PP degradation throughout this text refers to the reduction in molecular weight of PP during chemical modification in the grafting step. It should also be noted that the degree of crosslinking is one way to measure the grafting efficiency of the silane during the grafting reaction.

Chaudhary et al. (2011) compared three approaches in terms gel content, which is used to indicate the crosslinking degree. The first approach consists of two separate grafting steps. The first step begins with the creation of PP macroradicals via the action of peroxide radicals, followed by grafting a co-agent, such as triallyl trimetate (TATM) (Figure 2.2) onto PP macroradicals. Two kinds of PP macroradicals are assumed to participate in the grafting reaction with TATM, namely, those created initially and those resulting from initial radicals fragmentation. This step results in the attachment of unsaturated pendant groups to PP and the creation of PP low molecular weight chains containing double bonds resulting from the β -scission reaction. The second step involves grafting mercaptopropyltrimethoxysilane (MPTMS) (Figure 2.3) in the presence of peroxide to the unsaturation points formed during the first step. This reaction produces hydrolysable alkoxy silane groups attached to PP chains.

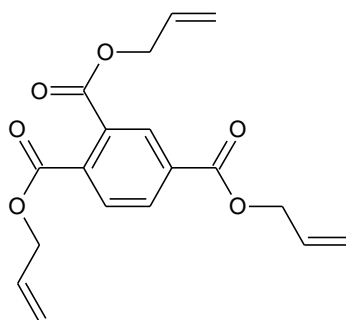


Figure 2.2 Chemical structure of triallyl trimetate (TATM)

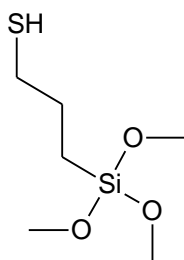


Figure 2.3 Chemical structure of mercaptopropyltrimethoxysilane (MPTMS)

The second approach explored by Chaudhary et al. (2011) involves a grafting step in which vinyltrimethoxysilane (VTMS) (Figure 2.4) is grafted onto PP in the presence of peroxide. First, peroxide radicals create PP macroradicals. VTMS is then grafted onto PP macroradicals by means of its vinyl group, and the resulting radical can combine with other radicals, disproportionate, or graft more VTMSs.

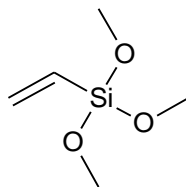


Figure 2.4 Chemical structure of vinyltrimethoxysilane (VTMS)

The third approach combines the above two approaches. VTMS is first grafted onto PP in the presence of peroxide, after which the grafted product is reacted in a separate step with MPTMS in the presence of peroxide. This approach takes advantage of the terminal unsaturation formed by chain scission during the first grafting reaction. Thiyl radicals originating from MPTMS are attached to the PP chain through the terminal unsaturation. (Chaudhary, 2011)

The highest gel contents, obtained after exposure to moisture, from the three approaches were 52 wt.%, 60 wt.%, and 59 wt.% for the first approach, the second approach, and the third approach, respectively. The second approach, which is the most common approach, was identified as the most efficient approach because it produced the highest gel content and required only one grafting step. (Chaudhary, 2011)

In an attempt to avoid the severe degradation caused by the presence of peroxide at elevated temperatures, An et al. (2008) grafted VTMS onto PP in a twin-screw extruder without adding peroxide. PP macroradicals were generated by the action of heat and mechanical shear and then grafted with VTMS. The grafting of VTMS was verified by FTIR, and a gel percentage of 42 wt% was obtained when only 4 wt% of VTMS was added to the grafting reaction medium.

Yang et al. (2007) proposed a new method to overcome the use of high peroxide concentrations. This method works only when the goal is to crosslink the PP-g-silane. Those authors combined the grafting and crosslinking steps into one step in the extruder. PP pellets, methacryloxypropyltrimethoxysilane (VMMS) (Figure 2.5), a small amount of water, benzoyl peroxide (BPO) (Figure 2.6), and styrene were blended (dry-mixed) and fed into a twin-screw extruder, in which the temperature in the first heating zone was maintained at 80°C, while the temperature was maintained at 160–190°C in the other heating zones. FTIR was used to verify that the VMMS was grafted, and the PP-g-VMMS was almost completely crosslinked by water in the extruder. Furthermore, the product was cured in boiling water, and curing was not found to change neither the gel content nor the MFR, indicating that few grafted chains were left after the extrusion process and that crosslinking of the grafted product actually occurred in the extruder. The gel content obtained was approximately 58 wt.%, and the amounts of VMMS and BPO were 1.0 phr and 0.36 phr, respectively.

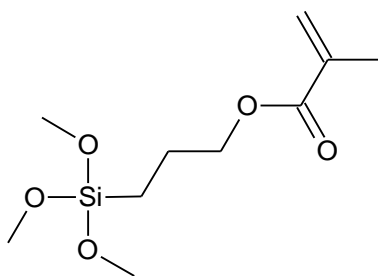


Figure 2.5 Chemical structure of methacryloxypropyltrimethoxysilane (VMMS)

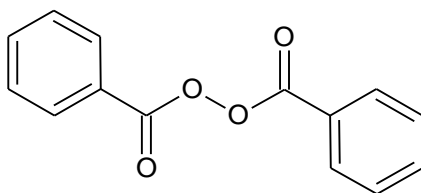


Figure 2.6 Chemical structure of benzoyl peroxide (BPO)

Those authors suggested that water hydrolyzed and condensed VMMS monomers in the first heating zone, in which it was kept at 80°C. This step combined silane monomers to form silane compounds with two or more vinyl groups. Then, in the other zones in which the temperature was high, PP macroradicals formed, and the new silane compound reacted with different PP macroradicals via its multiple vinyl groups to form silane-crosslinked PP. This mechanism was confirmed by FTIR results and supported by the fact that silane crosslinking by hydrolysis and condensation can easily occur at 80°C, while BPO peroxide cannot decompose at this low temperature, which means that PP macroradicals cannot form. In addition, crosslinking is impossible at temperatures higher than 100°C due to the complete escape of water via vaporization, while grafting is possible due to the formation of PP macroradicals as a result of the action of BPO formed radicals.

2.3.2 Effect of Silane Type and Concentration on PP Properties

The influence of silane type and concentration on the properties of PP-g-silane and silane-crosslinked PP has been investigated by numerous researchers.

Huang et al. (2000) compared three types of silane in terms of gel content and melt flow rate of isotactic polypropylene, which was initially in powder form with a melt flow rate of 6.7 g/10min. VMMS was found to be more efficient for grafting and crosslinking than VTMS and vinyltriethoxysilane (VTES) (Figure 2.7). In addition, the increase in the concentration of VMMS had a greater influence on the gel content, as demonstrated in Figure 2.8. The gel content was used as an indication of grafting and crosslinking efficiency. It was suggested that this influence might be due to the fact that the bulky alkoxy groups in VTMS and VTES are near the reactive sites, leading to larger steric hindrance. Another

reason might be the presence of the conjugated group in VMMS, which may stabilize the macroradicals, resulting in better grafting and crosslinking.

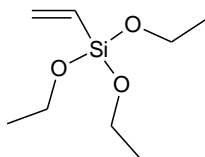


Figure 2.7 Chemical structure of vinyltriethoxysilane (VTES)

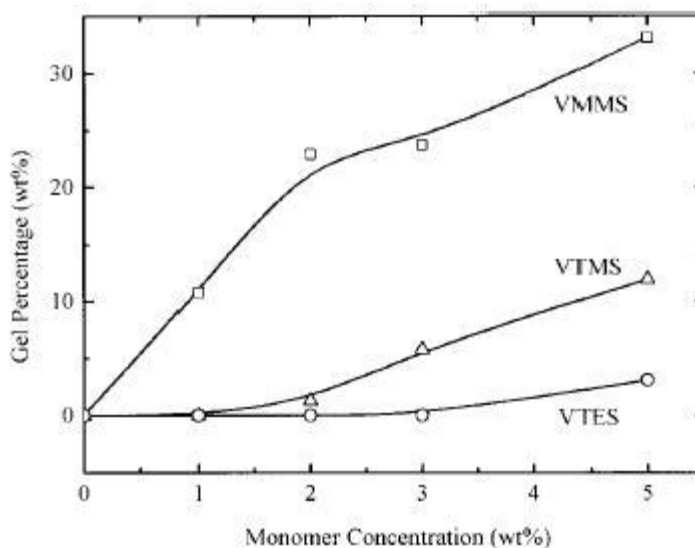


Figure 2.8 Effect of silane type and concentration on the gel content of crosslinked PP (from Huang et al., 2000)

Huang et al. (2000) and Wang et al. (2005) showed that VTMS is more effective at grafting and crosslinking than VTES under the same conditions as those displayed in Figure 2.9. This finding was attributed to the larger steric hindrance of VTES, leading to less grafting (Wang, 2005). However, the addition of styrene to the system greatly reduced the gel content obtained with VTMS, as demonstrated in the study conducted by Huang et al. (2000), which coincides with the research findings of Zhou et al. (2009).

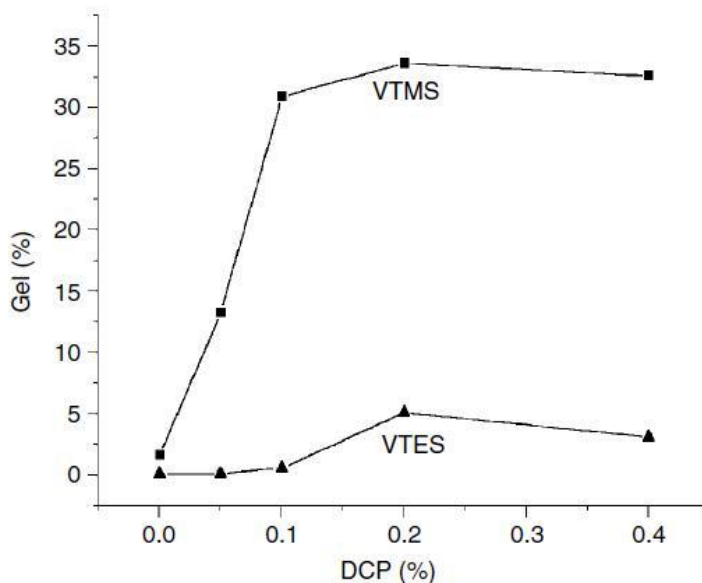


Figure 2.9 Effect of DCP concentration on the gel percentage of silane-crosslinked PP (silane 4%) (from Wang et al., 2005)

With regard to the melt flow rate, Huang et al. (2000) observed that the increase in concentration of both VMMS and VTES caused the melt flow rate of the grafted PP to decrease. However, grafting PP with VTES was observed to result in more degradation, as indicated by much higher flow rates compared to PP-g-VMMS at the same concentration of the silane monomer (Figure 2.10). The large hindrance in the case of VTES may inhibit the combination of radicals. Moreover, the stabilizing effect that the conjugated group in VMMS has on the macroradicals, it was suggested, could make the combination of radicals more favourable. At concentrations greater than 2 wt.%, an increased amount of combination was indicated by some degree of PP crosslinking that occurred during grafting with VMMS, as reflected by the melt flow rates of PP-g-VMMS, which were smaller than the pure PP melt flow rates. The equilibrium torque data obtained by Liu et al. (2000) supported this finding. In this study, the addition of VMMS to the system during the grafting reaction reduced the extent of degradation, unlike VTES, which did not affect the equilibrium torque, as seen in Figure 2.11.

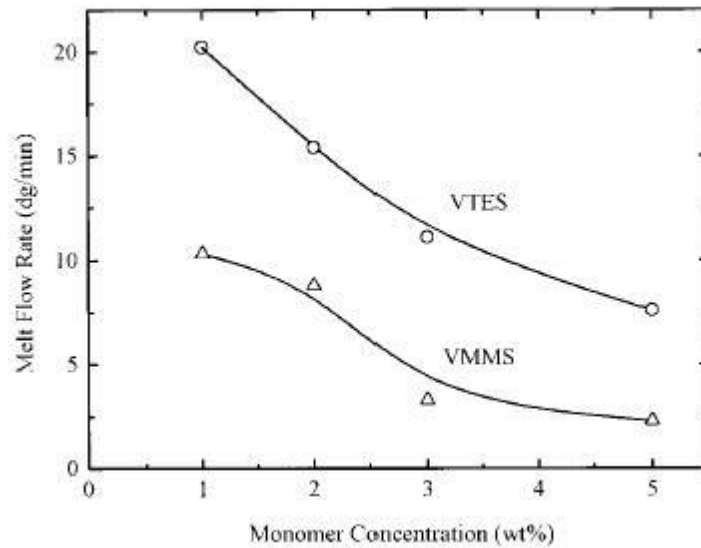


Figure 2.10 Effect of silane type and concentration on the MFR of grafted PP (from Huang et al., 2000)

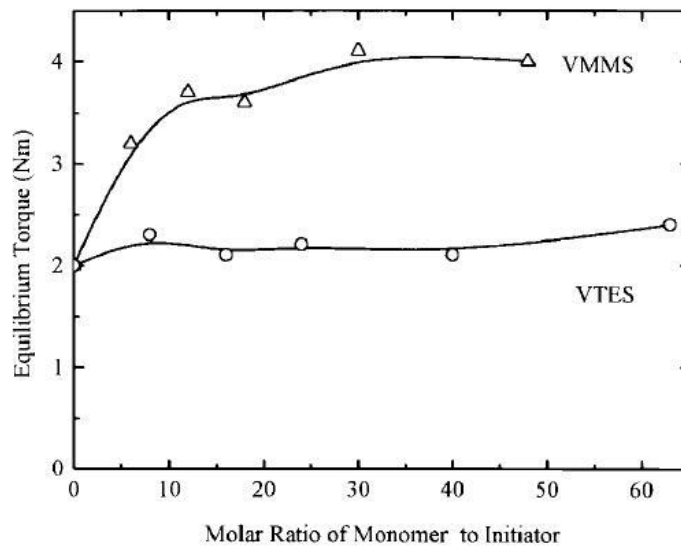


Figure 2.11. Effect of silane type and concentration on the equilibrium torque during the grafting reaction (from Liu et al., 2000)

The increase in concentration of VTMS was found to increase the amount of gel in VTMS-crosslinked PP (An, 2008; Wang, 2005). However, beyond a certain concentration value (Figure 2.12), there was a plateau, meaning that network formation did not involve new

chains. This finding may be due to the fact that short PP chains had more grafts due to a degradative chain transfer or because the tendency for intramolecular hydrogen transfer increased, resulting in many grafts on a single PP chain (Chaudhary, 2011).

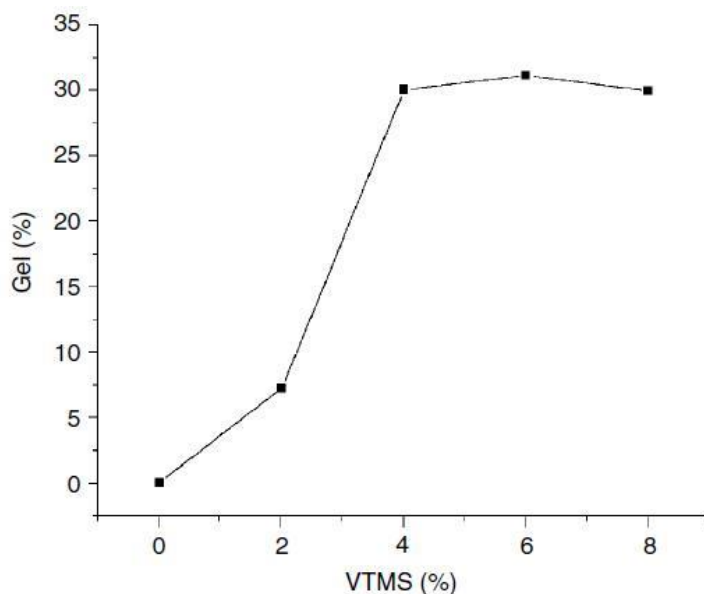


Figure 2.12 Effect of VTMS concentration on the gel content of crosslinked PP (from Wang et al., 2005)

Moreover, An et al. (2008) and Beltran and Mijangos (2000) observed that the concentration increase decreased the melt flow rate of the VTMS-crosslinked PP due to some crosslinking that decreased chain mobility (Figure 2.13). However, in the case of PP-g-VTMS, Beltran and Mijangos (2000) found that adding VTMS and increasing its concentration caused the viscosity of the grafting reaction mixture to drop, as indicated by the decrease in torque, which indicates that no crosslinking occurred during the grafting process. The drop in viscosity can be attributed to the lubricating effect that VTMS had on the PP melt or to the grafting process, which could have promoted internal plasticization in the melt. A similar trend was found with regard to the melt flow rate of PP-g-VTMS. However, the melt flow rate of PP-g-VTMS was observed to decrease once the concentration of VTMS exceeded a certain value due to the fact that some crosslinking took place during the preparation of the samples by the hot press. This crosslinking dominated the lubricant effect as the concentration increased (Beltran, 2000).

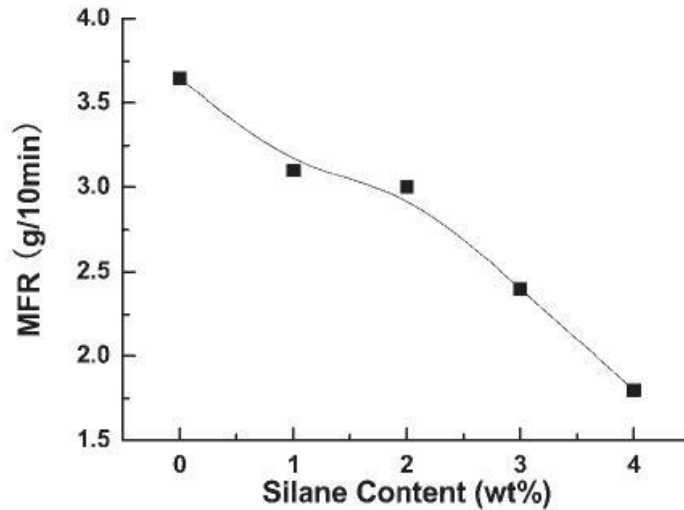


Figure 2.13 Effect of VTMS concentration on the MFR of crosslinked PP (from An et al., 2008)

According to Nachtigall et al. (1999), increasing the concentration of VTES had a positive influence on the grafting efficiency, as seen in Figure 2.14, indicating that VTES has a good reactivity. In addition, increasing the concentration from 5 % to 10 % at 0.1 % DCP had almost no influence on the mixing torque measured during the grafting reaction. Therefore, varying VTES concentration had no clear influence on molecular weight. But adding VTES without DCP to the system resulted in a drop in the equilibrium torque compared to pure PP. The authors suggested that this finding may be a result of the plasticization effect that VTES may have on the PP melt.

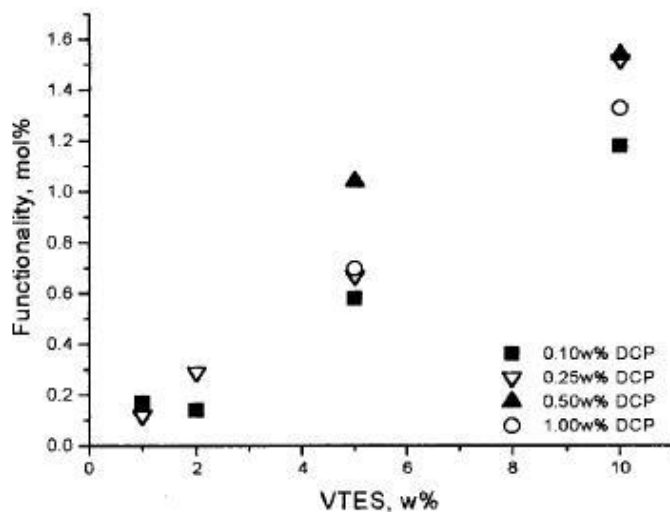


Figure 2.14 Effect of VTES concentration on the grafting degree of grafted PP (from Nachtigall et al., 1999)

Zhou et al. (2009) studied the crystallization behaviour and found that crosslinking of PP by VTMS accelerated PP crystallization, as indicated by higher onset temperatures of crystallization (T_o). On the other hand, the degree of crystallinity was lower than that of pure PP, which may be due to the formation of networks that hinder the chains' movement. An et al. (2008) prepared VTMS-crosslinked PP without any additives, and observed that increasing the concentration of VTMS shifted T_o to higher values, as shown in Figure 2.15. The latter study attributed the acceleration of crystallization to the increase in the nucleation density caused by crosslinking. However, the degree of crystallinity was noted to be higher than that of pure PP, which is the opposite of what Zhou et al. (2009) found. An increase in T_o with increasing VTMS concentration was also observed by Wang et al. (2005). In addition, these researchers found that the VTMS-crosslinked PP had a higher T_o than the PP-g-VTMS at the same VTMS concentration. In this study, the addition of VTMS had no influence on the degree of crystallinity. The crystallization process is typically hindered by crosslinking and promoted by a reduction in molecular weight. The acceleration of the crystallization process led to the conclusion that molecular weight reduction or chain scission, as indicated by the decrease in torque, is more dominant than crosslinking.

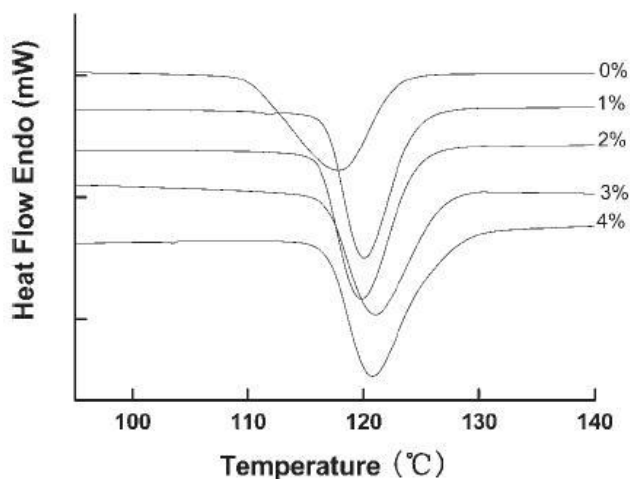


Figure 2.15 Effect of VTMS concentration on the crystallization curves of crosslinked PP (from An et al., 2008)

Crosslinking of PP by VTMS was found to improve PP thermal stability. Zhou et al. (2009) attributed this improvement to the Si-O-Si network, which has high thermal stability. Wang et al. (2005) observed that both PP-g-VTMS and VTMS-crosslinked PP were more thermally stable than pure PP, as indicated by higher degradation temperatures. The impact of VTMS concentration on thermal stability was studied by An et al. (2008) who found that after crosslinking, the heat resistance improved as VTMS concentration increased (Figure 2.16).

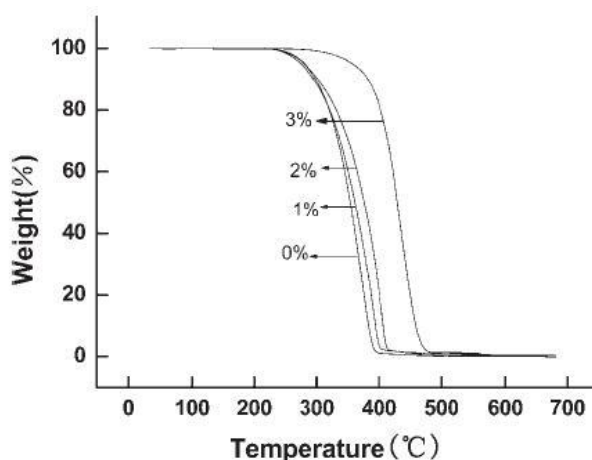


Figure 2.16 Effect of VTMS concentration on thermal stability of crosslinked PP (from An et al., 2008)

Isotactic PP has the ability to crystallize in the following three different crystalline forms, depending on crystallization conditions and composition: monoclinic (α), pseudo-hexagonal (β), and triclinic (γ). Wang et al. (2005) showed, by means of a WAXD study, that a peak corresponding to the β form disappeared completely after crosslinking PP with VTMS. This disappearance was caused by a change in the PP molecular structure, rather than by the crystallization conditions since the thermal history of the samples was erased. Zhou et al. (2009) and An et al. (2008) observed that the γ form appeared with VTMS-crosslinked PP but was absent for the pure PP. In addition, An et al. (2008) noticed that the intensities for some α peaks differed between VTMS-crosslinked PP and the pure PP, indicating that crosslinking caused slight changes in the growth of the crystals (Figure 2.17).

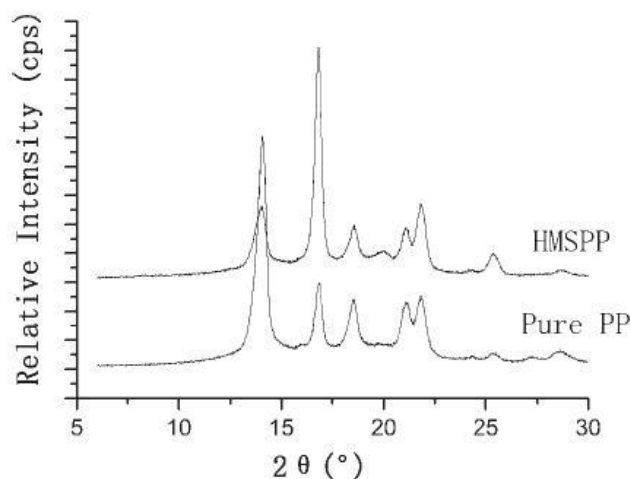


Figure 2.17 WAXD profiles for VTMS-crosslinked PP (HMSPP) and pure PP (from An et al., 2008)

2.3.3 Effect of Co-agents

Several studies have shown that the addition of co-agents influences unsaturated monomers grafting on polymers. However, research on the influence of co-agents in grafting of unsaturated silane monomers onto PP has been minimal (Zhou et al., 2009).

Huang et al. (2000) studied the influence of styrene on the gel content of silane-crosslinked PP. The gel content was found to increase rapidly as the styrene amount increased at low styrene to VMMS monomer molar ratios. After adding a certain amount of styrene, the gel percentage reached a plateau, as illustrated in Figure 2.18. The authors attributed this

behaviour to two reasons. First, since styrene is a good solvent for the silane monomer and PP, the solubility of the monomer in the PP melt was improved by the addition of styrene. Second, styrene is highly reactive towards PP macroradicals, which may have resulted in reducing radical termination. As a result, the macroradicals could easily react with the silane monomer, leading to improved grafting and crosslinking.

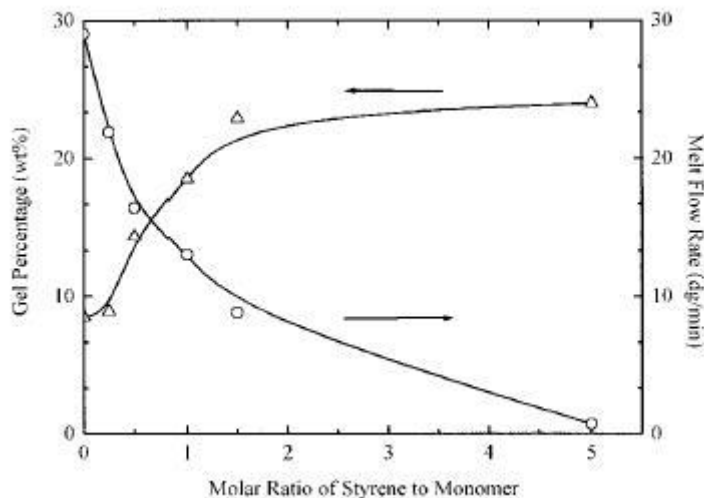


Figure 2.18 Effect of styrene concentration on the gel content of VMMS-crosslinked PP and the MFR of PP-g-VMMS (from Huang et al., 2000)

Zhou et al. (2009) noted that adding styrene caused the grafting degree of VTMS to drop, while adding divinylbenzene (DVB) (Figure 2.19), triallyl isocyanurate (TAIC) (Figure 2.20), and trimethylolpropane triacrylate (TMPTA) (Figure 2.21) improved the degree of grafting by VTMS onto PP. In reviewing monomer reactivity ratios, two conditions were observed to be essential for the co-agent to work. First, the co-agent must be more reactive towards PP macroradicals than the grafting monomer. Second, the reactivities of both the co-agent and the grafting monomer must be close to one another. The grafting of VTMS was inhibited by adding styrene because its reactivity is not very close to that of styrene. The styryl macroradicals tends to react with styrene rather than VTMS. On the other hand, the grafting of VTMS was improved with DVB, possibly due to the presence of a second double bond in DVB, which may increase the number of macroradicals and hence the number of grating points. TIAC and TMPTA are polyfunctional monomers and showed remarkable

improvement in the grafting degree because their reactivities are very close to the reactivity of VTMS.

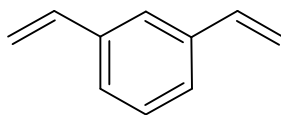


Figure 2.19 Chemical structure of divinylbenzene (DVB)

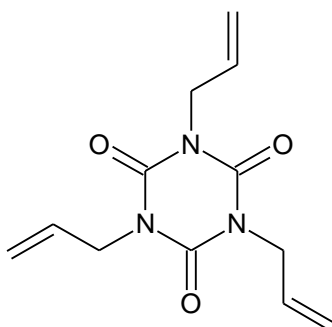


Figure 2.20 Chemical structure of triallyl isocyanurate (TAIC)

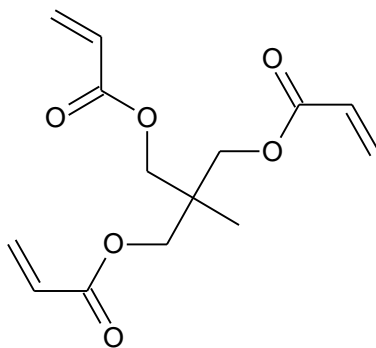


Figure 2.21 Chemical structure of trimethylolpropane triacrylate (TMPTA)

As a result of less grafting, the gel content in VTMS-crosslinked PP decreased with increasing styrene content. On the other hand, the gel content was found to be enhanced when the concentrations of DVB, TAIC, and TMPTA were low. Then, the gel content dropped when additional co-agent was added, as shown in Figure 2.22. With higher concentrations of DVB and TAIC, the side chains in these two co-agents may restrict the required movement of the grafted VTMS for crosslinking, leading to lower gel content.

TMPTA contains highly reactive acrylate groups; consequently, when the concentration is high, VTMS monomers may possibly react with the TMPTA monomer or graft copolymers. This process may increase the VTMS grafting degree but also contributes to the crosslinking of PP (Zhou, 2009).

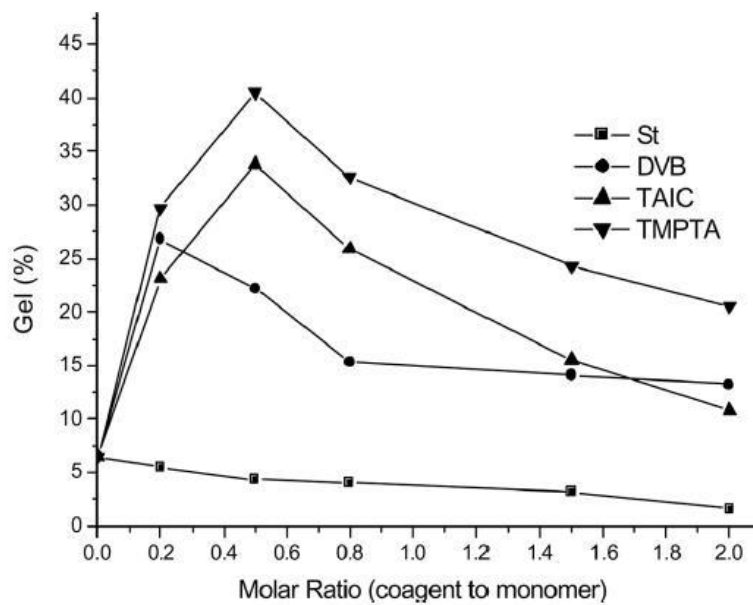


Figure 2.22 Effect of the co-agent concentration on the gel content of coagent-assisted VTMS-crosslinked PP (from Zhou et al., 2009)

The melt flow rate (MFR) of polymers is an indication of the polymers' degradation or crosslinking (Zhou, 2009). Huang et al. (2000) found that the MFR of PP-g-VMMS decreased gradually with increasing styrene content, indicating that PP degradation was reduced during the grafting reaction. A similar trend was observed when adding styrene or DVB to the VTMS-PP grafting system, as shown by Zhou et al. (2009) in Figure 2.23. These two co-agents are highly reactive and could rapidly consume the unstable tertiary radicals, preventing their fragmentation. However, DVB was found to be more effective since it contains more double bonds, causing it to be more reactive. Another reason may be that DVB is able to crosslink PP since it is a polyfunctional monomer. The trend was different with TAIC and TMPTA. The MFR of the grafted PP first decreased and then increased progressively as more co-agent was added. These two co-agents contain high contents of

double bonds. Therefore, increasing their concentrations leaves the system with residues of unconsumed co-agent that greatly increases the MFR (Zhou, 2009).

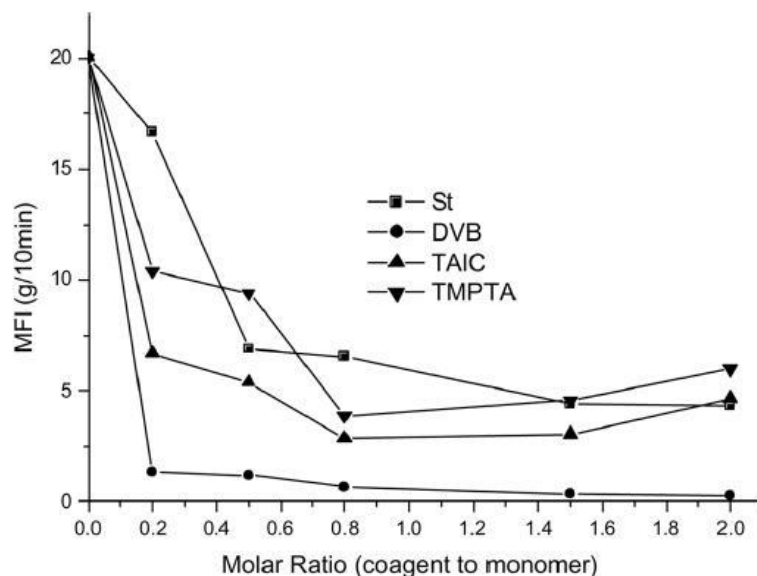


Figure 2.23 Effect of co-agent concentration on the MFR of co-agent-assisted PP-g-VTMS (from Zhou et al., 2009)

The crystallization behaviour of VTMS-crosslinked PP assisted by co-agents was researched by Zhou et al. (2009). The addition of co-agents to the VTMS-PP system results in relatively complicated behaviour since both crosslinking and restricted degradation affect crystallization behaviour and are associated with the incorporation of the co-agents. Moreover, crosslinking PP by VTMS units with co-agents resulted in the formation of γ PP crystals that were not present in the pure PP. The appearance of such crystals was attributed to defects resulting from grafting and crosslinking.

2.3.4 Effect of Peroxides

Huang et al. (2000) studied the influence of the organic peroxide type and concentration on the gel content of VMMS-crosslinked PP and the melt flow rate of PP-g-VMMS. Both dicumyl peroxide (DCP) (Figure 2.24) and benzoyl peroxide (BPO) (Figure 2.6) demonstrated a similar influence on the gel content. The gel content increased rapidly as the concentration increased. However, BPO showed a slightly higher level of gel content

compared to DCP. The trend in the melt flow rate was different. Increasing the concentration of DCP caused a gradual increase in the melt flow of the PP-g-VMMS, indicating that PP degradation increased during the grafting reaction (Figure 2.25). However, increasing the concentration of BPO resulted in decreasing the MFR of the grafted PP, as shown in Figure 2.26, indicating that the grafting reaction was not accompanied by degradation reactions. The authors suggested that this finding may be due to the fact that when using BPO, the termination mostly occurred via combination rather than disproportionation.

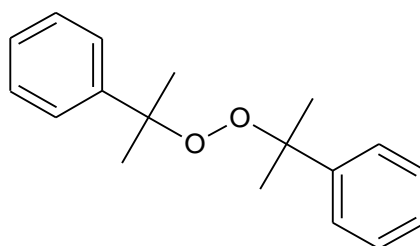


Figure 2.24 Chemical structure of dicumyl peroxide (DCP)

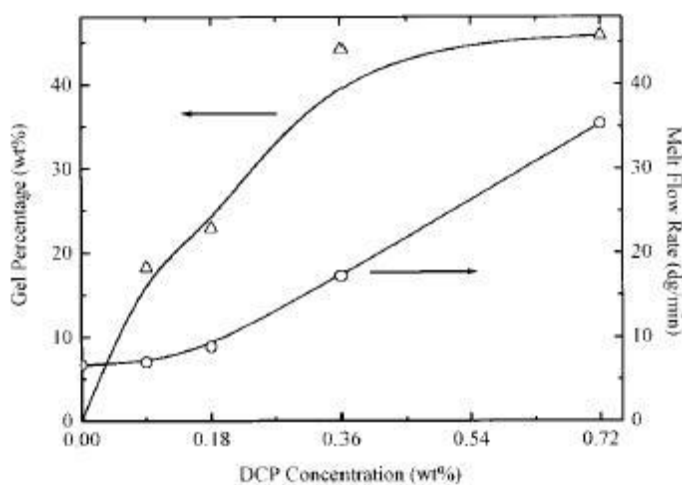


Figure 2.25 Effect of DCP concentration on the gel content of VMMS-crosslinked PP and on the MFR of PP-g-VMMS (from Huang et al., 2000)

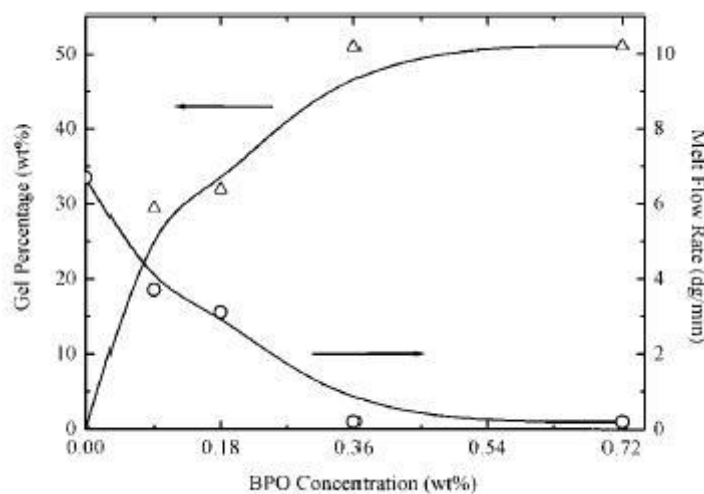


Figure 2.26 Effect of BPO concentration on the gel content of VMMS-crosslinked PP and on the MFR of PP-g-VMMS (from Huang et al., 2000)

Wang et al. (2005) investigated the effect of DCP on the gel percentage of VTMS- and VTES-crosslinked PPs. DCP was found to increase the gel content of the VTMS-crosslinked PP compared to a minor increase in the gel content of the VTES-crosslinked PP (Figure 2.9). This finding may be due to the larger steric hindrance of VTES, which could lead to a lower degree of grafting of the VTES units onto the PP backbone. The degree of grafting is known to be greatly influenced by the peroxide half-life and the reactivity of the radicals that are formed from the peroxide decomposition.

Liu et al. (2000) found that the gel content of VMMS-crosslinked PP increases gradually with increasing DCP concentration until the gel content reaches a value of approximately 55 wt.%. There is no significant increase in gel content as DCP concentration increases further. Moreover, PP degradation was found to increase with the increase in DCP concentration until very high concentrations were reached, as indicated by the equilibrium torque values (Figure 2.27). The authors tested the performance of DCP with VTES and found that unlike VMMS, there was no gel obtained at low DCP concentrations and the degradation was severe, even at these concentrations, confirming the low efficiency of VTES in grafting and crosslinking, as depicted in Figure 2.28.

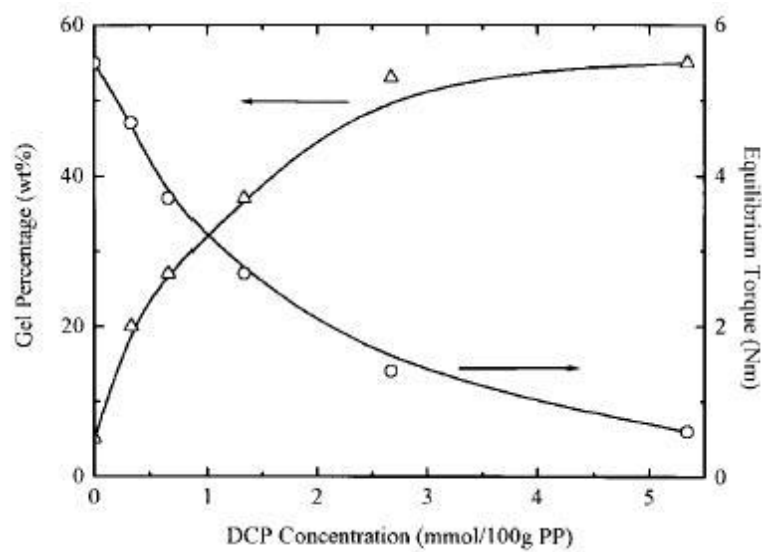


Figure 2.27 Effect of DCP concentration on the gel content of VMMS-crosslinked PP and on the equilibrium torque during the grafting reaction (from Liu et al., 2000)

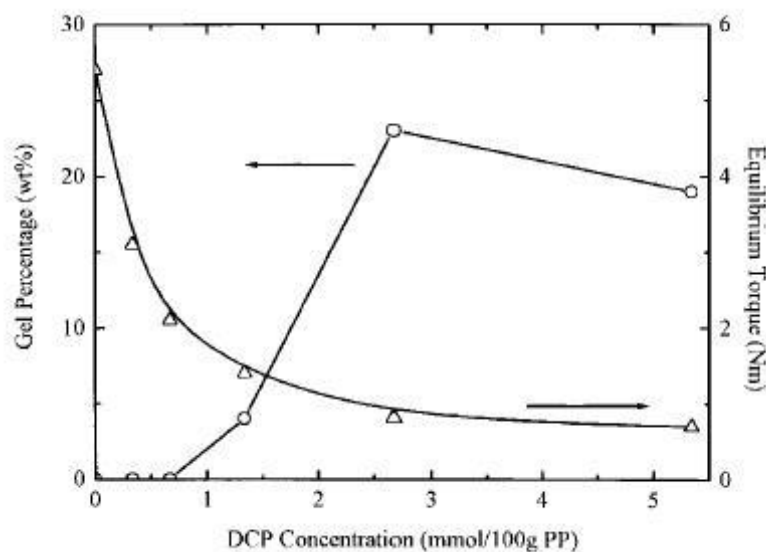


Figure 2.28 Effect of DCP concentration on the gel content of VTES-crosslinked PP and on the equilibrium torque during the grafting reaction (from Liu et al., 2000)

The latter study compared DCP with BPO at the same concentration and half life time. BPO performed better than DCP, as it resulted in higher gel content, as presented in Figure 2.29. Moreover, the equilibrium torque when PP was processed with BPO was high with no

monomer used, indicating minor degradation (Figure 2.30). Unlike DCP, which was added to the batch mixer at 180°C, BPO was added at 130°C, after which the temperature was increased to approximately 170°C in order to compare the performance of both peroxides at the same half life time. The minor degradation, in the case of BPO, was in part a result of the greater stability of PP macroradicals at the low processing temperatures. At low temperatures, PP macroradicals favour termination by combination rather than disproportionation. In addition, the steric hindrance in the case of BPO radicals is smaller compared to DCP radicals, leading also to favoured combinations of PP macroradicals. When the monomer was added with BPO and increased in concentration, the extent of degradation was observed to increase as a result. This increase was attributed to the reaction of BPO with the monomer, reducing the probability of the combination of radicals. In contrast to BPO, the degradation was higher with DCP without adding the monomer. When the monomer was added and its concentration increased, the extent of degradation was reduced, indicating that grafting the monomer onto the macroradicals probably reduced the disproportionation of the macroradicals.

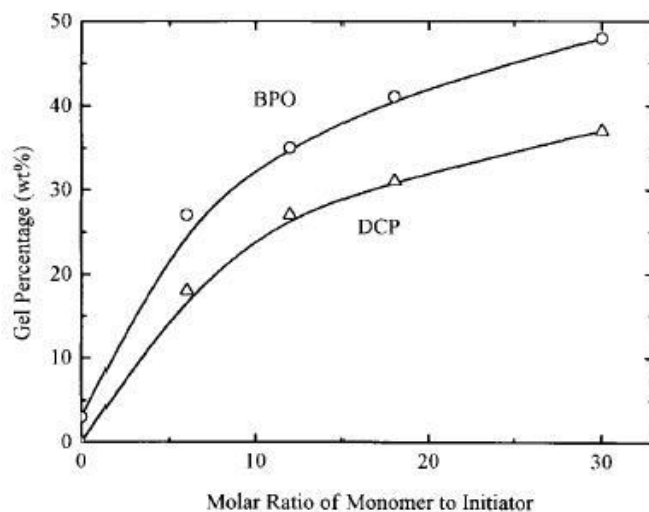


Figure 2.29 Effect of the type of peroxide on the gel content of crosslinked PP (from Liu et al., 2000)

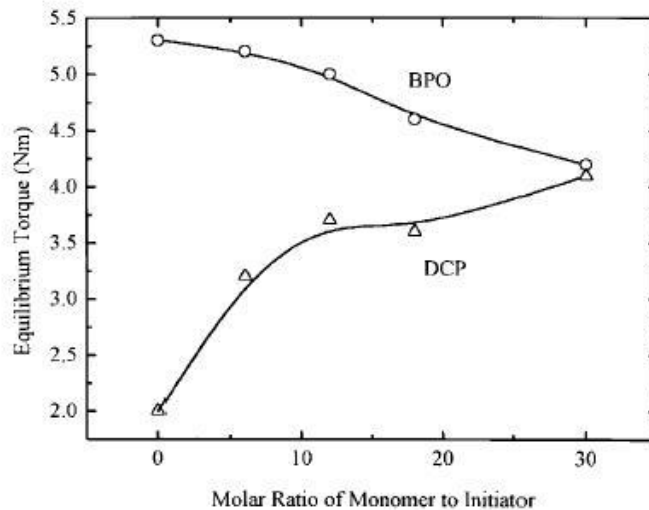


Figure 2.30 Effect of the type of peroxide on the equilibrium torque during the grafting reaction (from Liu et al., 2000)

In terms of grafting efficiency, Nachtigall et al. (1999) found that the grafting efficiency of VTES passed through a maximum as DCP concentration increases (Figure 2.31). For 5 wt.% and 10 wt.% VTES, this maximum occurred between 0.5 wt.% and 0.75 wt.% DCP; it took place at lower ranges for lower VTES concentrations. Those authors suggested that the production of more free radicals by peroxide decomposition probably resulted initially in the formation of more reactive sites in the PP chains, hence increasing the grafting efficiency. The decrease in grafting efficiency at higher DCP concentrations was attributed to the higher probability of side reactions promoted by the presence of more peroxide free radicals.

It is worth noting that VTES was significantly grafted, even when no DCP was present in the system. In this case, macroradicals were generated by high temperature and/or mechanical shear (not by oxidative degradation since carbonyl absorption bands were absent in the FTIR spectra). A low concentration of macroradicals can result in a high degree of grafting since the grafted macroradical abstracts a hydrogen atom from another chain, generating a new radical; the grafting efficiency thus depends only on the concentration of VTES (Nachtigall, 1999).

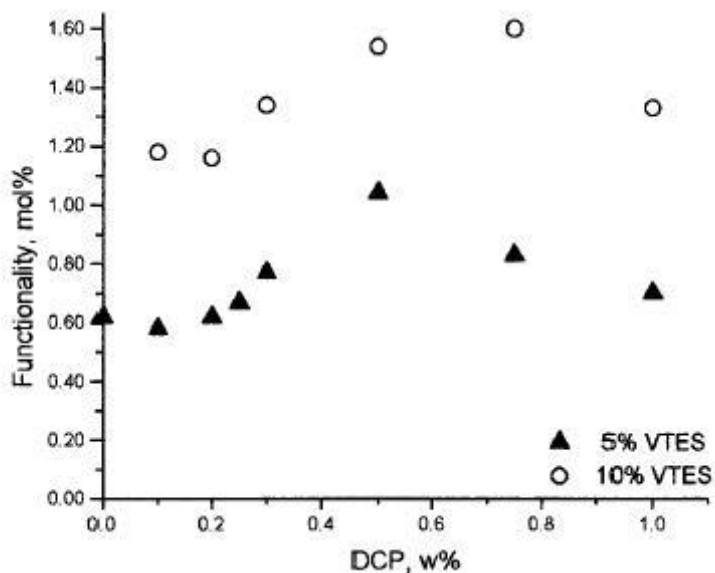


Figure 2.31 Effect of DCP concentration on the grafting degree of VTES in PP-g-VTES for different VTES concentrations (from Nachtigall et al., 1999)

Both the number average molecular weight and the weight average molecular weight were observed to decrease as the concentration of DCP increased at a constant VTES concentration. This degradation was attributed to the chain scission reactions that became severe when the concentration of the free radicals was high.

Hu et al. (2006) vapourized VTMS and grafted it onto PP powder at 150°C. The researchers found that the grafting degree of VTMS increased as the DCP concentration increased. The degree of grafting was expected to reach a plateau with a further increase in DCP concentration. The gel content is directly proportional to the grafting degree. However, the gel content reached a maximum 0.6% DCP and then decreased as DCP concentration increased. The decrease in the gel content has been suggested to be a result of serious degradation occurring at high DCP concentrations. In addition, FTIR spectra revealed that a large number of single VTMS units were grafted at low and high DCP concentrations, while multiple units appeared to exist only at high DCP concentrations, with their amount increasing as DCP concentration increased. This phenomenon led researchers to conclude that VTMS is not easily homopolymerized and its grafts are probably short.

The study exploring the influence of DCP and di-tertbutyl peroxide (TBP) (Figure 2.32) on the gel content of VTMS-crosslinked PP showed that DCP is more effective at producing higher gel content, as shown in Figure 2.33. This result indicates that a higher degree of grafting is achieved when this type of peroxide is used (Wang, 2005).

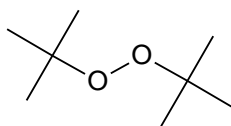


Figure 2.32 Chemical structure of di-tertbutyl peroxide (TBP)

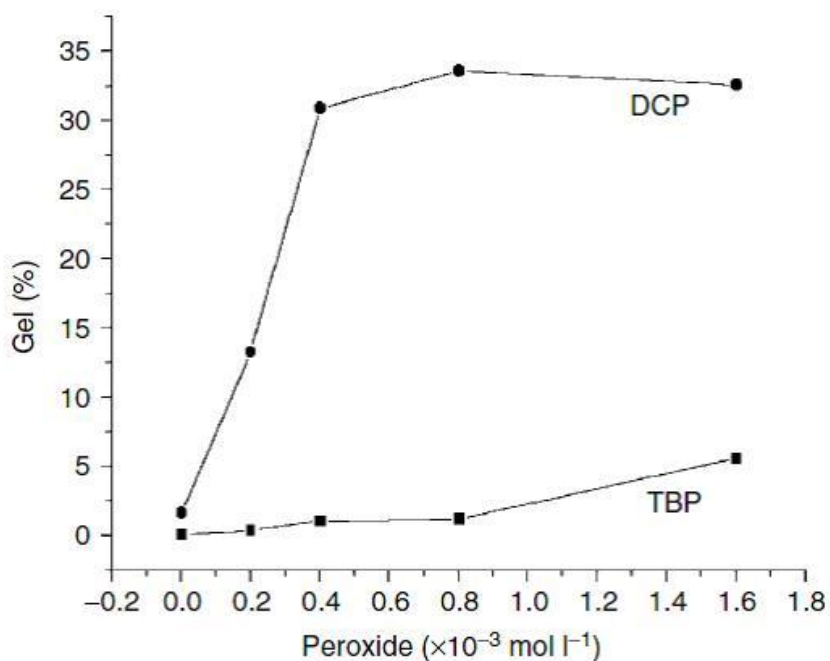


Figure 2.33 Effect of the type of peroxide on the gel content of crosslinked PP (from Wang et al., 2005)

Song et al. (2006) carried out grafting and crosslinking in one step in a twin-screw extruder. The researchers used BPO as the initiator and VMMS as the silane monomer. They noticed that an increase in BPO concentration rapidly increased the gel content and decreased the MFR up to 0.4 wt.%. Beyond this concentration, the trend was the same but at a slower pace.

2.3.5 Effect of Processing Conditions

Huang et al. (2000) studied the influence of processing temperatures (175 to 240°C) on the melt flow rate and the gel content. They conducted the experiment in a twin-screw extruder and showed that the melt flow rate of the PP-g-VMMS increased when the processing temperature was increased. This behaviour indicated that increasing processing temperatures during grafting led to a higher extent of degradation. On the other hand, the gel content of the VMMS-crosslinked PP decreased as the temperature was raised (Figure 2.34). The authors suggested the optimum temperatures to be in the range between 180 and 190°C. Within this range, the desired gel content can be achieved while maintaining desired PP processability.

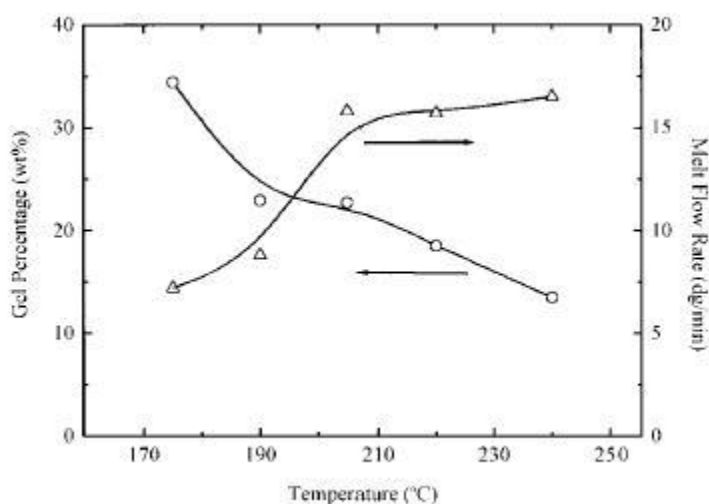


Figure 2.34 Effect of processing temperature on the gel content of crosslinked PP and on the MFR of grafted PP (from Huang et al., 2000)

The authors studied the influence of screw speed (20 to 90 rpm) on the gel content and the melt flow rate. An increase in screw speed in the range between 20 to 60 rpm was shown to positively influence and increase the gel content of VMMS-crosslinked (Figure 2.35). However, beyond this range, the gel content remained constant and stable. At high screw speeds, mixing efficiency improved, and hence, higher gel contents were expected. However, at these high speeds, the residence time was not long enough to completely decompose the peroxide, which is necessary for grafting and crosslinking (Huang, 2000).

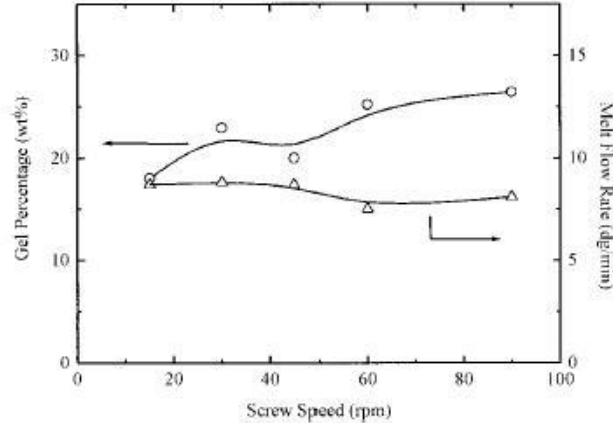


Figure 2.35 Effect of screw speed on the gel content of crosslinked PP and on the MFR of grafted PP (from Huang et al., 2000)

Liu et al. (2000) examined the effect of processing temperature (165 to 220°C) on the equilibrium torque and the gel content in a batch mixer. In agreement with Huang et al. (2000), more degradation, indicated by lower torque values, was observed as the processing temperature increased. However, the gel content passed through a maximum near 180°C, as shown in Figure 2.36. The optimum temperature to achieve a higher gel content and less degradation has been suggested to fall between 170 and 180°C.

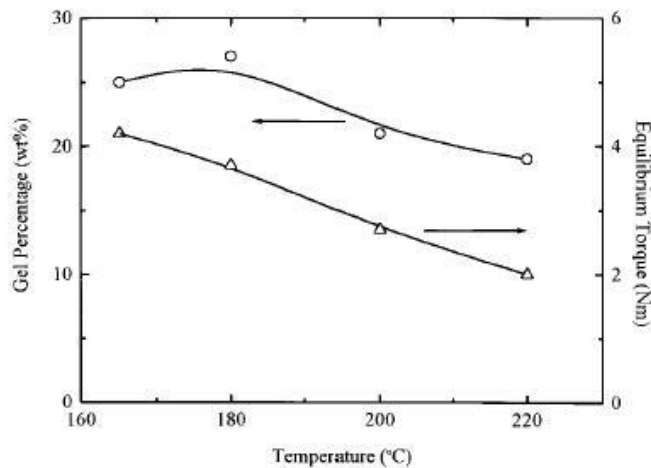


Figure 2.36 Effect of the processing temperature on the gel content of crosslinked PP and on the equilibrium torque during the grafting reaction (from Liu et al., 2000)

The influence of PP initial particle size on the gel content of the VMMS-crosslinked PP and the equilibrium torque was examined by Liu et al. (2000). The highest gel content and the least degradation was found to occur between 190 and 330 μm . The researchers suggested that large particle sizes do not allow sufficient mixing of PP with the additives before processing, leading to less grafting and crosslinking. Although mixing can be uniform with very small particles, the possibility that PP macroradicals react with monomers or terminate with monomer radicals is reduced due to the low localized concentration of radicals. It was suggested that the initial particle size should have a narrow distribution in order to achieve higher amounts of gel in the crosslinked PP.

2.4 Introduction of Long Chain Branching onto PP through Silane

Long chain branches can be introduced onto PP by the use of vinyl silane compounds. The steps involved here are the same as in silane-PP crosslinking mentioned earlier except that crosslinking here is carried out to an extent that is just below the gel point. El Mabrouk et al. (2009) compared this two-step approach with the approach that involves grafting polyfunctional co-agents onto PP in the presence of a peroxide in a single step. Both fragmentation and crosslinking of PP chains occur simultaneously during the course of the co-agent-based method. The long chain branched PP can be produced by the latter method by using relatively low concentrations of the co-agent, which has more than two double bonds, and the peroxide in order to minimize the amount of insoluble gel and the extent of degradation (Wang et al., 1996). The long chain branched PP produced by this single-step method has been found to have a bimodal molecular weight distribution as seen in Figure 2.37 (El Mabrouk, 2009).

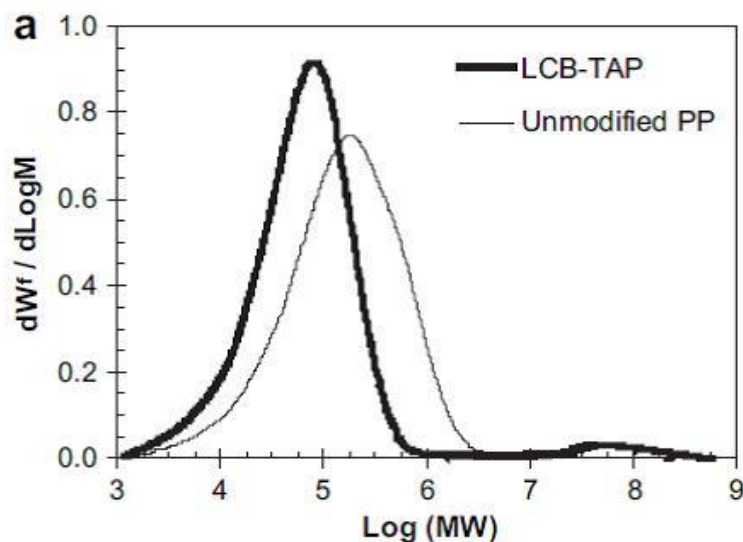


Figure 2.37 GPC data for pure PP and long chain branched PP (LCB-PP) prepared by grafting triallyl phosphate (TAP) in the presence of DCP (from El Mabrouk et al., 2009)

El Mabrouk et al. (2009) showed that long chain branched gel-free PP produced by the silane approach has more uniform molecular weight and branching distributions. The advantage of this approach comes from the separation between the first step that reduces the molecular weight and the second step that increases molecular weight and introduces branches. Those authors grafted 5 wt.% of VTES onto PP powder in the presence of 0.2 wt.% DCP. The molecular weight and dispersity decreased, and 0.7 wt.% of VTES was grafted as a result of the grafting reaction. Then, treating the grafted product with moisture in the presence of 5 μL of dibutyltin dilaurate (Figure 2.38), which is a crosslinking catalyst, created a long chain branched gel-free PP with increased molecular weight and dispersity. It can be seen from Figure 2.3 that the molecular weight of a significant number of chains was raised after the moisture treatment step. However, the majority of chains were not significantly affected. This non-uniformity was attributed to the fact that silane grafts were not distributed uniformly. It was suggested that some chains were grafted with multiple silanes while others remained ungrafted due to what is called intramolecular hydrogen transfer which is followed by silane addition to the resulting radical. Nevertheless, the silane

approach can provide much more uniform branching distributions than the co-agent based approach.

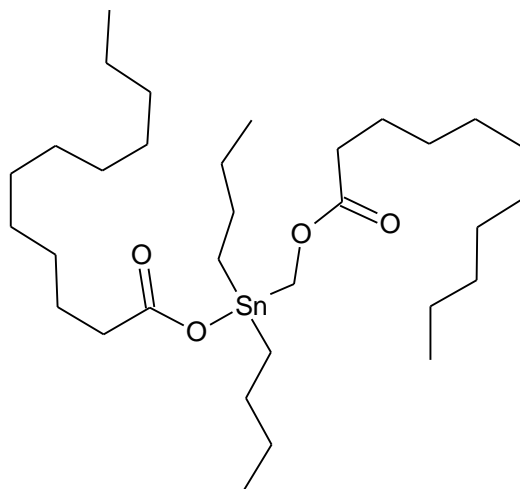


Figure 2.38 Chemical structure of dibutyltin dilaurate (DBTDL)

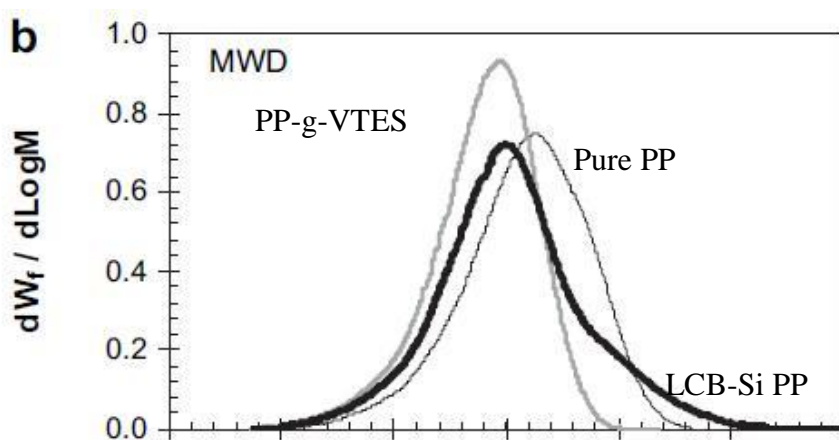


Figure 2.39 GPC data for pure PP, PP-g-VTES and long chain branched PP prepared by grafting VTES (LCB-Si PP) in the presence of DCP (from El Mabrouk et al., 2009)

2.5 Use of Polypropylene-g-silane as a Coupling Agent in Natural-fiber/Polypropylene Composites

Composite materials are produced by combining different materials with significantly different properties to achieve useful properties that could not be attained with the separate materials. Natural fiber/thermoplastic composites have been extensively studied and have received significant attention in recent years (Arbelaiz, 2005; Nachtigall, 2007). Their markets are growing currently in major industrial sectors, such as the construction and automotive industry (Rachini, 2012). Their applications involve sidings, window and door frames, decks, and use in various automotive parts, such as door panels, package rays, dashboards, and the like (Khanam, 2014).

Natural fibers are biodegradable and derived from natural resources, such as wood, cotton, vegetable, and cereal straw (Arbelaiz, 2005; Xie, 2010). The use of natural fibers in thermoplastic composites offers numerous advantages when compared with inorganic fillers, such as carbon fibers and glass fibers. They are abundant and widely available at low cost. Compared with inorganic fillers, they pose fewer health hazards and result in less machine wear since they are non-abrasive. Their flexural and tensile moduli are fairly high, and the density of the composites containing natural fiber is significantly less than those containing synthetic fibers, such as glass fibers. Therefore, incorporating them into polymer matrices creates composites with a high specific strength and stiffness. The utilization of natural fibers in composite production reduces the consumption of oil-based materials. Due to their biodegradability and renewability, they can be disposed of with less of an environmental impact, unlike most synthetic fibers (Nachtigall, 2007; Xie, 2010). Moreover, natural fiber/thermoplastic composites require less energy and cost less to be properly disposed of and treated at the end of their life cycle (Rachini, 2012).

However, two main drawbacks are associated with natural fibers. First, they are susceptible to high water uptake due to their hydrophilic character, which, in turn, swells the fibers (Arbelaiz, 2005) and has a weakening effect on the composite materials containing these fibers. Water absorption may weaken the resulting composite dimensional stability and deteriorate the interfacial adhesion between the fiber and the polymer (Xie, 2010). Second,

natural fibers are sensitive to heat treatment and can be degraded during processing or during the service time (Rachini, 2012). The degradation of the natural fiber components, such as hemicellulose and lignin, during processing may change the structure of the fiber and create microvoids across the interfacial region by generating volatile compounds, thus weakening the mechanical properties of the composite (Nachtigall, 2007).

In addition, thermoplastics, such as polypropylene and polyethylene, are hydrophobic; therefore, the interaction between the hydrophilic fiber and the polymer at the surface is weak due to low compatibility. The lack of compatibility leads to poor dispersion of the fiber and fiber agglomeration in the polymer melt due to the non-polar nature of the polymer and the possible formation of hydrogen bonds between the fibers. This incompatibility also leads to poor adhesion between the two materials due to the poor wetting of fibers by the hydrophilic polymer (Arbelaz, 2005). As a result, the stress is not sufficiently transferred from the polymer matrix to the fibers (Xie, 2010). It is thus essential to improve the compatibility between these two materials in order to obtain durable composites with better mechanical properties (Rachini, 2012).

Several methods have been reported in the literature for improving adhesion and bonding between natural fibers and polyolefin matrices and to minimize the adverse effects of water uptake and low degradation temperatures of the fiber on the mechanical properties of the composite. Among these methods is fiber surface treatment by coupling agents, such as alkoxy silanes. When treating the surface of the fiber with an alkoxy silane, the alkoxy groups (-Si-O-CH₃) are hydrolyzed by water, forming silanol groups (-Si-OH) that react with the cellulose hydroxyl groups in the fiber, thus forming covalent bonds (-Si-O-C-) between the fiber and the silane coupling agent. Such reactions reduce the water absorption by consuming the hydroxyl groups on the fiber surface and minimize the possibility of water interacting with the fiber surface through hydrogen bonds (Rachini, 2012). However, the interaction between the organic part of the silane and the non-polar matrix, on the other hand, is often unsatisfactory since the silane monomers, if not grafted onto the polymer chains by covalent bonds, cannot effectively couple with the polymer chains by means of mechanical intermolecular entanglement (Paunikallio, 2008). Improvement in the mechanical properties

of the resulting composite is limited with such physical compatibility between the silane-treated fiber and the thermoplastic matrix (Xie, 2010). Marginal improvement is mainly caused by improved compatibility, which leads to uniform distribution of the fiber into the polymer matrix. However, note that reactions may still occur when using certain types of alkoxy silane, such as amino silanes, in which the amino groups can react with oxidation products produced on the matrix at high processing temperatures (Nachtigall, 2007).

Covalent bonds are required between the organo-functionalities of the silane and the polymer matrix in order to significantly improve the interfacial adhesion between the fiber and matrix. Consequently, another method has been suggested to create chemical bonding between the two materials. It involves grafting alkoxy silanes with double bonds onto the thermoplastic matrix using initiators. One approach in this method involves the preparation of the silane-grafted polymer in a separate step, which can then be used as a coupling agent in the composite preparation step. Another approach is implemented by combining the peroxide-mediated grafting with the composite compounding in one step (Xie, 2010). It should be noted that in the latter approach, the peroxide radicals could create cellulose radicals, thus grafting them onto PP chains (Arbelaiz, 2005).

Arbelaiz et al. (2005) modified flax fiber with VTMS and observed that mechanical properties of the flax fiber bundle/PP composite were not improved significantly compared to the non-coupled composite. In addition, the mechanical performance of these treated composites was lower than that of the composites coupled with PP-g-MAN. However, grafting VTMS onto PP in the presence of peroxide along with the composite compounding resulted in superior mechanical properties when compared with the fiber surface treatment approach. In addition, mechanical properties were improved over those present when using PP-g-MAN and nearly similar to those obtained with an unmodified glass fiber/PP composite.

Rachini et al. (2012) carried out the grafting of VTMS and the preparation of hemp fibers/PP composites using the same processing steps in the presence of peroxide. The tensile strength and the impact strength of the coupled composites were improved considerably, while the Young's modulus and degradation temperatures of PP and hemp fibers in the

composites remained unchanged. The authors attributed the improvement in tensile strength and impact strength to the good adhesion, as revealed by SEM results, which indicated improved compatibility between the hemp fibers and the PP matrix. However, the use of VTMS increased the water take-up of the composites. It was suggested that this increase is due to the fact that the covalent bond (-Si-O-C-) formed between the fibers and VTMS is not stable towards hydrolysis in a humid environment, and thus can be hydrolyzed forming silanol groups (-Si-OH), increasing the water take-up capacity of the composites as a result. In an attempt to avoid this unfavourable hydrolysis reaction, the authors repeated the same procedures, except that the surface of the fibers was treated with 3-(triethoxysilyl)propylsuccinic anhydride (SiAn) in addition to grafting PP with VTMS. A great reduction in water absorption was observed compared to the non-coupled and the VTMS-coupled composites. It was suggested that the anhydride groups in SiAn reacted with the hydroxyl groups on the fiber surface at high temperatures, forming ester bonds, which are less hydrolysable compared to (-Si-O-C-) bonds. In addition, the water resistance could also be improved by the formation of non-hydrolysable siloxane bonds (-Si-O-Si-) as a result of the hydrolysis and condensation reactions between VTMS that is grafted on PP and SiAn that is bonded to the fiber. The resulting composites were also more thermally stable. The bonding between the fiber and SiAn and the possible formation of very thermally stable (-Si-O-Si-) bonds between the two silanes were suggested to be responsible for the significant improvement in the fibers' thermal stability. The higher degradation temperature of PP was attributed to VTMS grafting and the possible crosslinking between PP chains induced by the peroxide. The tensile strength, impact strength, and Young's modulus were also higher in this case compared to the other two types of composites due to the influence of the chemical bonds formed in this system, leading to better adhesion and dispersion.

Paunikallio, Suvanto, and Pakkanen (2008) grafted PP with VMMS in a separate step and used it as a coupling agent in viscose fiber/polypropylene composites. This coupling agent was found to improve the mechanical properties of the composites significantly. For example, the increase in tensile strength was 59% percent compared with the non-coupled composites. For the sake of comparison, the authors treated the surface of the viscose fibers

with VMMS and observed that the improvement in mechanical properties in this case was noticeably less than that obtained with PP-g-VMMS.

The coupling effect of PP-g-VTES was compared with that of PP-g-MAN by Nachtigall et al. (2007). In this study, the preparation steps of both coupling agents were separated from the composite-making step. Due to better compatibility and interfacial adhesion between the wood flours and PP matrix, tensile strength obtained with PP-g-VTES was higher than that obtained with PP-g-MAN. Water absorption was substantially lower with PP-g-VTES due to the reduction in the number of hydroxyl groups available for hydrogen bonding with water. Both coupling agents improved the thermal stability of the PP matrix, while the presence of the wood flours without coupling agents reduced the PP thermal stability.

Chapter 3

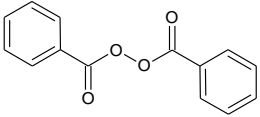
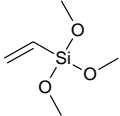
Materials and Methods

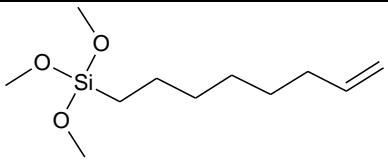
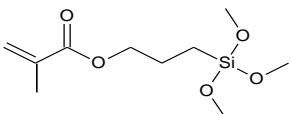
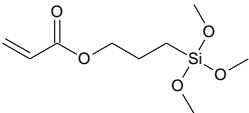
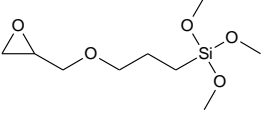
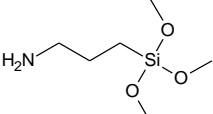
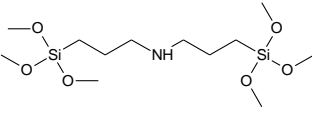
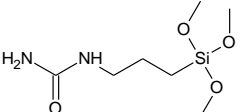
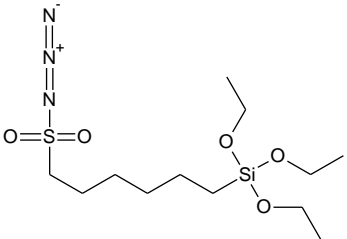
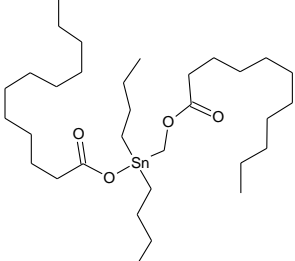
3.1 Materials

The resin used throughout this study was a polypropylene homopolymer (PP) kindly provided by Saudi Basic Industries Corporation (SABIC). It was in white pellet form with a melt flow index of 3 g/10min (measured at 230°C and 2.16 kg load, ASTM D1238).

Nine different liquid organo-functional silanes were obtained from Gelest, Inc. and used as received. They differ only in the organic functional group type except for 6-azidosulfonylhexyltriethoxysilane where it differs also in the alkoxy group which is ethoxy instead of methoxy. The organo-functional groups are azido, vinyl, acryloxy, methacryloxy, epoxy, amino, and ureido. In addition, one peroxide type was obtained from Sigma Aldrich and used as received throughout this work. It was dibenzoyl peroxide in powder form. The moisture cure catalyst used was dibutyltin dilaurate from Alfa Caesar and it was used without purification. Chemical names, abbreviations, and structures for the silanes and the peroxide are shown in Table 1.

Table 3.1 Organo-functional silanes and peroxide used in this study

Chemical name	Chemical structure	Abbreviation
Dibenzoylperoxide		BPO
Vinyltrimethoxysilane		VTMS

7-octenyltrimethoxysilane		ONTMS
3-methacryloxypropyltrimethoxysilane		VMMS
(3-acryloxypropyl)trimethoxysilane		APTMS
(3-glycidoxypropyl)trimethoxysilane		GPTMS
3-aminopropyltrimethoxysilane		AMPTMS
Bis(3-trimethoxysilylpropyl)amine		BTMSPA
Ureidopropyltrimethoxysilane		UPTMS
6-Azidosulfonylhexyltriethoxysilane		Azido-silane
Dibutyltin dilaurate		DBTDL

The wood fiber used in the preparation of the wood-fiber/PP composites was obtained from Sonae Industria with a product name of WoodForce. It was received in the form of wood fiber dice (square 5x5mm, 3.5mm thick) with 7% average moisture content. The dices were disentangled before use and their moisture content was reduced to below 4 %. The drying was carried out in an oven under vacuum and 60⁰C for 6 hours. Drying fibers before composite preparation negatively influences mechanical properties of the composite since water evaporation may create voids in the polymer matrix. In addition, water present on the fiber surface can increase separation in the interface between the fibers and the matrix. (Bledzki, 1999)

3.2 Sample Preparations

3.2.1 Grinding

PP pellets were ground to reduce the particle size to allow even dispersion of other ingredients. The grinding process took place in a Retsch Ultra Centrifugal Mill ZM200 (Figure 3.1). Particle size reduction in this grinding machine is achieved between a fixed ring sieve and a rotor in two steps by impact and shearing forces. First, the material is fed through a hopper onto the rotor that it is rotating at a high speed. Once the material hits the center of the rotor it is thrown outward with high energy, created by centrifugal acceleration, and crushed by impact force on the rotor sharp teeth. Second, the material is ground between the ring sieve and the rotor creating finer particles. The ground material finally accumulates in a collecting cassette enclosing the grinding chamber.

The size of the PP pellets as received was in the range between 1.7 mm and 4.75 mm. Before grinding, the pellets were immersed in liquid nitrogen for 5 minutes to lower the temperature and consequently to prevent melting during grinding as well as to improve the breakage behavior and embrittle the pellets as well as to prevent melting during grinding. Prior cooling of the pellets in the freezer for 24 hours gave good results but the feed rate had to be reduced compared to liquid nitrogen cooling. The grinding of the pellets was performed using a 1 mm sieve at 6,000 rpm. Liquid nitrogen was added intermittently to the grinding chamber during the grinding operation. The particle size was reduced to less than 500 µm for

80% of the material and between 1 mm and 500 μm for the rest of the material. The PP powder produced was denoted as pure PP in this study.

For the wood-fiber/PP composites preparation, PP-g-APTMS and PP-g-Azidosilane were also ground according to the above procedure. The purpose was to better mix these polymeric coupling agents with the pure PP and wood fibers before compounding.



Figure 3.1 Retsch Ultra Centrifugal Mill ZM200 (Retsch GmbH 2012)

3.2.2 Preparation of PP-g-silane Samples

The grafting reaction between the pure PP and the silanes was performed in a co-rotating twin-screw mini-extruder Haake Minilab II with intermeshing screws (Thermo Electron Corporation) (Figure 3.2 & 3.3). The Haake MiniLab II was designed to compound and extrude samples with a small volume (7 cm^3). It is equipped with a backflow channel (depth = 1.5 mm; width = 10 mm) and a bypass valve which allow to extrude the sample in a

circulation mode and to easily control the residence time for the reaction mixture. In addition, two pressure transducers are built in the backflow channel; one is located at the capillary entrance and one at the exit. The distance between the two transducers is 64 mm.

The reaction is monitored by reading the pressure values in the back flow channel, and the torque of the drive motor. The pressure values can also be used to measure the relative melt viscosity up to 350°C since the back flow channel acts as a rheological slit capillary die. When the time for the circulation mode is over, the bypass valve is opened by air pressure to extrude the material as a strand through a small die. The extruder is said to be in a flush mode after opening the bypass valve.

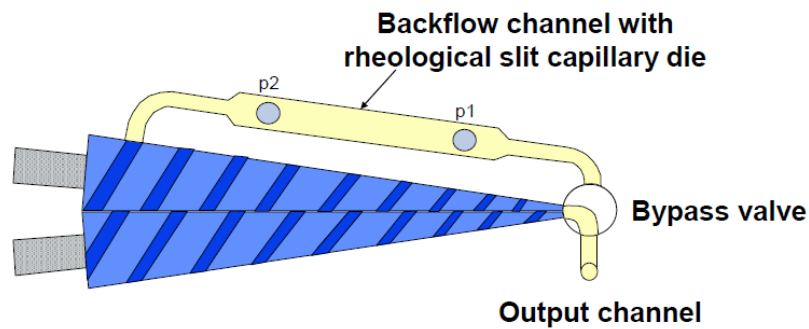


Figure 3.2 Parts in Haake Minilab extruder (Thermo Electron Corporation)



Figure 3.3 The view inside Haake Minilab extruder (Thermo Electron Corporation)

The mixture of the pure PP powder, peroxide (0.20 wt.%), and the organo-functional silane (5 wt.%) was manually mixed in a small beaker to make it homogeneous before the reactive extrusion. The mixture (6.5 grams) was then fed continuously and evenly (in 1 minute and 30 seconds) into the extrusion chamber through a funnel. The reaction time (5 minutes) was started after the complete loading of the material by one minute. The mini-extruder was set at 180°C under nitrogen atmosphere and its screw speed was set at 60 rpm. It should be noted that nitrogen was not introduced in the case of Azido-silane, AMPTMS, BTMSPA, UPTMS, and GPTMS. It should be noted also that no peroxide was used in the preparation of PP-g-Azidosilane. The PP-g-silane samples prepared according to this procedure were used for chemical analyses by FT-IR.

3.2.3 Preparation of Silane-crosslinked PP Samples

The PP-g-silane samples used in the crosslinking reactions were prepared following the same grafting procedure mentioned above except that two drops of the moisture cure catalyst were added to the mixture before the grafting reaction. The PP-g-silane samples were then put in small conical flasks filled with demineralized water. To perform the crosslinking reactions, the flasks were immersed in a hot water bath at 90°C for 18 hours. At the end, the silane-crosslinked PP samples were dried at 60°C under vacuum for 24 hours.

3.2.4 Preparation of Wood-fiber/PP Composites

The wood-fiber/PP composites had five different formulations prepared to study the influence of the coupling agent PP-g-APTMS concentrations on the mechanical performance of the composites. The grafting procedure mentioned in Section 3.2.2 was followed to prepare PP-g-APTMS here except that the concentration of the peroxide in the reaction mixture was 0.10 wt.% instead of 0.20 wt.% and no moisture cure catalyst was added. In addition the above five formulations, one more formulation was prepared using PP-g-Azidosilane to compare its performance with PP-g-APTMS. PP-g-Azidosilane used here was prepared according the grafting procedure mentioned in Section 3.2.2 but with no moisture cure catalyst.

The wood fibers were first blended by hand with the pure PP powder and PP-g-APTMS or PP-g-Azidosilane. The blend was then fed into the mini-extruder and conveyed by the screws. The processing temperature was set at 185⁰C and the screw speed was set at 30 rpm. Continuous melting and mixing took place while the mixture was flowing in between the intermeshing screws. The extruder was completely operated in the flush mode where the material was flowing out through the die in the form of a strand. These strand was then air-cooled and cut to smaller pieces with an average size of 1.0 cm in length.

Those small pieces were then injection molded using a lab-scale bench top injection molding apparatus (Ray-Ran). The temperature in the barrel was set at 200⁰C while the mold temperature was set at 120⁰C. The applied pressure was maintained at 7 bar and the time for injection period was 15 seconds. Specimens with two different geometric were prepared. Dumbbell-shaped specimens were used for the tensile tests (ASTM D1708) while plain rectangular bars were used for the impact strength and flexural strength tests (ASTM D256 and ASTM D790).

The injection molded specimens were annealed according to the following procedure. They were put into an oven and annealed at 120⁰C for 15 minutes. Then they were cooled down at a rate of 10⁰C/min. Finally before characterization, the annealed specimens were put into a conditioning chamber for 48 hours where the temperature was set at 23 ± 1⁰C and the humidity was kept at 50 ± 5 %.

3.3 Characterization

3.3.1 Fourier Transform Infrared Spectroscopy (FT-IR) Analysis

In infrared spectroscopy, a sample is exposed to infrared radiation (IR). Molecules in the sample absorb specific radiation frequencies and some of the radiation is transmitted (not absorbed) through the sample. The absorbed frequencies depend on the functional groups present in the molecules within the sample. They also depend on the symmetry of each molecule. Only specific radiation frequencies are absorbed because bonds within a molecule

can only absorb infrared radiation when the radiation has specific energy to interact with the vibration energy of the bond.

The generated IR spectrum presents the transmittance for each wavenumber. In the spectrum, a decrease in detected signals indicate the absorbed frequencies. No two chemical compounds give the same IR spectrum because each material has its unique combination of atoms. Therefore, FT-IR can be used to identify unknown materials. The concentration can also be identified using the size of the peaks, thickness of the sample, and the molar absorptivity.

Fractionation Procedure

The PP-g-silane samples were purified by fractionation with solvent before the FT-IR analysis to remove nonreacted silane and possible polymerized silane. Each sample was first put into a flask containing 200 ml of xylene. The temperature was raised to 140°C using a hot plate to dissolve the sample. The evaporated xylene was recovered using a condenser attached to the top of the flask. The extraction (fractionation) under stirring lasted 2 hours. Longer extraction times did not have a significant effect on the FT-IR results. The purified sample was then precipitated in 800 ml of acetone at room temperature for 18 hours. The precipitation in the case of PP-g-BTMSPA was carried out with ethanol. The precipitated material was then collected by vacuum filtration where the mixture of solid and liquid was allowed to flow through a filter paper in a Buchner funnel. The collected material was then dried under vacuum at 60°C for 24 hours.

Preparation of Films

A Carver Inc. hydraulic press was used to prepare thin films of the purified and dried PP-g-silane. Two temporary smooth plates were used to protect the main heated plates of the press. The samples were placed between two overhead vinyl transparencies which in turn were put between the temporary plates. By doing that the melt was kept clean and the film was detached easily from the plates after the experiment. The samples were heated at 190°C for 2 minutes and then pressed to a pressure of 20,000 pounds at 190°C for an additional 2 minutes. The thin films were finally cooled at room temperature.

FT-IR Analysis

A Bruker Optics Tensor 27 FT-IR spectrometer was used to record the FT-IR spectra of the PP-g-silane samples. The infrared spectra were used to verify the occurrence of the grafting performed in the extruder and to compare the grafting efficiencies of the silanes onto PP backbone. Each thin film of PP-g-silane was introduced into the FT-IR cell and characterized at 4 cm⁻¹ resolution. Two spectrum ranges were selected for this research's scope. The first range was in the wavenumbers from 600 to 2000 cm⁻¹ and each thin film was scanned 64 times within this range. The second range was scanned 1,024 times within the wavenumbers from 1550 to 1850 cm⁻¹ and used for certain silanes, namely, AMPTMS, UPTMS, BTMSPA, and GPTMS.

3.3.2 Gel Content Determination

The crosslinking ability of the PP-g-silane samples was compared by determining the percentage of gel formed after the crosslinking reactions performed in the hot water bath. This test was also used to confirm FT-IR results. About 1.0 g of each silane-crosslinked sample was wrapped in a 120-mesh steel cloth and placed inside a flask filled with 200 ml of xylene. The flask was heated to 140⁰C on a hot plate to extract the soluble material from the material inside the mesh with the aid of refluxing xylene for 2 hours. The evaporated xylene was recovered using a condenser attached to the top of the flask. At the end of the extraction, the insoluble material (gel) inside the cloth was dried at 60⁰C under vacuum for 24 hours. The gel content of the samples was calculated using the following formula:

$$Gel\ Content\ (wt\%) = \frac{Gel\ weight}{Sample\ initial\ weight} \times 100\%$$

3.3.3 Differential Scanning Calorimetry (DSC)

In the DSC used here, two pans sit on top of a thermoelectric disk. The pan where the sample is encapsulated is called the sample pan while the other pan is empty and called the reference pan. Heat is supplied by a furnace that surrounds the thermoelectric disk which in turn transfers heat to the two pans. Area thermocouples are used to measure the heat flow to

the pans. When the experiment starts, the two pans are heated at a specific heating rate (10⁰C per minute) which is fixed for both pans to keep them at the same temperature throughout the entire experiment. Therefore, heat flow to the pans is different because the sample pan contains extra material. The area thermocouples measure the change in heat input (heat flow) between the sample pan and the reference pan due to thermal energy changes. Thermal transitions occurring during the experiment are marked by release or absorption of energy by the sample.

The TA Instruments DSC Q2000 was used to obtain crystallization temperatures of the silane-crosslinked samples as well as the soluble materials left after gel extraction. The soluble materials were collected by precipitation in 800 ml of acetone at room temperature. The precipitation in the case of BTMSPA-crosslinked PP was carried out with ethanol. The precipitated materials were collected by vacuum filtration using a filter paper and a Buchner funnel. The collected soluble materials were then dried under vacuum at 60⁰C for 24 hours.

For each sample, approximately 5-7 mg was encapsulated in a hermetically sealed pan and loaded automatically. The sample was first heated at a rate of 10⁰C/min from 35⁰C to 200⁰C and maintained for 5 minutes at 200⁰C. This heating step was performed to erase the sample thermal history. Then, the sample was cooled at the same rate to 35⁰C. Finally, it was heated further at the same rate of 10⁰C/min. to 200⁰C. All DSC analyses were performed under 50 ml/min. of nitrogen purge.

3.3.4 Melt Flow Index (MFI)

The test was carried out using a Dynisco D4001DE MFI indexer. The melt flow tester device comprises four main components:

1. A capillary tube.
2. A heated barrel surrounding the capillary tube.
3. A die located at the end of the capillary tube.
4. A piston attached to a weight used to force the melted material in the capillary tube to flow through the die.

The melt flow index (MFI) was determined for selected crosslinked samples with low gel contents: APTMS-crosslinked PP (prepared with lower peroxide concentration, 0.020 wt.%) and ONTMS-crosslinked PP. It was also determined for the pure PP and PP reacted with two levels of peroxide (0.20 wt.% and 0.020 wt.%).

The test was performed according to ASTM D1238 (method A). For each sample, three independent MFI runs were carried out. Seven grams in every run was loaded inside the MFI apparatus capillary which was at 230°C. After loading the entire sample, a weight of 2.16 kg was placed on top of the capillary. The material was allowed to melt and stay inside the capillary for 360 seconds. After the melt time was over, the extrudate running out of the die was collected over a fixed period of time. The collected extrudate was then weighed and the flow rate was converted to grams that would have run out of the die over 10 minutes. The result was reported in g/10 min.

3.3.5 Oscillatory Shear Rheology Experiments

Oscillatory shear rheology experiments were carried out on the same samples selected for the MFI test except for the PP reacted with lower peroxide concentration. The rheometer used was a parallel plate rheometer (TA Instruments AR 2000). The test involves placing the sample between two parallel circular plates (diameter = 25 mm) surrounded by a heated chamber. The upper plate is rotated by a rotor while the lower plate remains stationary. During the test, the rheometer applies controlled sinusoidal oscillation on the sample and measures stress, strain, frequency, and phase angle. Using the measured variables, many viscoelastic properties can be determined. Examples of these properties are:

$$G'(\text{storage modulus}) = \frac{\text{stress}}{\text{strain}} \times \cos(\delta)$$

$$G''(\text{loss modulus}) = \frac{\text{stress}}{\text{strain}} \times \sin(\delta)$$

$$G^*(\text{complex modulus}) = \frac{\text{stress}}{\text{strain}}$$

$$\eta^*(\text{complex viscosity}) = \sqrt{(\eta' + \eta'')^2} = \frac{G^*}{\text{frequency}}$$

$$\tan(\delta) = \frac{G''}{G'}$$

where:

δ is the phase angle.

$$\eta'(\text{in phase viscosity}) = \frac{G'}{\omega}$$

$$\eta''(\text{out of phase viscosity}) = \frac{G''}{\omega}$$

All experiments were carried out at 180°C and the gap was fixed at 1 mm between the two plates. Four samples in the disc form (diameter = 25 mm; thickness = 1 mm) were prepared using the hot press at 190°C and 20,000 pounds. In each run, the disc was placed between the two plates after calibrating the rheometer for the inertia and the gap. The normal force value increased dramatically when the upper plate touched the disc and started to decrease when the temperature approached 162°C which is the melting point of the sample.

Before running the oscillatory frequency sweep, a strain sweep was recorded in order to verify the region of linear viscoelasticity of each sample. In the strain sweep, the temperature and frequency were kept constant and successive measurements were taken at particular step increases in strain. The strain sweep experiment was performed for each sample at 180°C and revealed a linear viscoelastic region.

The oscillatory frequency sweep followed the strain sweep. During the frequency sweep, successive measurements were taken at selected frequencies in rad/sec. while keeping the strain and temperature constant. The selected strain was within the linear viscoelastic region for each sample and the frequency sweep was recorded at 180°C. Viscoelastic properties such as the complex viscosity (η^*), the storage modulus (G'), the loss modulus (G''), and the phase shift angle (δ) were determined by the frequency sweep. The imposed frequency covered a

range from 0.01 to 100 rad/sec. As a result, the time it took to complete the test for each sample was approximately 2 hours. The experiments were carried out under constant nitrogen flow (3.5 l/min.) to prevent any possible sample degradation.

3.3.6 Mechanical Properties

3.3.6.1 Tensile Properties

Tensile tests were performed according to ASTM D1708 using Q Series Mechanical Test Machine (Test Resources Inc.) to obtain tensile strength and modulus data for the pure PP and the wood-fiber/PP composites. A preconditioned dumbbell-shaped bar was clamped in the testing machine between two grips. A distance of 22 ± 0.5 mm was fixed between the two grips after clamping the bar. The rectangular portion in the middle of the bar was then exposed to a tensile force at a rate of 1.33 mm/min. Six bars were tested for each sample and the obtained results were averaged and reported with the standard deviation. The machine measured the applied force and the elongation of the rectangular portion in the middle of the bar. Using these measurements, the tensile strength, tensile modulus, and elongation at break were calculated using the following formulas:

$$\text{Tensile strength} = \frac{\textit{maximum force}}{\textit{unit cross - sectional area}}$$

$$\text{Tensile modulus} = \frac{\textit{stress}}{\textit{strain}} = \frac{(\textit{maximum force})/(\textit{unit cross - sectional area})}{(\textit{change in length})/(\textit{original length})}$$

$$\text{Elongation at Break(\%)} = \frac{\textit{Final gauge length} - \textit{original gauge length}}{\textit{original gauge length}} \times 100\%$$

3.3.6.2 Flexural Properties

Flexural tests were also performed on the above mentioned samples according to ASTM D790. The testing machine used for the tensile test was used here where the three point flex system was utilized to obtain the flexural strength and modulus data. The plain rectangular bar was placed on two supporting pins and subjected to a load on the center using a loading

pin from the opposite direction. The load was kept acting continuously until the sample broke or until it stretched to 5% of strain. For each sample, six plain rectangular bars were subjected to the flexural test and the obtained results were averaged and reported with the standard deviation. The following formulas were utilized to calculate the flexural strength and modulus:

$$\text{Flexural strength (MPa)} = \frac{3PL}{2bd^2}$$

$$\text{Flexural strain } \left(\frac{\text{mm}}{\text{mm}}\right) = \frac{6Dd}{L^2}$$

$$\text{Flexural modulus (MPa)} = \frac{\text{Flexural strength}}{\text{Flexural strain}}, \text{ within the elastic region}$$

where:

P = load at a given point in N

L = support span in mm

b = width of plain rectangular bar in mm

d = depth of plain rectangular bar in mm

D = maximum deflection at the center of plain rectangular bar in mm

3.3.6.3 Izod Impact Strength

Izod impact strength was determined for the pure PP and the wood-fiber/PP composites using a Monitor Impact Tester (Testing Machine Inc.) according to ASTM D256 (Method A). Before testing, each plain rectangular bar was notched at a depth of 2.5 mm and an angle of $45 \pm 1^\circ$. The notch was created to increase the tendency to a brittle failure by concentrating the stress on the bar. Each notched bar was placed vertically and fixed into a clamping device in the test machine. The top half was then hit at a 90° angle by a swinging pendulum weighing 5 ft-lb. The results were recorded in J/m which is the energy absorbed per unit of bar thickness at the notch. The test was carried out 6 times for each sample and the average of the results was reported with the standard deviation.

3.3.7 Gel Permeation Chromatography (GPC)

High-temperature Gel Permeation Chromatography (GPC) analysis was kindly performed by Saudi Basic Industries Corporation's laboratories in Riyadh, Saudi Arabia. It was carried out to measure the molecular weights and the molecular weight distributions of the soluble fraction of ONTMS-crosslinked PP (prepared with 0.20 wt.% peroxide). It was also performed for the PP reacted with 0.20 wt.% peroxide to evaluate the impact of ONTMS addition (grafting and crosslinking) on the molecular structure of PP.

The following procedure was followed. The sample was dissolved in 1,2,4-trichlorobenzene (TCB) to form a solution at a concentration of 2.0 mg/ml. TCB was stabilized by 500 mg/L of butylated hydroxytoluene (BHT). The solution was then heated to a temperature of 160°C. The analysis was performed at 160°C and a solvent flow rate of 1.0 ml/min. Narrow molecular weight distribution polystyrene standards were used for calibration.

Chapter 4

Results and Discussions: Chemical Modification of Polypropylene with Organo-functional Silanes and its Impact on Crystallization Temperature and Melt Properties of Polypropylene

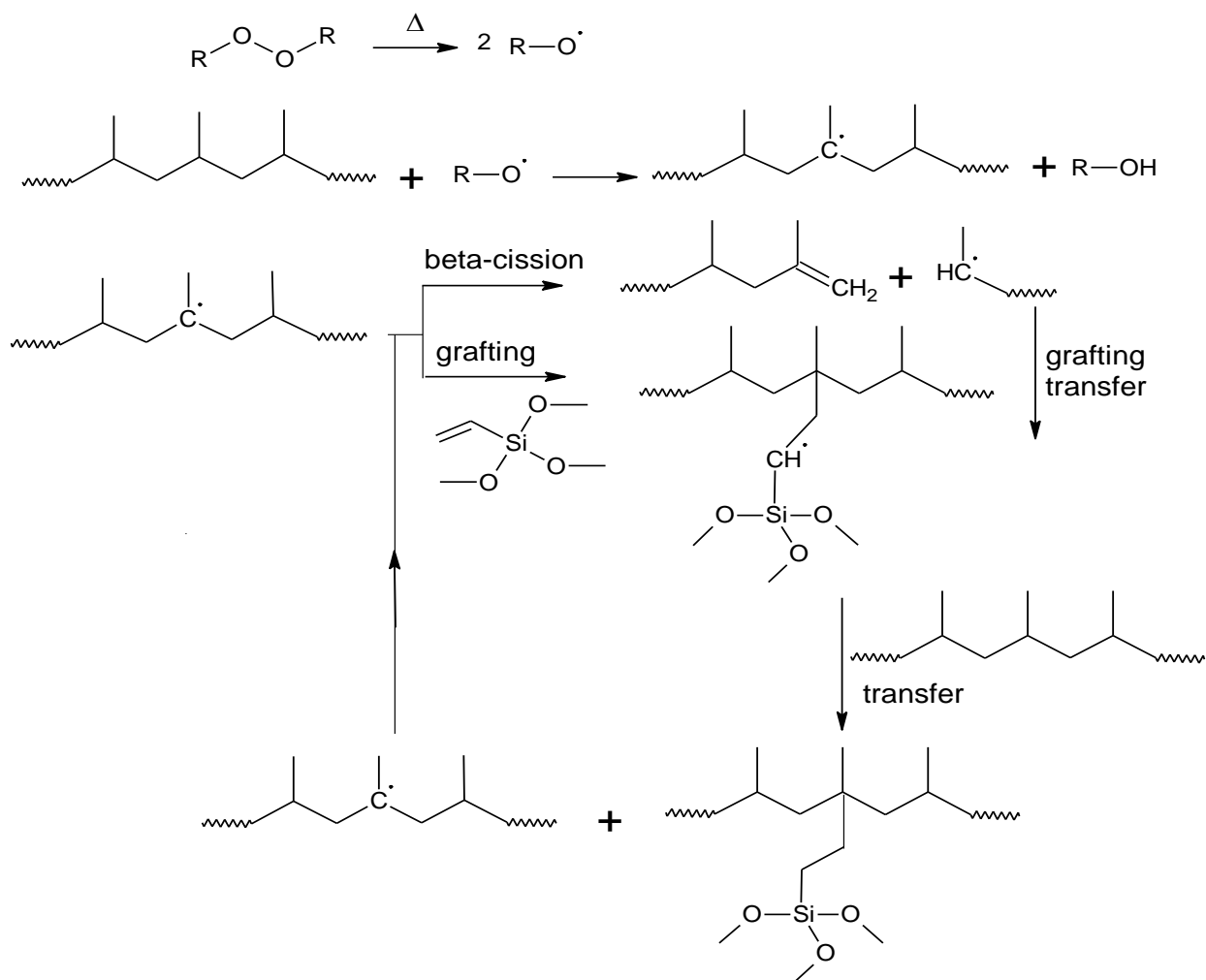
4.1 Grafting Organo-functional Silanes and Chemical Analyses

Fourier Transform Infrared (FT-IR) spectroscopy was used to verify the grafting of the organo-functional silanes onto PP, and compare the grafting efficiencies of these silanes. Beside the pure PP and PP reacted with peroxide, nine different samples of PP grafted with different silanes were prepared according to the procedures mentioned previously in Chapter 3 (Sections 3.2.1/2). Unreacted silane and polymerized silane were removed from these samples by fractionation and solvent extraction. Table 4.1 presents these grafted samples used for chemical analyses. Only one peroxide type was used in this work and it was dibenzoyl peroxide. All these samples were prepared at 180°C and 60 rpm.

Table 4.1 Samples prepared for FT-IR analysis

Sample	Silane Concentration (wt.%)	Peroxide Concentration (wt.%)	N₂ Atmosphere
Pure PP	0	0	N/A
PP-g-APTMS	5	0.20	√
PP-g-VMMS	5	0.20	√
PP-g-ONTMS	5	0.20	√
PP-g-VTMS	5	0.20	√
PP reacted with peroxide	0	0.20	×
PP-g-BTMSPA	5	0.20	×
PP-g-AMPTMS	5	0.20	×
PP-g-UPTMS	5	0.20	×
PP-g-GPTMS	5	0.20	×
PP-g-Azidosilane	5	0	×

Free radical grafting of (3-acryloxypropyl)trimethoxysilane (APTMS), 3-methacryloxypropyltrimethoxysilane (VMMS), vinyltrimethoxysilane (VTMS), and 7-octenyltrimethoxysilane (ONTMS) onto PP follows the same basic mechanism (a free-radical mechanism) shown in Scheme 4.1. (Rätzsch, 2002; Wang, 2005)



Scheme 4.1 Schematic representation of VTMS grafting onto PP

The FT-IR spectra of the pure PP, PP-g-APTMS, and PP-g-VMMS are shown in Figure 4.1. It can be seen clearly from the spectrum of PP-g-APTMS that the intensity of the carbonyl groups peak centered around 1730 cm^{-1} (Salimi, 2009) increased significantly after the introduction of APTMS. This indicates that APTMS was indeed grafted onto PP since APTMS contains a carbonyl group in its structure. A second evidence of grafting APTMS onto PP is the broad band at $1080\text{-}1100\text{ cm}^{-1}$ which is attributed to the stretching vibration of the bond O-C in Si-O-C group. (Stuart, 2004; Li, 2013) In addition to these two evidences, a

new peak can be clearly seen at 1191 cm^{-1} which was assigned to the rocking vibration of O-CH_3 in Si-O-C group. (Li, 2013)

With regard to VMMS grafting onto PP, similar three changes were also observed in the spectrum of PP-g-VMMS confirming the occurrence of grafting. However, the intensities were weaker indicating that VMMS was not as effective as APTMS. Nevertheless, APTMS and VMMS had higher grafting degrees compared to the other silanes used in this study except Azido-silane. It has been suggested that the conjugated structure in the silane improves grafting onto PP. (Huang, 2000) Such structure is present in APTMS and VMMS and it is the C(=O)R- moiety which draws electrons away from the double bonds in these two silanes. (Backer, 2013)

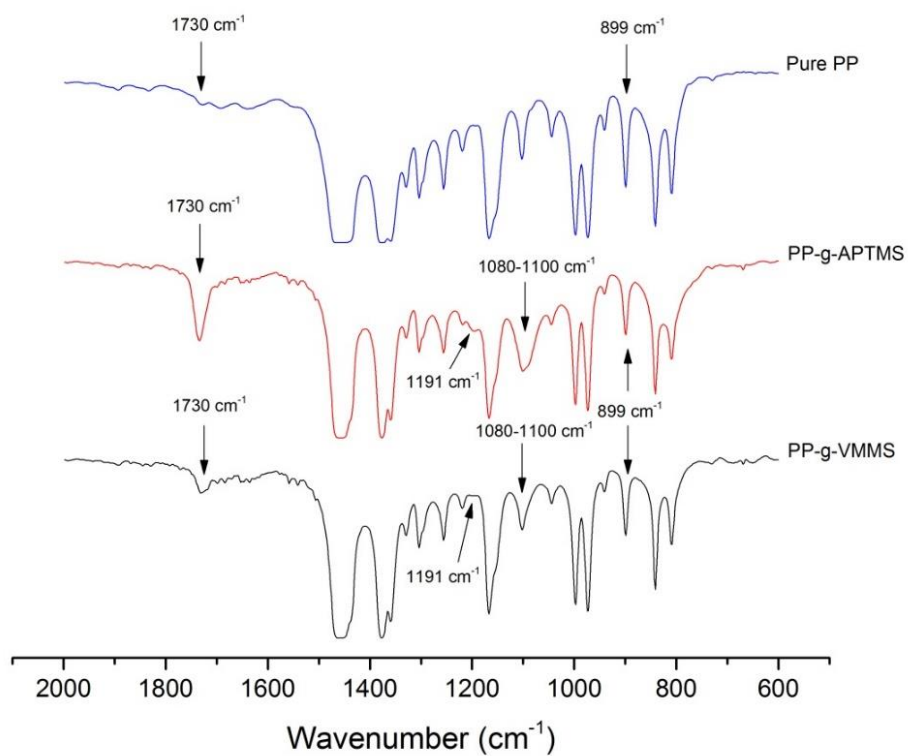


Figure 4.1 FTIR spectra of the pure PP, PP-g-APTMS, and PP-g-VMMS

Figure 4.2 shows the FT-IR spectra of the pure PP, PP-g-ONTMS, and PP-g-VTMS. The broad band at 1080-1100 cm^{-1} can be seen although not as clear as in the modification of PP with APTMS and VMMS. In several studies, VTMS was shown to have less grafting efficiency compared to VMMS. (Huang, 2000; Backer, 2013) The spectrum of ONTMS indicates that its grafting degree was slightly less than VTMS grafting. Gel content determination was used to further confirm the grafting of VTMS and ONTMS as will be shown later.

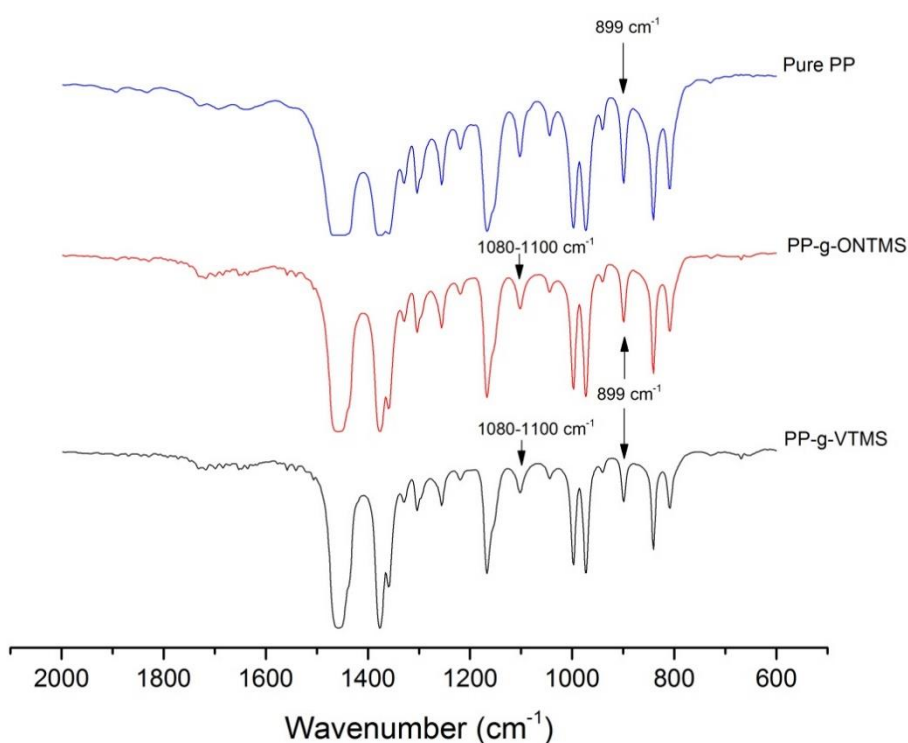
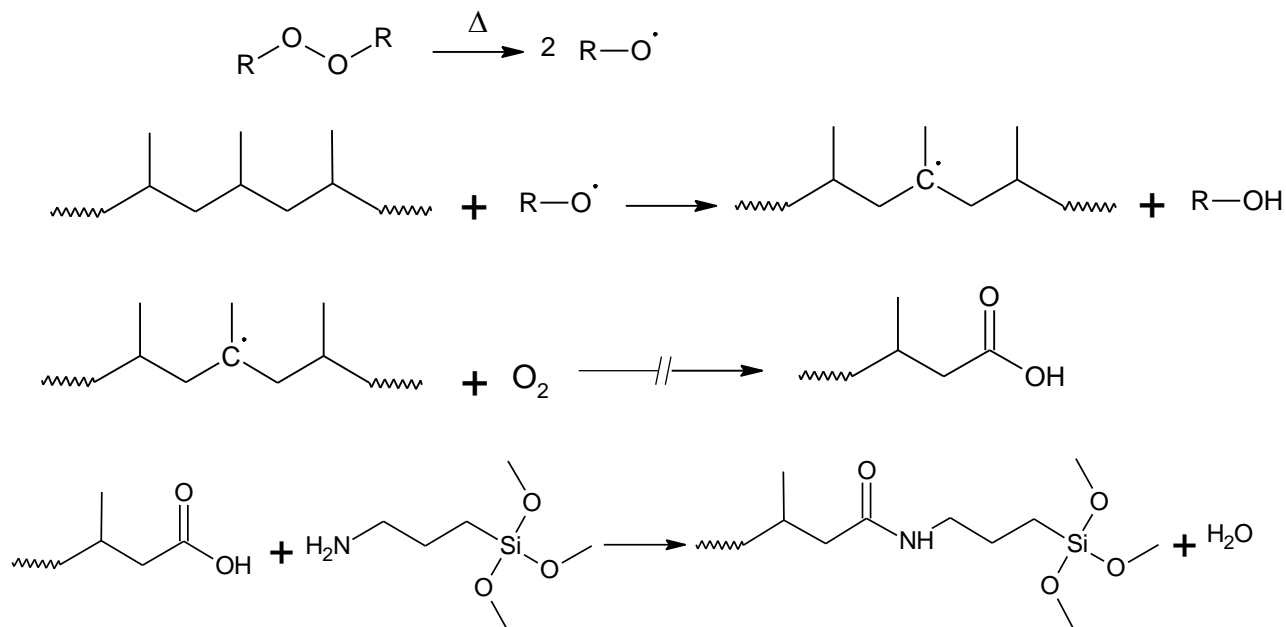


Figure 4.2 FTIR spectra of the pure PP, PP-g-ONTMS, and PP-g-VTMS

AMPTMS, UPTMS, BTMSPA, and GPTMS were expected to react with PP through a different mechanism (see Scheme 4.2 below). The organic functional groups in these silanes (the primary amine in APTMS and UPTMS, secondary amine in BTMSPA, and epoxy in GPTMS) may react with the carboxylic acid groups that result from PP oxidation during

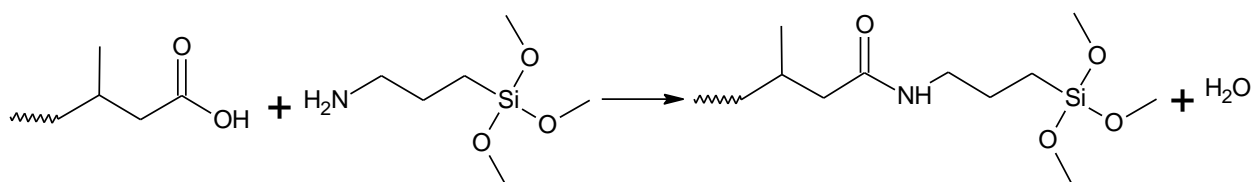
reactive extrusion in the presence of air. (Demje'na, 1999; Blonk, 2002) Dibenzoyl peroxide was added to accelerate the formation of carboxylic acid groups.



Scheme 4.2 Schematic representation of AMPTMS grafting onto PP

It can be seen from Figure 4.3 that the PP reacted with peroxide in the presence of air contained some carboxylic acid groups as can be seen from its spectrum around 1730 cm^{-1} . It should be noted that the PP reacted with peroxide here was prepared at reaction conditions similar to those selected for AMPTMS, UPTMS, and BTMSPA, and GPTMS grafting systems except that silane was not added. The purpose was to observe the concentration of carboxylic acid groups which were expected to be consumed during the reactions with those four silanes.

The addition of AMPTMS caused the intensity of the carboxylic acid groups region in the spectrum of the PP reacted with peroxide to decrease indicating that some of these groups were consumed in the reaction with the primary amine groups in AMPTMS to generate secondary amide groups according to the following reaction:



In addition, two new peaks were observed. The new peak appeared at 1640 cm^{-1} can be assigned to the carbonyl group vibration of the secondary amide and the other new peak observed at 1564 cm^{-1} can be attributed to the N-H deformational vibration in the secondary amide. (Demje'na, 1999)

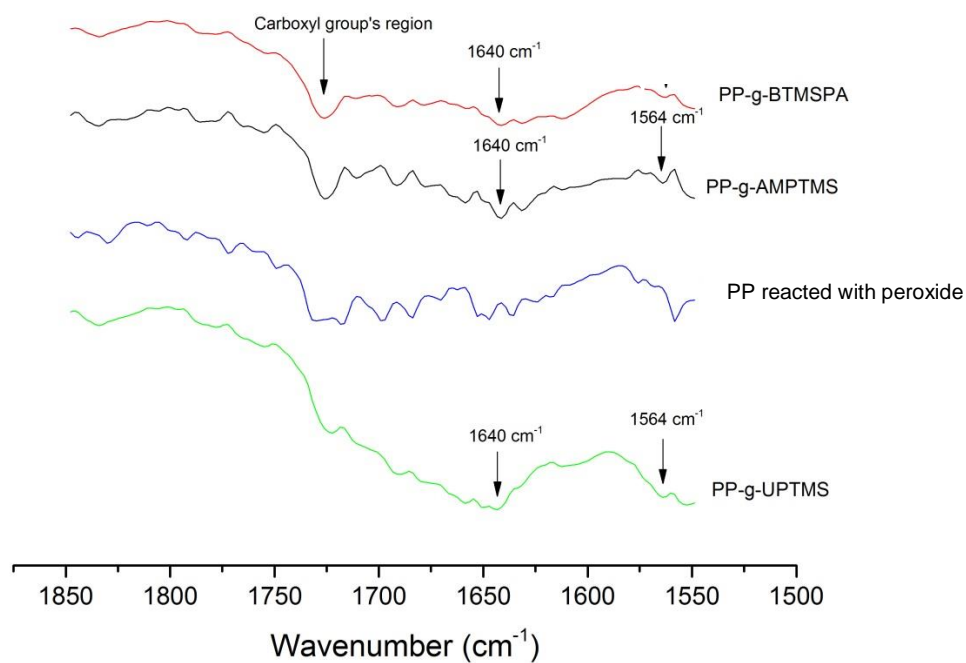
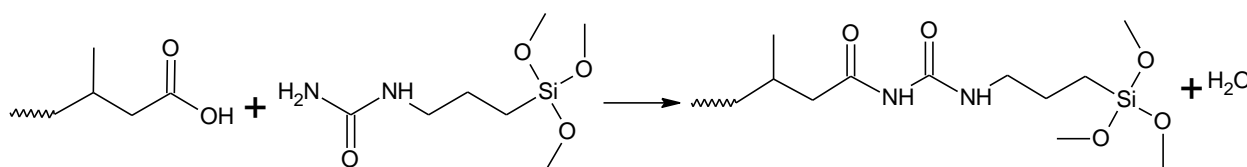


Figure 4.3 FTIR spectra of the PP reacted with peroxide, PP-g-BTMSPA, PP-g-AMPTMS, and PP-g-UPTMS (Wavenumber range: $1500\text{-}1850\text{ cm}^{-1}$)

The same changes were observed with PP-g-UPTMS. However, the peak at 1640 cm^{-1} in this case seems to be broader than in the case of PP-g-AMPTMS and PP-g-BTMSPA. This may be explained by the existence of two carbonyl groups resulting from the reaction

between a single carboxylic acid PP macromolecule with a single UPTMS molecule unlike the previous reaction with AMPTMS. However, the peak at 1191 cm^{-1} (see Figure 4.4) attributed to the rocking vibration of O-CH₃ in Si-O-C group can be seen clearly in PP-g-UPTMS spectrum unlike PP-g-AMPTMS and PP-g-BTMSPA. This may indicate that the cause of higher intensity of the peak at 1640 cm^{-1} was simply the high grafting efficiency of UPTMS compared to AMPTMS and BTMSPA. The reaction between the single carboxylic acid PP macromolecule and UPTMS is shown here:



For PP-g-BTMSPA, there are is also a new peak at 1640 cm^{-1} that can be assigned to C=O vibration in the tertiary amides resulting from the reaction between the carboxylic acid groups in the oxidized PP and the secondary amine groups in BTMSPA according to the reaction:

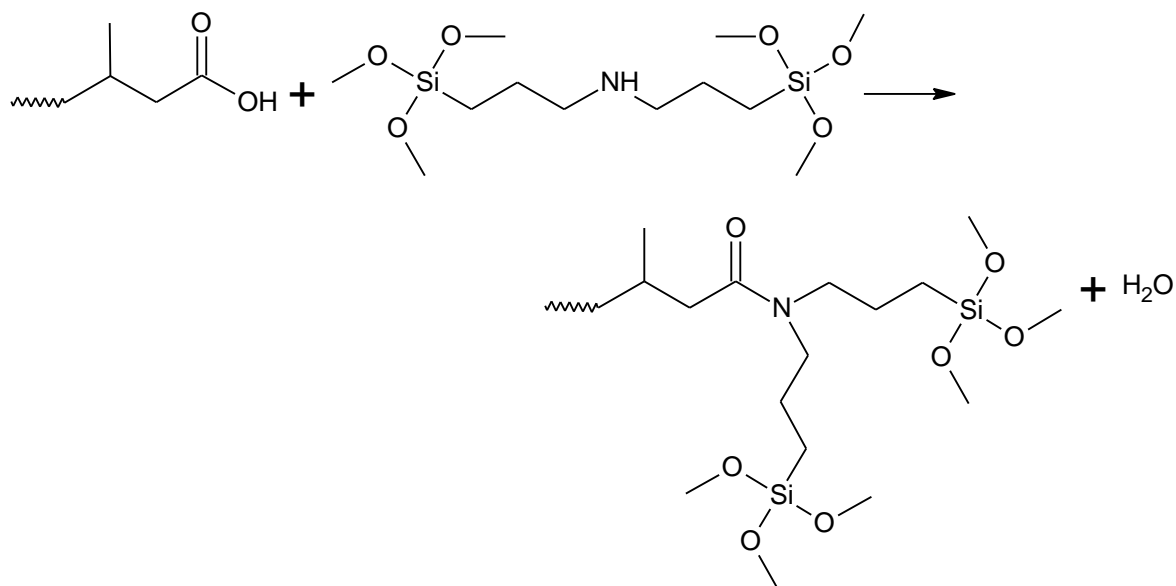


Figure 4.4 shows the FTIR spectra of the PP reacted with peroxide, AMPTMS, UPTMS, and BTMSPA with a wider wavenumber range. All three PP-g-silanes seem to exhibit a

slightly broad peak at 1080-1100 cm^{-1} . However, the peak at 1191 cm^{-1} appears only in the spectrum of PP-g-UPTMS indicating that UPTMS was grafted more effectively onto PP.

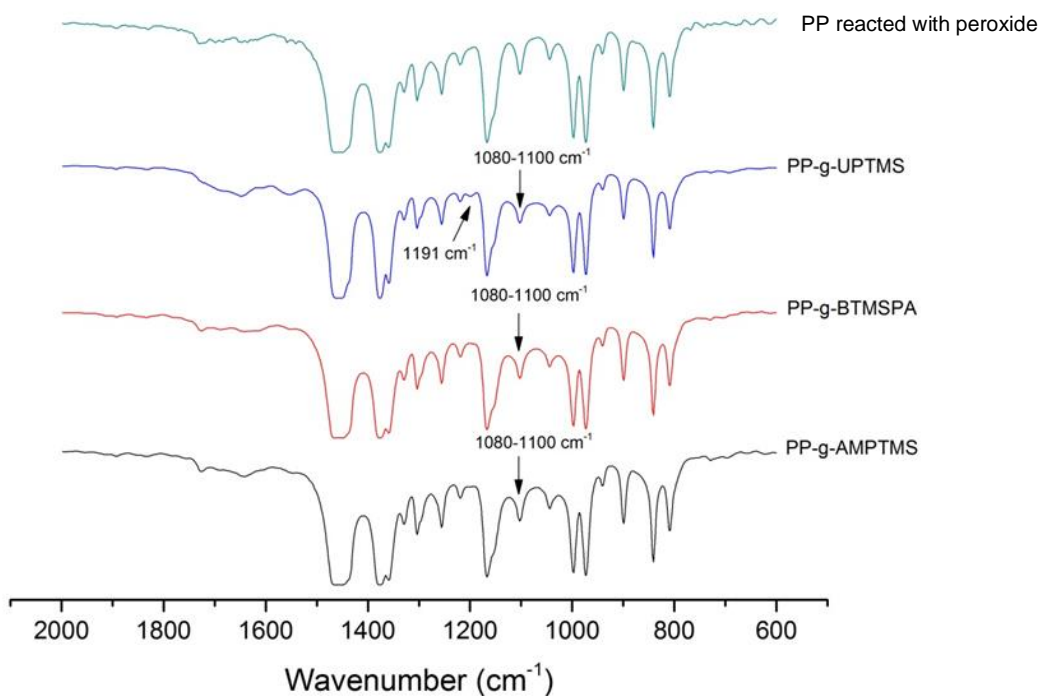


Figure 4.4 FTIR spectra of the PP reacted with peroxide, PP-g-BTMSPA, PP-g-AMPTMS, and PP-g-UPTMS

All of the above observations indicate that AMPTMS, UPTMS, and BTMSPA were grafted onto PP. Furthermore, the grafting degrees of these silanes can be increased by increasing the concentration of carboxylic acid groups present in the PP backbone as a result of oxidation. The carboxylic acid groups' concentration can be enhanced by increasing the reaction temperature, increasing the oxygen concentration by introducing pure oxygen instead of air, increasing the peroxide concentration, using PP grafted with monomers capable of reacting with these silanes such as PP-g-maleic anhydride, or increasing the reaction time.

The concentration of carboxylic acid groups increases with reaction time. Thus, significant grafting of amino-silanes onto PP can be achieved by increasing the reactive extrusion time.

The effect of reaction time on the grafting of AMPTMS onto PP is illustrated in Figure 4.5. Three different reaction times (5, 10, and 20 minutes) were chosen. In five minutes, the new peak at 1640 cm^{-1} was detected and the intensity of the peak around 1730 cm^{-1} decreased indicating that AMPTMS grafting can be achieved at this reaction time under the reaction conditions mentioned earlier in the experimental part. After ten minutes, the intensity of the new peak increased and a further decrease in the intensity of the peak at 1730 cm^{-1} can be observed. These changes can be seen more clearly in 20 minutes reaction time. This is supported by the appearance of the peak at 1191 cm^{-1} after 10 and 20 minutes as shown in Figure 4.6.

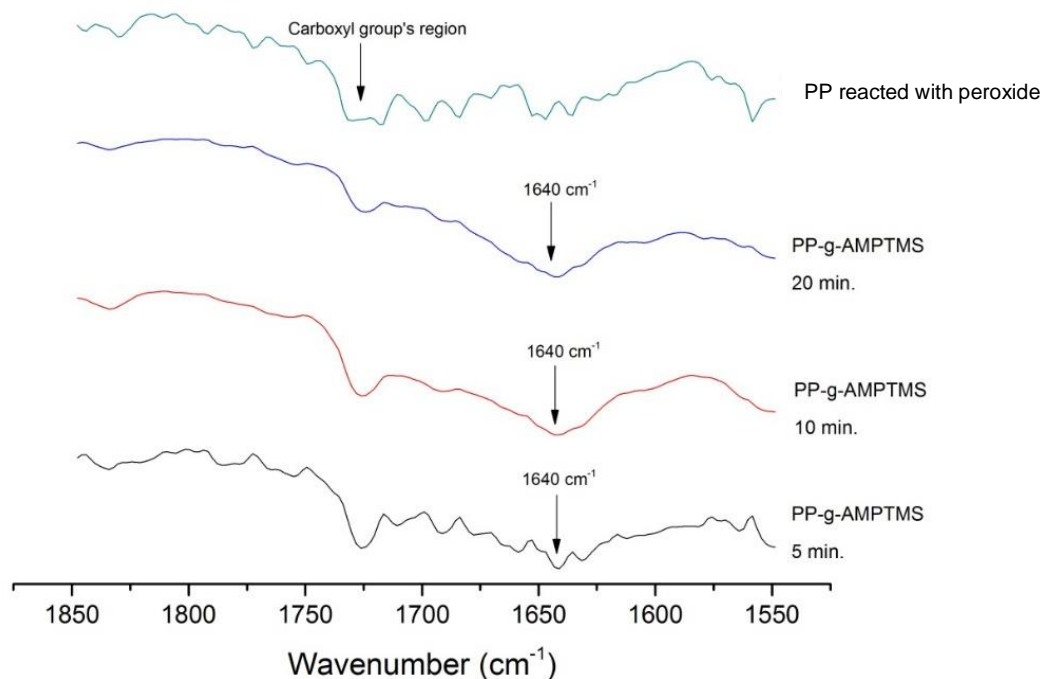


Figure 4.5 FTIR spectra of the PP reacted with peroxide, and PP-g-AMPTMS prepared at different reaction times (Wavenumber range: $1500\text{-}1850\text{ cm}^{-1}$)

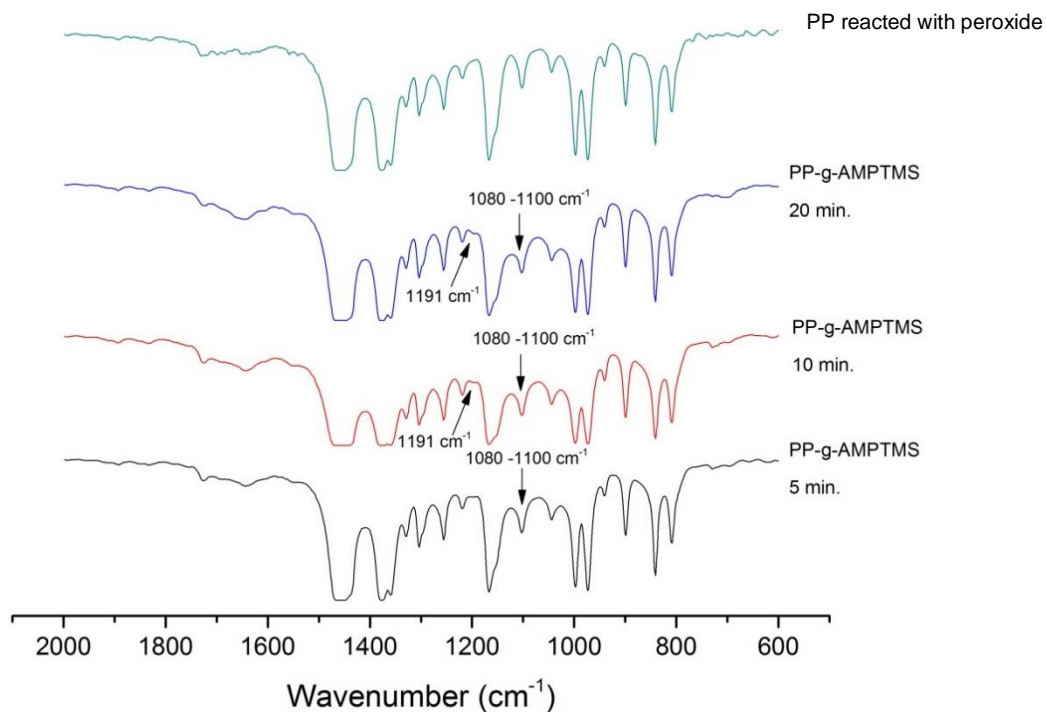


Figure 4.6 FTIR spectra of the PP reacted with peroxide, and PP-g-AMPTMS prepared at different reaction times

With regard to GPTMS, its introduction to the reaction system consumed some carboxylic acid groups as can be seen from the reduced intensity of the carboxylic acid groups' region in the spectrum of the PP reacted with peroxide (see Figure 4.7). In addition, the peak at 1191 cm⁻¹ can be seen in the spectrum of PP-g-GPTMS shown in Figure 4.8. These changes can confirm the grafting of GPTMS onto PP. The expected reaction between the epoxy group in GPTMS and the carboxylic acid group in the oxidized PP is as follows:

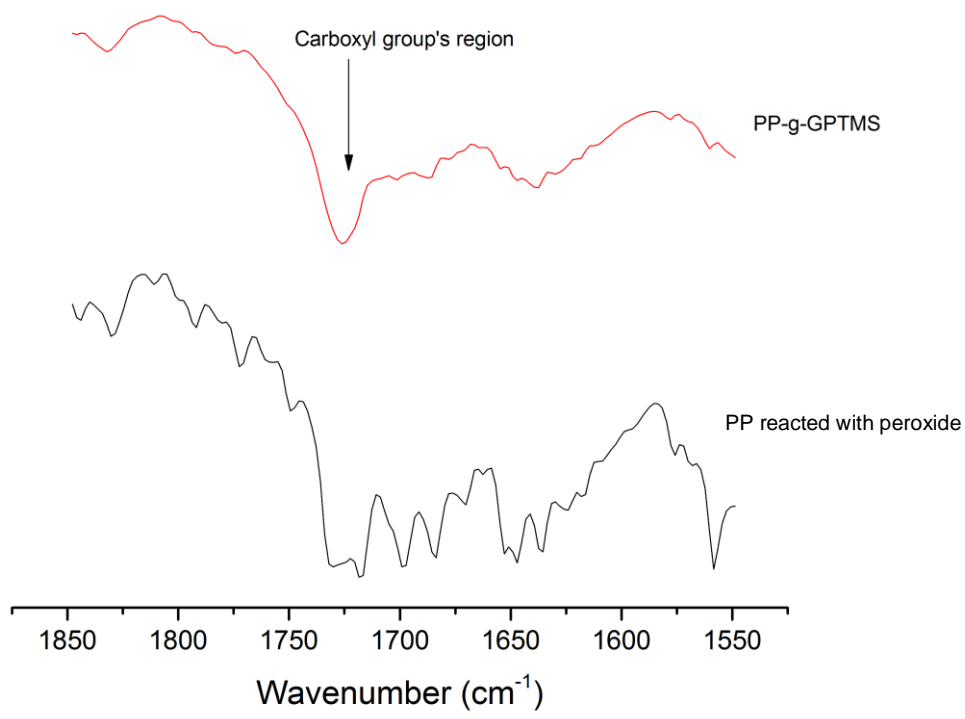
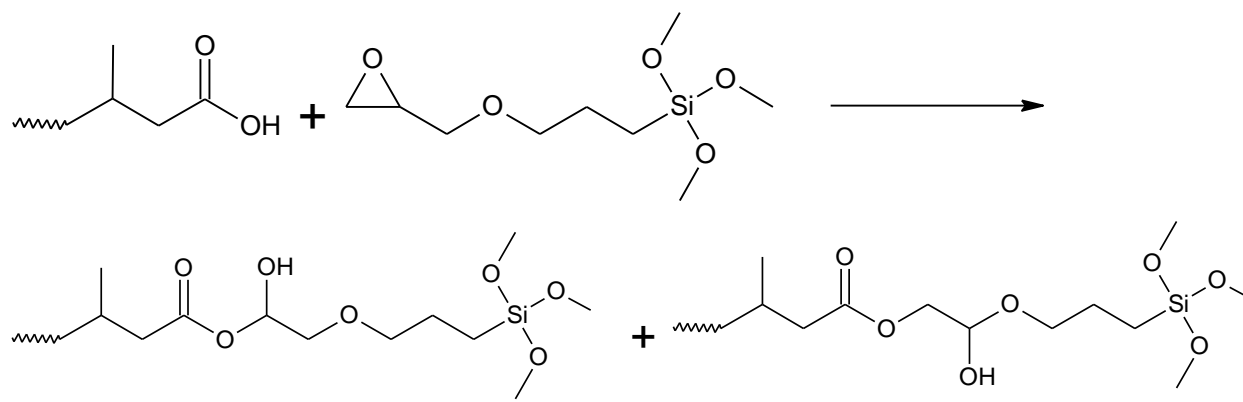


Figure 4.7 FTIR spectra of the PP reacted with peroxide, and PP-g-GPTMS (Wavenumber range: 1500-1850 cm^{-1})

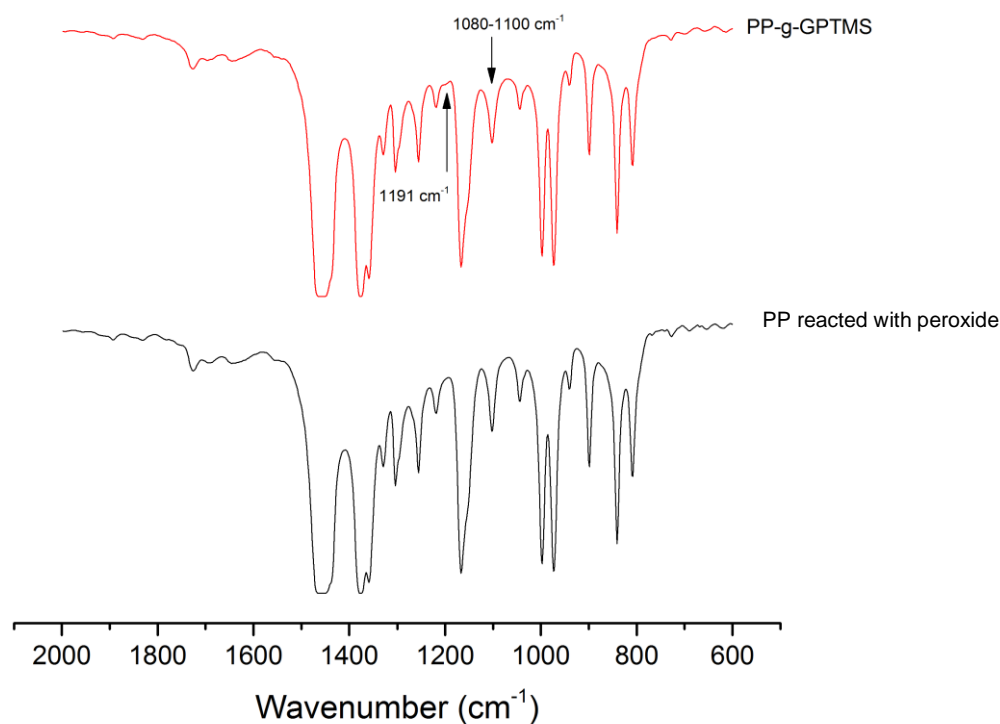
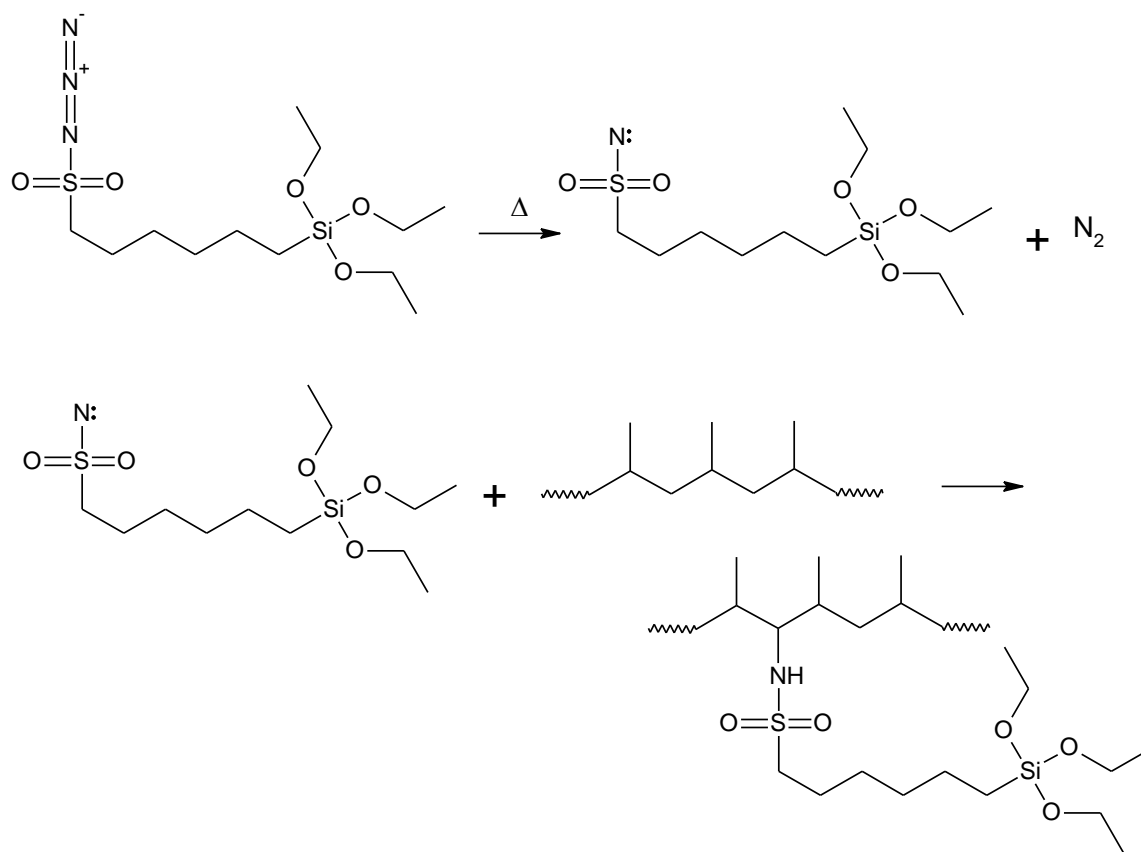


Figure 4.8 FTIR spectra of the PP reacted with peroxide, and PP-g-GPTMS

Finally, 6-Azidosulfonylhexyltriethoxysilane, via its organo-functional azido group, can react differently with PP forming covalent bonds according to the grafting reaction mechanism shown in Scheme 4.3. In this case, no peroxide is needed since the formation of PP macroradicals is not required to accomplish the grafting. Heating the reaction mixture to temperatures below 200°C is enough to decompose the azido group generating two products, namely, a nitrene molecule and a nitrogen gas molecule. The highly reactive nitrene molecule can then insert itself into the C-H bonds in the PP chains. It can also react with the double bonds that may be formed as a result of PP oxidation during the reactive extrusion process (β -scission reactions). (Xie, 2010; Jørgensen, 2007)



Scheme 4.3 Schematic representation of Azido-silane grafting onto PP

In Figure 4.9, a strong absorption can be seen between 1000 cm^{-1} and 1130 cm^{-1} which can be attributed to the siloxane groups (Si-O-Si). Some crosslinking of PP chains via Si-O-Si seem to occur before FT-IR analysis. It should be noted that this strong band can mask the band that results from the absorption of the Si-O-C₂H₅ groups between 1080 cm^{-1} and 1100 cm^{-1} . (Launer, 2013) The siloxane groups were formed as a result of hydrolysis and condensation reactions of the grafted Si-O-C₂H₅ groups with moisture in air and these reactions started even during the reactive extrusion. The torque decreased at the beginning of the reaction but then started to increase at the end of the reaction and became even higher than that observed when extruding PP only. This means that an increase in the melt viscosity and the molecular weight occurred during the reaction process as a result of hydrolysis and condensation (crosslinking) reactions. Similar behavior was not observed with all other silane grafting systems. In these systems, the torque decreased initially and reached a plateau at the

end of the reaction indicating that only grafting reactions occurred. This was confirmed by the absence of the strong bands of the siloxane groups in the FT-IR spectra of these silanes.

This observation might indicate that the Azido-silane here was highly grafted onto PP since moisture in air was enough to hydrolyze some of the grafted Si-O-C₂H₅ groups to form silanol groups (Si-OH) and crosslinking the PP chains as a result. It is interesting to note that hydrolysis reactions occurred even though Si-O-C₂H₅ tend to be hydrolyzed much more slower compared to S-O-CH₃ present in the other silanes tested in this work. In addition, this silane contained a longer alkyl spacer between the silicon atom and the organo-functional group which can also slow down the hydrolysis process. (Xie, 2010) The high grafting degree of this silane onto PP was confirmed by the gel content test as will be shown later.

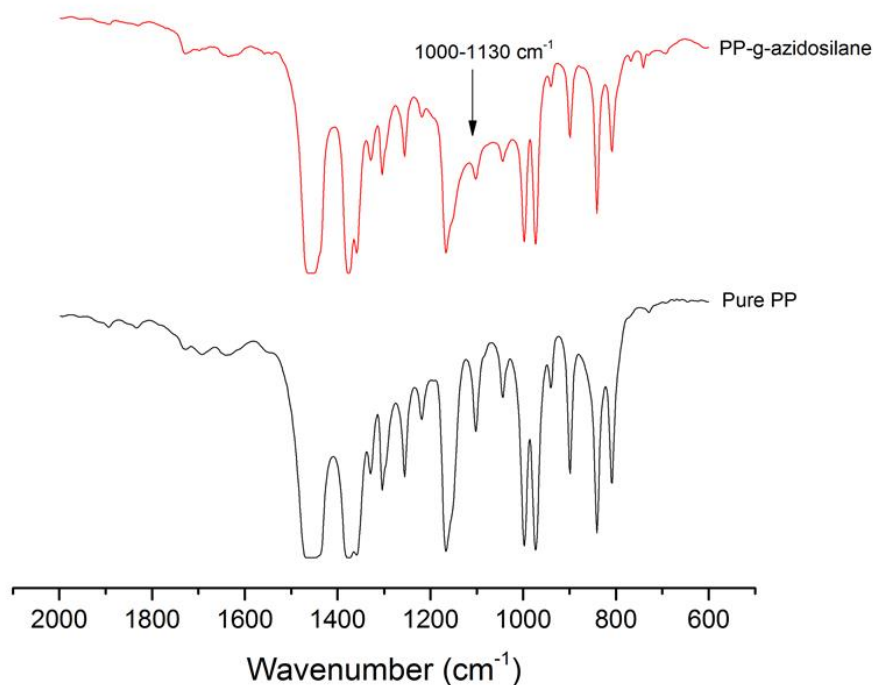


Figure 4.9 FTIR spectra of the pure PP and PP-g-Azidosilane

Figure 4.10 shows the absorption ratios of the region 1080-1100 cm⁻¹ to the peak at 899 cm⁻¹ which is a characteristic absorption of PP and picked as an internal reference. These

ratios are based on FTIR peak areas and indicate the relative grafting degrees of APTMS, VMMS, VTMS, and ONTMS onto PP. They can be used for comparing the grafting efficiencies of these silanes. As mentioned earlier, the broad band at 1080-1100 cm^{-1} is assigned to the stretching vibration of O-C in the Si-O-C group. The figure shows that ONTMS has the lowest grafting degree (ratio = 0.95) while APTMS has the highest grafting degree (ratio = 3.11). VTMS grafting degree (ratio = 1.11) is slightly higher than that of ONTMS. VMMS has a significant grafting degree that is higher than that of VTMS (ratio = 1.31).

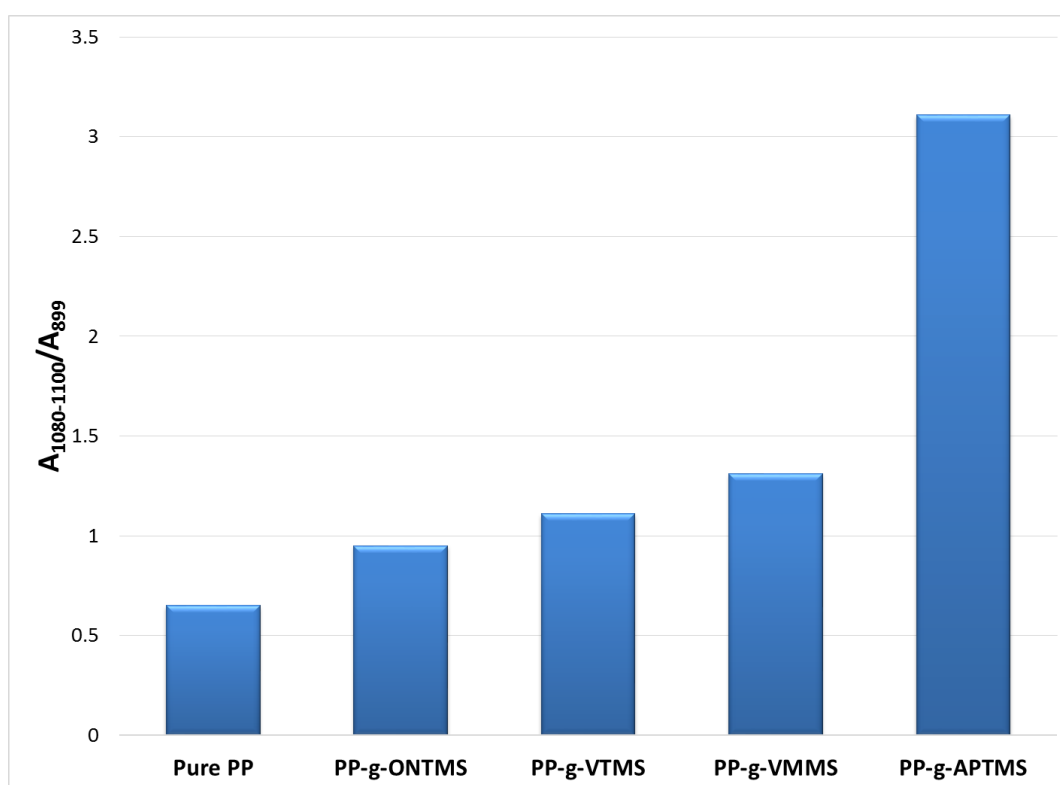


Figure 4.10 FT-IR absorption ratios of the pure PP, PP-g-ONTMS, PP-g-VTMS, PP-g-VMMS, and PP-g-APTMS

The relative grafting degrees of AMPTMS, UPTMS, BTMSPA, and GPTMS were compared separately since they are expected to follow a different grafting mechanism. They were grafted to less extent onto PP due to the low concentration of carboxylic acid groups in PP.

Figure 4.11 compares the relative grafting degrees of AMPTMS, UPTMS, BTMSPA, and GPTMS. In this case, the absorption ratios of the band around 1730 cm^{-1} to the band at 899 cm^{-1} were chosen to indicate the relative grafting degrees. These ratios can be used as a measure of the concentration of the carboxylic acid groups in PP and they are expected to decrease as a result of the reactions. In this case, a low absorption ratio indicates a high degree of grafting. Among these silanes, UPTMS (ratio = 0.05) and GPTMS (ratio = 0.172) were clearly the most effective ones in this family of silanes as can be seen by their low absorption ratios. The absorption ratio of UPTMS is even lower than that of pure PP (ratio = 0.09). This finding is supported by the presence of the peak at 1191 cm^{-1} which can be seen more clearly only in the spectra of UPTMS and GPTMS. The absorption ratios of AMPTMS (ratio = 0.251) and BTMSPA (ratio = 0.214) indicate that some carboxylic acid groups were consumed during the reaction of these silanes with PP.

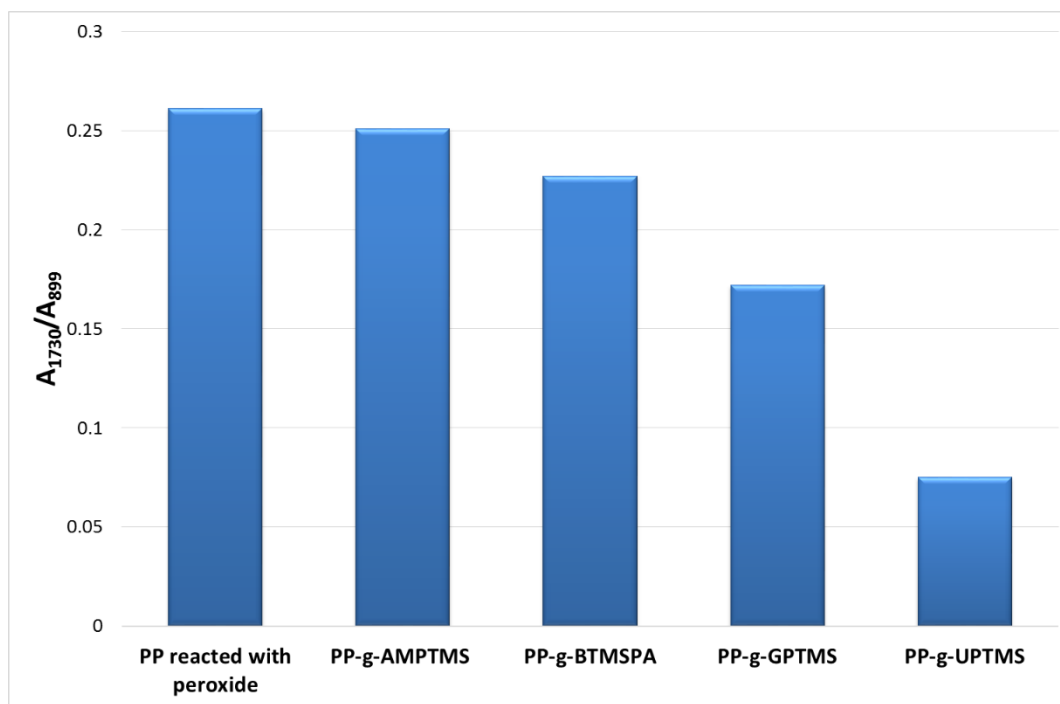


Figure 4.11 FT-IR absorption ratios of the PP reacted with peroxide, PP-g-AMPTMS, PP-g-BTMSPA, and PP-g-UPTMS

Finally, the comparison of the relative grafting degree of AMPTMS onto PP as a function of the reaction time is illustrated in Figure 4.12. As expected, the relative grafting degree increases with time as indicated by the steady decrease in the ratio attributed to the concentration of carboxylic acid groups.

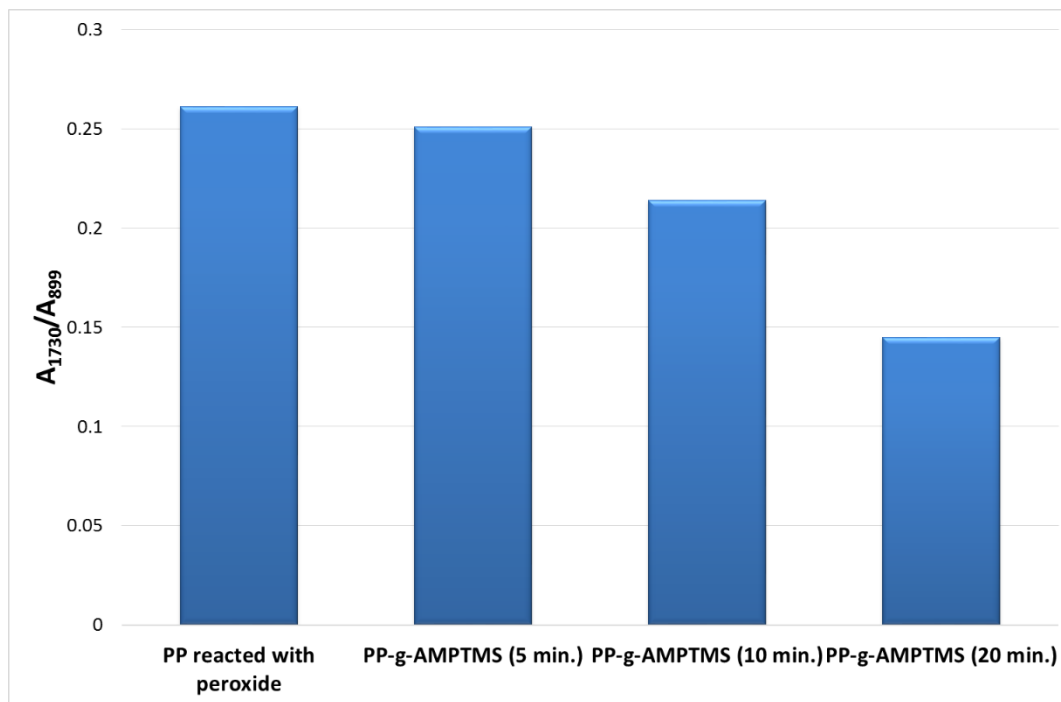
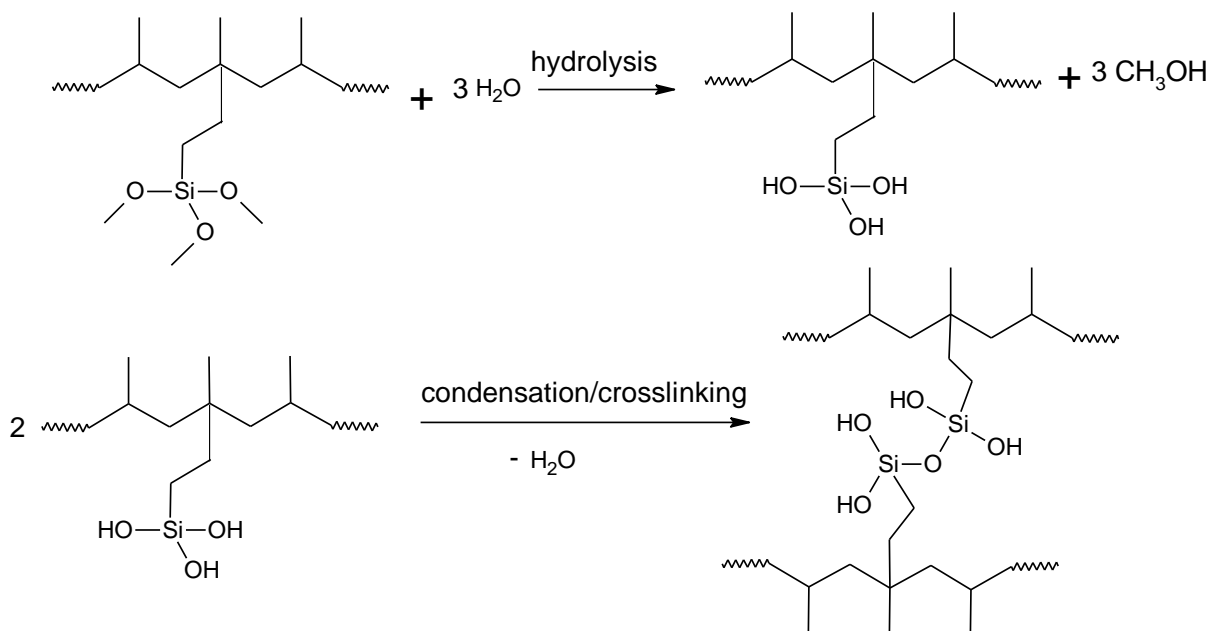


Figure 4.12 FT-IR absorption ratios of the PP reacted with peroxide, and PP-g-AMPTMS at different reaction times

4.2 Gel Contents

The gel material in this context refers to the crosslinked material within the crosslinked PP sample. It is not soluble in hot xylene due to its high molecular weight. Its content was measured (in wt.%) and used as another indication of the grafting efficiencies of the silanes used here. The grafted samples shown in Table 4.1 were treated with hot water to trigger a reaction where the alkoxy groups (Si-O-R) in the silane are hydrolyzed with water to form silanol groups (Si-OH). Then the silanol groups undergo condensation reactions forming crosslinks between the grafted PP chains (see Scheme 4.4). Thus, the presence of high silane contents on the PP backbone should generate high gel contents and vice versa.



Scheme 4.4 Schematic representation of water crosslinking of PP via VTMS grafts

The high grafting efficiencies of APTMS, VMMS, and Azido-silane were confirmed by the high gel contents obtained after treating their grafted products with hot water. Figure 4.13 compares the gel contents obtained with these silanes. The gel contents of APTMS-crosslinked PP (66.5 wt.%) and VMMS-crosslinked PP (25.8 wt.%) systems followed the same trend seen with FTIR data (relative grafting degrees) indicating that the increase in gel content was a result of the high content of grafted silane. The use of Azidosilane produced a crosslinked product with 82.0 wt.% gel content indicating that it is the most effective silane for grafting onto PP.

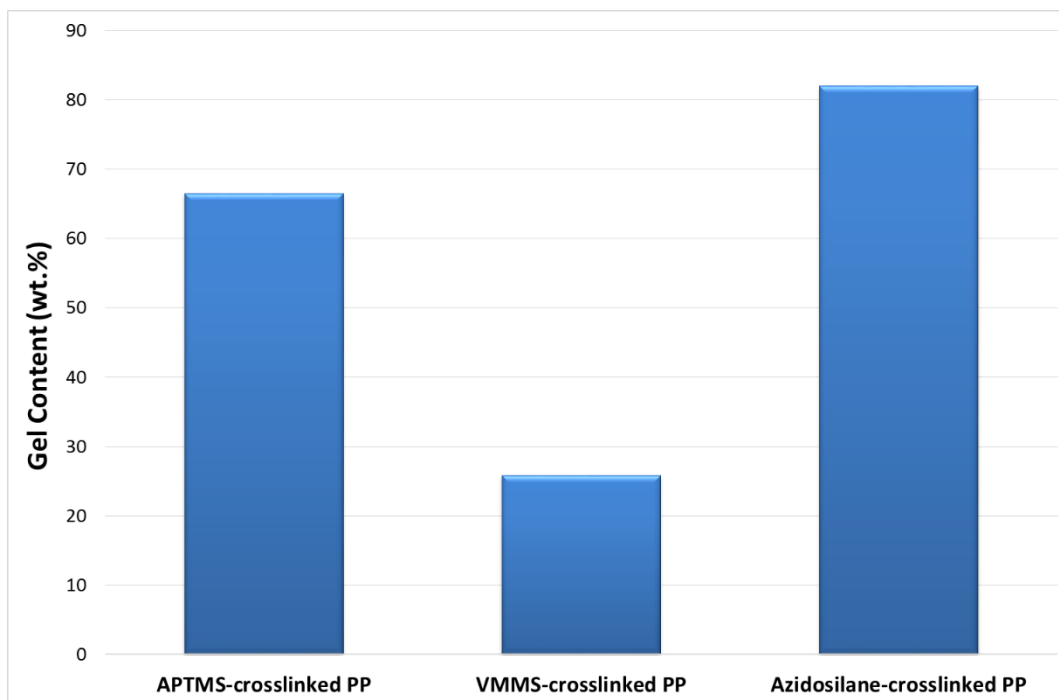


Figure 4.13 Gel contents of APTMS-crosslinked PP, VMMS-crosslinked PP, and Azidosilane-crosslinked PP

All other silanes produced PP with low gel contents ($\leq 5\text{wt.}\%$) as shown in Figure 4.14. PP crosslinked via UPTMS or GPTMS gave higher gel contents compared to the other crosslinked systems except with BTMSPA. VTMS-crosslinked PP and ONTMS-crosslinked PP gave low gel contents due to their low grafting degrees. These results confirm the results obtained with the FT-IR analysis. With regard to BTMSPA, it gave a higher gel content compared to, for example, UPTMS although it exhibited a lower grafting efficiency as shown earlier. One reason could be the nature of its molecular structure where each molecule contains two hydrolysable methoxy groups increasing the tendency of crosslinking PP compared to UPTMS. Another reason could be simply the nature of gel content analysis where a typical noise is always present especially at low crosslinking levels. Nevertheless, the gel contents associated with all of these silanes confirm their successful grafting onto PP.

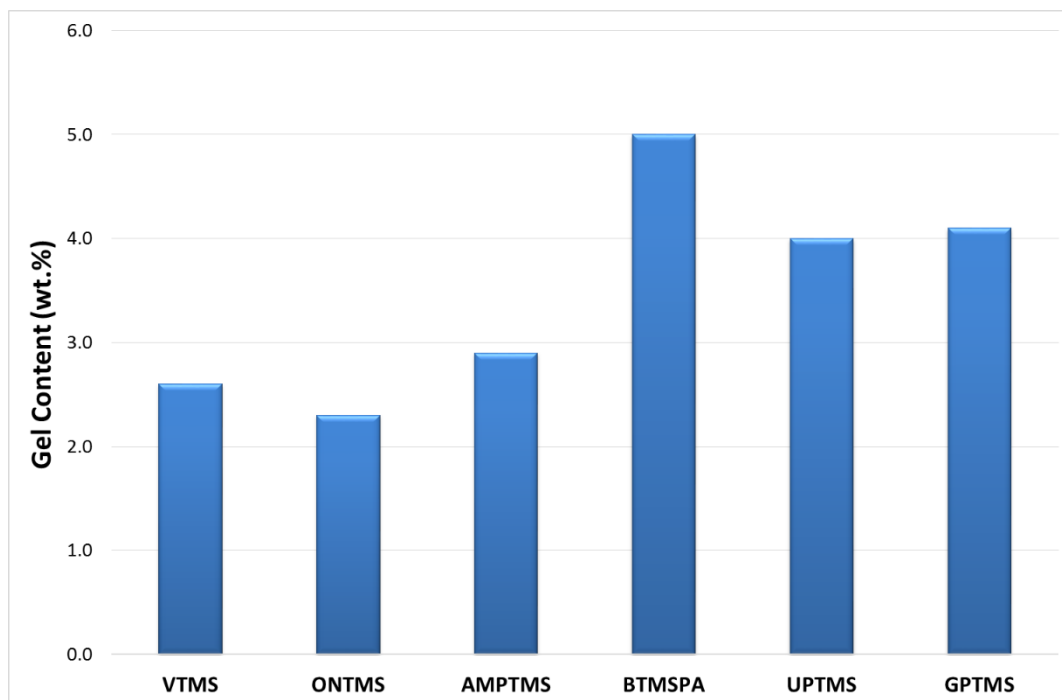


Figure 4.14 Gel contents of PP crosslinked with VTMS, ONTMS, AMPTMS, BTMSPA, UPTMS, and GPTMS

It should be noted that a gel content of approximately 1 wt.% was present with the PP reacted with peroxide, which might be a result of carbon-carbon crosslinking induced by peroxide and heat. This finding could be used to confirm that the low levels of gel (between 2 wt.% and 5 wt.%) resulted mainly from the crosslinking reactions of the grafted PP chains.

4.3 Crystallization Peak Temperatures

4.3.1 Crosslinked Samples

The crystallization peak temperatures (T_c) of the above crosslinked samples (see Section 4.2) were determined using DSC. They are shown in Figure 4.15 to help visualize the influence of the tested silanes on the bulk crystallization rate of PP. The DSC exotherms under non-isothermal conditions of the pure PP, PP reacted with peroxide, and all crosslinked samples can be seen in the Appendix section. It should be noted that higher T_c can be used as a sign of faster crystallization. (Wang, 1996)

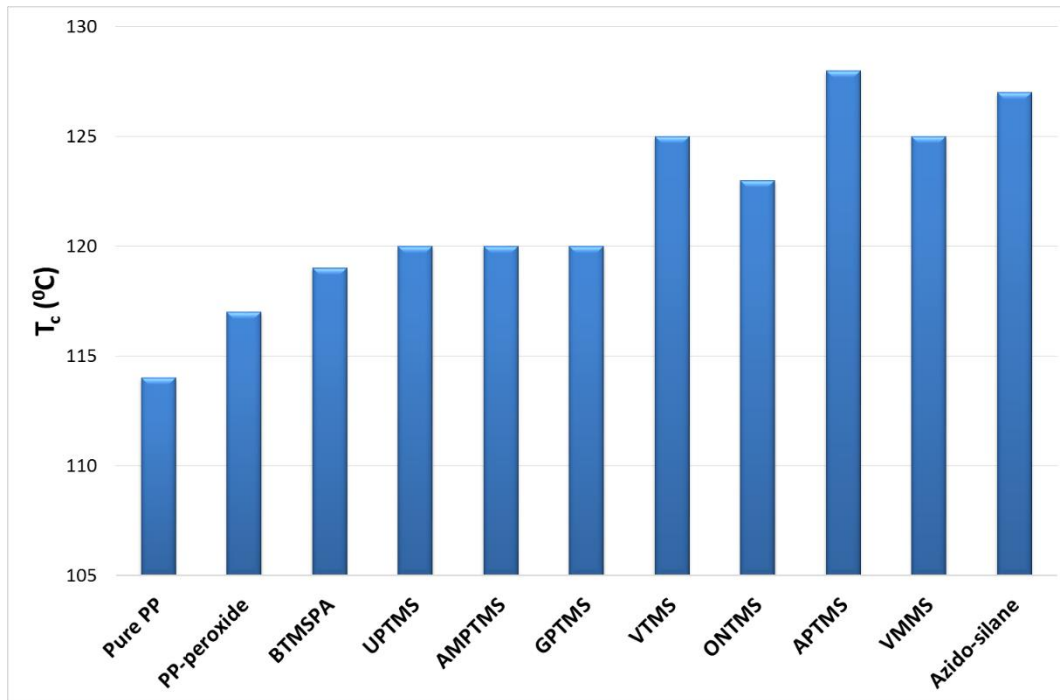


Figure 4.15 The crystallization peak temperatures of the pure PP, PP reacted with peroxide, and PP crosslinked with different silanes

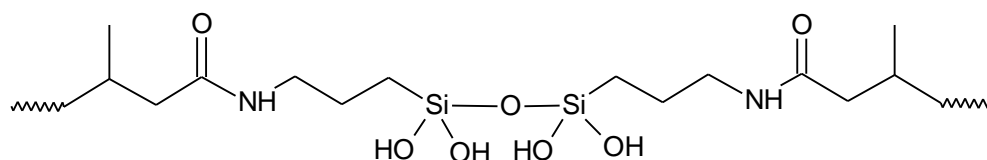
It can be seen that the crystallization peak temperature (T_c) of the PP reacted with peroxide is higher than that of the pure PP. The increase in T_c in this case can be explained by the reduction in molecular weight resulting from beta-scission reactions induced by the peroxide. It is a well-established mechanism that segments of chains with lower molecular weights exhibit enhanced mobility leading to faster crystallization. (Su, 2010; Garcia, 2013)

It can also be clearly seen that T_c of all crosslinked samples shifted to higher values compared to the pure PP and PP reacted with peroxide. It was suggested by many authors that the presence of crosslinking points increases T_c by increasing the nucleation density of the PP melt leading to faster crystallization. (An, 2008; Wang, 1996) Another factor that could also contribute to the crystallization behavior is the silane grafting points that might have a nucleating effect. (Shieh, 2001) However, the second factor might not be influential here since UPTMS and GPTMS produced more grafting points compared to VTMS and ONTMS but their influence on T_c was not considerable unlike with VTMS and ONTMS. It

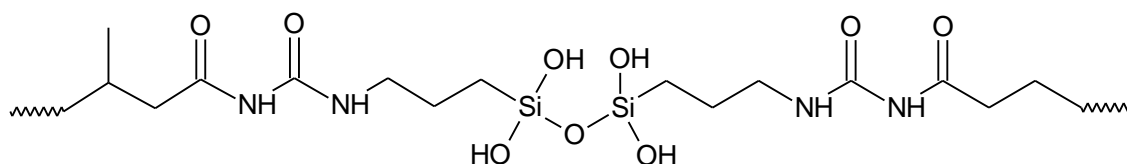
should be noted that the gel contents, the appearance of the peak at 1191 cm^{-1} in the FT-IR spectra of PP-g-UPTMS and PP-g-GPTMS and its absence in the FT-IR spectra of PP-g-VTMS and PP-g-ONTMS indicate that UPTMS and GPTMS were more grafted onto PP compared to the other two silanes.

Crystallization peak temperature (T_c) did not increase significantly with the silanes that reacted with terminal carboxylic acid groups in the oxidized PP, namely, AMPTMS, BTMSPA, UPTMS, and GPTMS. This could be due to the fact that the modification with these silanes requires more than two molecules to produce crosslinking points capable of inducing a nucleating effect. In this case, two molecules would produce an extended linear chain instead of a crosslinked chain as a result of hydrolysis and condensation reactions as can be seen below.

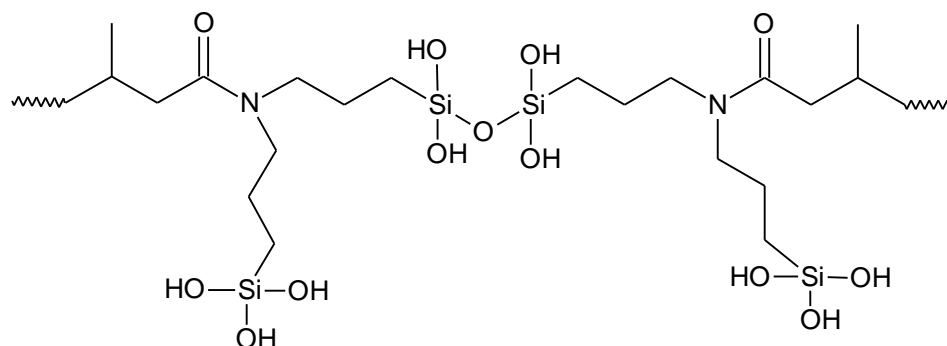
PP-g-AMPTMS



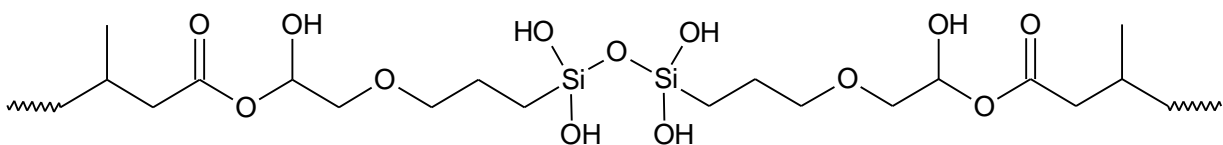
PP-g-UPTMS



PP-g-BTMSPA



PP-g-GPTMS



On the other side, VTMS and ONTMS produced PP crosslinked products with higher T_c although they generated less gel contents compared to the above four silanes. This behavior could be attributed to the topology of the crosslinked products. VTMS and ONTMS are able to produce crosslinked products with only two molecules as can be seen in Scheme 4.4 which shows a typical crosslinked product that would be obtained with VTMS, ONTMS, APTMS, VMMS, and Azido-silane. Such crosslinked products are capable of inducing a nucleation effect. Highly crosslinked products obtained with APTMS and Azido-silane exhibited the highest T_c 's as expected.

4.3.2 Soluble Materials

Figure 4.16 shows the T_c for APTMS, VMMS, VTMS, ONTMS, and Azido-silane systems before and after gel removal to visualize the influence of gel or crosslinked material on T_c and to see if there is any molecular structure changes within the soluble material. It was found that highly crosslinked samples with high gel contents produced soluble materials with slower crystallization, except with Azido-silane, as can be seen from the T_c values for the soluble materials of both APTMS-crosslinked PP and VMMS-crosslinked PP. The T_c of these samples shifted considerably to lower values after removing the gel portions. The difference in T_c was obvious in the case of APTMS-crosslinked PP where the soluble material had a T_c of 117⁰C which is lower than that of the sample containing the gel by 11⁰C.

The significant difference in T_c observed with these samples indicates that the soluble materials might have mostly linear and un-grafted chains since they gave T_c values close to that of the PP reacted with peroxide. As seen earlier by the FT-IR data and the high gel contents of these samples, they exhibited high grafting degrees causing probably most of the grafted chains to participate in the crosslinking reactions forming highly crosslinked chains which were not soluble in boiling xylene. This means that most of the grafted silane was

found within the gel. This explanation can be supported by what Parent et al. (2008) found as a result of the grafting reaction between atactic PP and triallyl trimesate (TAM). Using ^1H NMR, they found that the insoluble hyper-branched fraction contained most of the grafted allylic ester while the extracted fraction contained relatively small amounts.

This finding could indicate that the grafting with these methacryloxy (VMMS) and acryloxy (APTMS) silanes was not uniform resulting in multiple silane grafts in some chains. The non-uniform distribution could be a result of an intramolecular chain-transfer mechanism of grafting that left many other chains un-grafted and unable to form branching or crosslinking. Shing et al. (1995) investigated the grafting of 2-(di-methyl-amino)-ethyl methacrylate onto hydrocarbon substrates and found that intramolecular chain-transfer mechanism plays an important role in the grafting process. In addition, Parent et al. (2009) showed that the grafting of tri-methylol-propane-tri-acrylate (TMPTA) onto PP produced bimodal branching distributions.

Interestingly, the T_c drop after gel removal was not significant with Azido-silane. The fast crystallization rate of the soluble material here might indicate that most of the PP chains were grafted with the Azido-silane and the distribution of grafting was more uniform compared to APTMS and VMMS. Consequently, the faster crystallization could be attributed to the presence of soluble long chain branched chains within the soluble material. These chains are capable of inducing nucleation and thus increasing the crystallization rate. (Zhao, 2013; Su, 2010; Garcia, 2013; Wang, 1996)

Similarly, PP crosslinked with vinyl-silanes (VTMS and ONTMS) did not exhibit significant drop in T_c after gel removal. Again, the high T_c and fast crystallization observed with these soluble materials compared to the pure PP and PP reacted with peroxide could be mainly due to the nucleation effect induced by the presence of long chain branched chains in the soluble materials. Both samples produced low gel contents and the removal of the gel did not cause any significant drop in T_c as a result. The low number of grafted chains as revealed by the FTIR data was not enough to produce a considerable amount of highly crosslinked

material. Instead, most of the grafted chains were probably converted (after water treatment) to long chain branched chains that had a considerable nucleating effect.

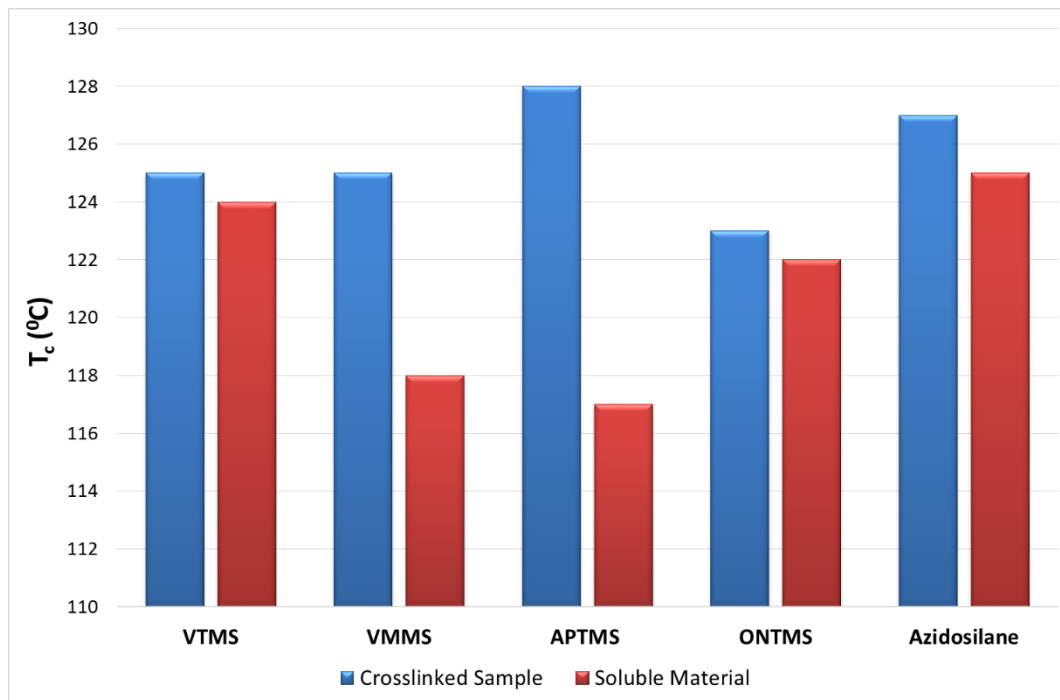


Figure 4.16 T_c for APTMS, VMMS, VTMS, ONTMS, and Azido-silane systems before and after gel removal

For further evidence, the soluble material of ONTMS-crosslinked PP was selected to be evaluated with Gel Permeation Chromatography (GPC) to determine its molecular weight and molecular weight distribution compared to the PP reacted with peroxide which was treated with the same amount of peroxide. However, the treatment here was carried out under nitrogen atmosphere since this sample was compared with ONTMS-crosslinked PP sample which was prepared under nitrogen atmosphere. It was found that nitrogen had a great influence on the molecular weight when treating PP with peroxide.

The weight-average molecular weight of the soluble material of ONTMS-crosslinked PP was found to be higher than that of the PP reacted with peroxide by 11% and the molecular weight distribution (indicated by PDI) was broader by almost 25% as can be seen in Table 4.2. Thus, this increase in molecular weight and the broader molecular weight distribution

indicate that the soluble material of ONTMS-crosslinked PP most probably contained long chain branched chains. Therefore, it can be said that the increase in T_c in this case was caused by the presence of some degree of branching in the soluble materials. The GPC data including the distribution curves for the soluble material of ONTMS-crosslinked PP and the PP reacted with peroxide can be found in the Appendix section.

Table 4.2 Mn, Mw, Mz, and PDI for the PP reacted with peroxide, and the soluble material of ONTMS-crosslinked PP

Sample	Mn (kg/mol)	Mw (kg/mol)	Mz (kg/mol)	PDI (Mw/Mn)
PP reacted with peroxide	72.36	259.71	609.80	3.59
ONTMS crosslinked PP*	64.58	289.08	770.01	4.48

***TCB-soluble material only, no gel.**

Finally, it is worth noting that El Mabrouk et al. (2009) used PP-g-VTES to produce long chain branched PP (LCB-PP) and verified the existence of long chain branches by GPC and rheology techniques. Those authors found that the soluble material of the sample with a very low gel content (0.1 wt.%) and low amount grafted VTES contained long chain branched chains. However, their sample with a higher gel content (12 wt.%) and higher amount of grafted VTES gave a soluble material with low molecular weight indicating that it contained fewer long chain branched chains or even only degraded linear chains. Using GPC and extensional viscosity measurement, Chaudhary et al. (2011) proved that VTMS-crosslinked PP with < 5 wt% gel contained long chain branches. Therefore, based on the literature and results produced here it can be concluded that long chain branched PP can be prepared with APTMS, VMMS, VTMS, and ONTMS by controlling the grafting reactions conditions to obtain grafted products with low gel contents.

4.4 Melt Properties

The melt properties of ONTMS-crosslinked PP and APTMS-crosslinked samples were selected and studied to evaluate the effect of silane grafting and crosslinking on the melt properties of lightly crosslinked PP (i.e. with low gel content). It was seen earlier that ONTMS-crosslinked PP (prepared with 0.20 wt.% peroxide) contained a gel amount of 2 wt.%. In order to prepare APTMS-crosslinked PP with low gel content, it was prepared with less amount of peroxide (0.02 wt.%) and as a result a gel content of ~5 wt.% was obtained.

4.4.1 Melt Flow Index (MFI)

It is well established that long chain branched chains and crosslinked chains dramatically influence the melt flow behavior of the modified polymer. The melt flow index (MFI) was determined for the pure PP, two PP samples reacted with two different levels of peroxide (0.20 wt.% and 0.020 wt.%) under nitrogen atmosphere, and the two crosslinked PP samples mentioned above (see Figure 4.17).

The MFI for the pure PP was found to be 3.0 g/10min. By adding a small quantity of peroxide (0.20 wt.%), the MFI increased to 5.21 g/10min. indicating a reduction in molecular weight caused by β -scission reactions induced by the peroxide. However, the MFI dropped from 5.21 to 3.21 g/10min. after the introduction of ONTMS into the system and after the crosslinking reactions. The reduction in MFI in this case indicates that the molecular weight increased which could be caused by the presence of crosslinked chains and long chain branched chains.

With regard to APTMS-crosslinked PP, PP reacted with 0.020 wt.% was used as a control sample that was prepared under the same conditions except that APTMS was not added along with the peroxide. The addition of only 0.02 wt.% peroxide caused the MFI to increase slightly from 3.0 to 4.36 g/10min. It should be noted that all samples tested here were prepared under nitrogen atmosphere. It was observed that the absence of nitrogen during the reaction leads to substantial increase in MFI. A dramatic drop in the MFI to 0.95 g/10min. was seen after crosslinking the PP with APTMS in the presence of 0.020 wt.% peroxide. This

reduction in MFI shows a significant increase in the molecular weight which was most probably caused by the presence of the gel portion (~5 wt.%).

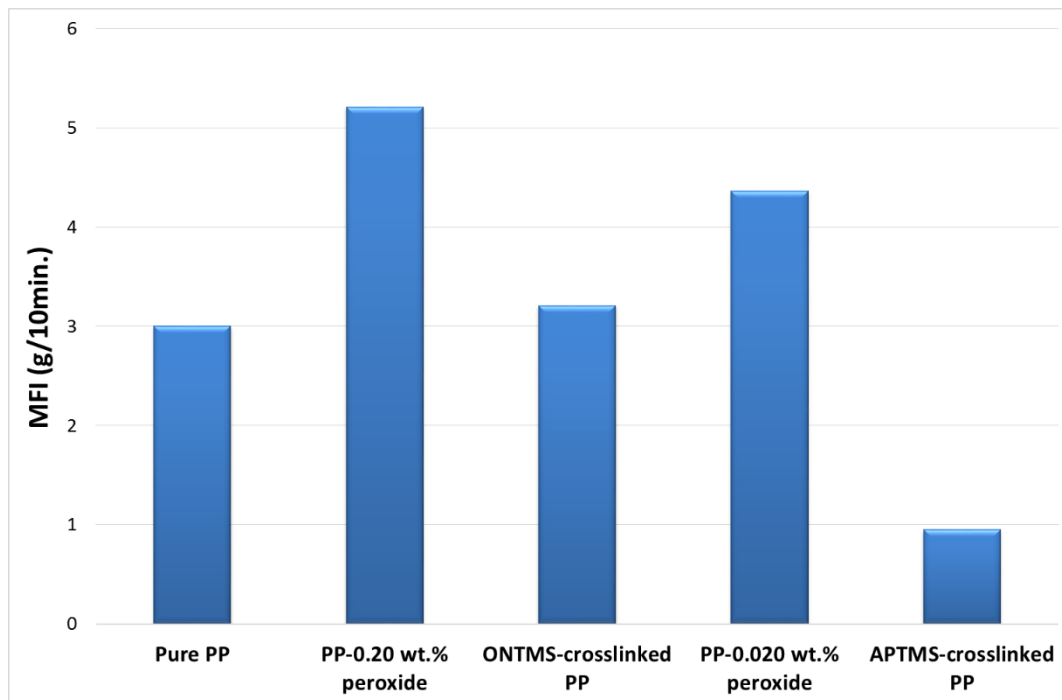


Figure 4.17 Melt flow Index (MFI) of pure PP, PP reacted with two levels of peroxide, ONTMS-crosslinked PP (0.20 wt.% peroxide), and APTMS-crosslinked PP (0.020 wt.% peroxide)

4.4.2 Melt Rheological Properties

Oscillatory shear rheology is sensitive to structural changes in PP chains. Dynamic oscillatory measurements were carried out for the pure PP, ONTMS-crosslinked PP, APTMS-crosslinked PP, and PP reacted with 0.20 wt.% peroxide. Different rheological plots are presented below to demonstrate the effect of silane grafting and crosslinking on the linear viscoelastic properties of lightly crosslinked PP (≤ 5 wt.% gel).

Figure 4.18 presents the plot of complex viscosity (η^*) versus angular frequency. The rheological behaviour of the pure PP and PP reacted with peroxide is consistent with that of linear polymers since they exhibited the presence of Newtonian plateau at low frequency where complex viscosity is independent of frequency. When only peroxide was added to PP,

the complex viscosity dropped at all frequencies and the Newtonian region became broader indicating that the molecular weight decreased as a result of β -scission reactions induced by the peroxide. This behavior is well known in the literature. (Tian, 2006; Su, 2011) The drop in viscosity was not very significant because the treatment of PP melt with the peroxide was carried out under nitrogen atmosphere as stated earlier.

After the addition of ONTMS to the system and carrying out the crosslinking reactions, the complex viscosity at low frequency became higher than that of PP reacted with the same amount of peroxide (0.20 wt.%) indicating that more chain entanglements and a higher molecular weight were formed. In addition, no Newtonian plateau can be seen with this sample and its shear thinning behaviour started at lower frequency. It can be seen also that the complex viscosity became slightly smaller at high frequency. The behaviour of this sample at low frequency can be ascribed mainly to the low amount of highly crosslinked material (gel) present in the sample (2 wt.%) which could create sufficient chain entanglements and in turn increase the complex viscosity at low frequency. (Parent, 2009)

The presence of higher amount of gel in APTMS-crosslinked PP sample caused the complex viscosity to apparently exceed that of the pure PP at low frequency where the relaxation behaviour governs the viscosity. Moreover, the influence of the chain entanglements effects imposed by the gel fraction was clear that, compared to all other samples, the shear thinning regime started at lower frequency and the Newtonian plateau was not evident.

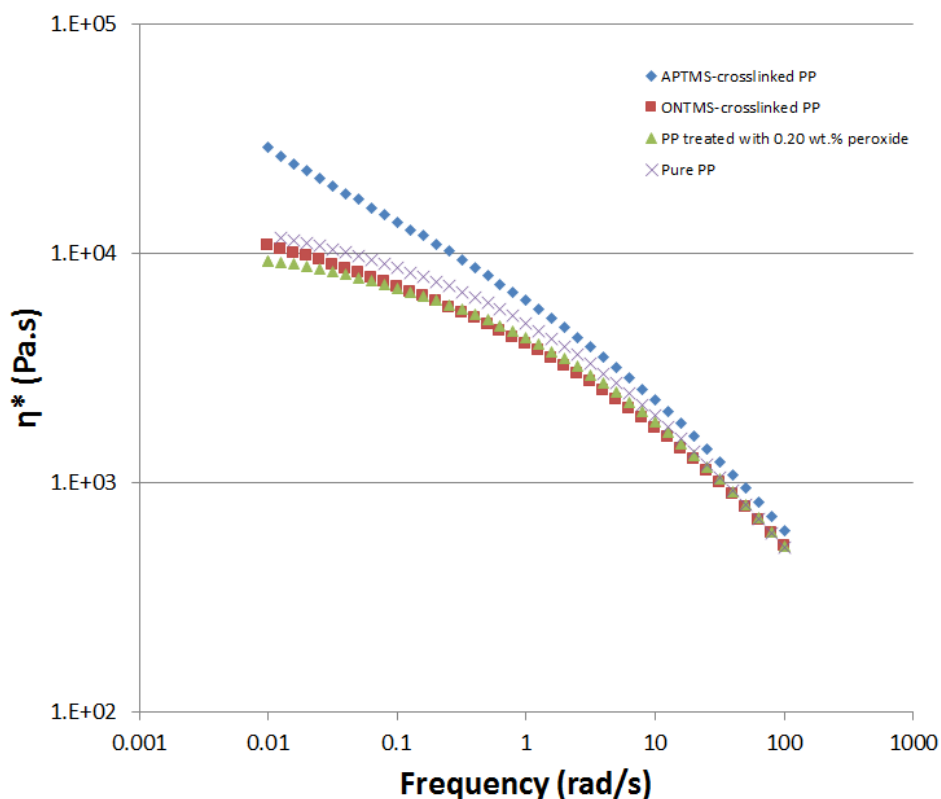


Figure 4.18 Complex viscosity (η^*) versus angular frequency of the pure PP, PP reacted with 0.20 wt.% peroxide, ONTMS-crosslinked PP (0.20 wt.% peroxide), and APTMS-crosslinked PP(0.020 wt.% peroxide) at 180°C

The storage modulus (G') of the above four samples plotted as a function of the angular frequency is shown in Figure 4.19. The storage modulus is more sensitive to the molecular structure changes of macromolecules. At low frequency, the longest relaxation time is the only factor contributing to the viscoelastic behavior. Linear viscoelastic polymers exhibit a typical terminal behavior at low frequency where the storage modulus (G') scales with ω^2 . (Li, 2009) This typical terminal behavior can be seen clearly for the pure PP and PP reacted with peroxide indicating that their chain structure is linear. A slight increase in the terminal slope of G' and a lower G' value can be seen in the terminal zone for the PP reacted with peroxide compared to the pure PP. This confirms the reduction in molecular weight induced by the peroxide leading to a less elastic polymer.

After crosslinking PP with ONTMS, it can be seen that ONTMS-crosslinked sample deviated from the above mentioned terminal behavior. G' value at low frequency increased significantly while the terminal slope decreased which indicates a higher level of elasticity compared to the pure PP and PP reacted with peroxide. This behavior in the terminal zone suggests that there was a longer relaxation time which can be ascribed to the chain entanglements induced by the crosslinked material (2 wt.%) present in this sample. This behaviour has also been reported elsewhere. (Romani, 2002) The deviation from the terminal behavior became more distinct with APTMS-crosslinked PP. This sample exhibited a dramatic increase in the value of G' at low frequency. The presence of the 5 wt.% gel material within this sample is believed to be responsible for this clear elastic response and the higher elasticity of this material.

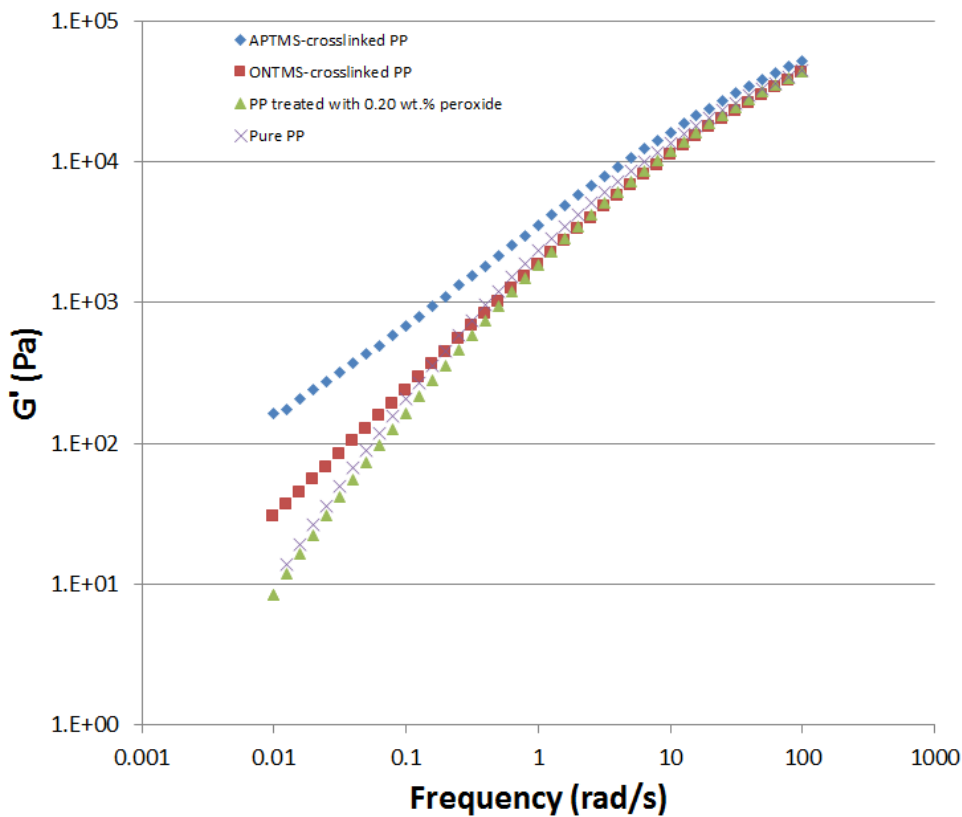


Figure 4.19 Storage modulus (G') versus angular frequency of the pure PP, PP reacted with 0.20 wt.% peroxide, ONTMS-crosslinked PP (0.20 wt.% peroxide), and APTMS-crosslinked PP (0.020 wt.% peroxide) at 180°C

Further insight into the viscoelastic behavior can be gained from the plot of $\tan \delta$ as a function of sweeping frequency. $\tan \delta$ is defined as the ratio of G'' (the loss modulus) to G' (the storage modulus) and it can be used to indicate melt elasticity of a polymer. Figure 4.20 displays the $\tan \delta$ curves for all four samples. $\tan \delta$ curves of the pure PP and PP reacted with peroxide showed higher values of $\tan \delta$ at low frequency. They also exhibited a rapid decrease with frequency increasing. This behavior is typical for linear polymers; similar results for the behavior of unmodified PP and PP reacted with peroxide were obtained by Su and Huang (2010). Here, the $\tan \delta$ of ONTMS-crosslinked PP was lower at low frequency indicating a higher elastic response and longer relaxation time. The elastic response was more obvious with APTMS-crosslinked PP where $\tan \delta$ is much lower than that of ONTMS-crosslinked PP. It is clear from these findings that the crosslinked materials increased the melt elasticity of these two samples.

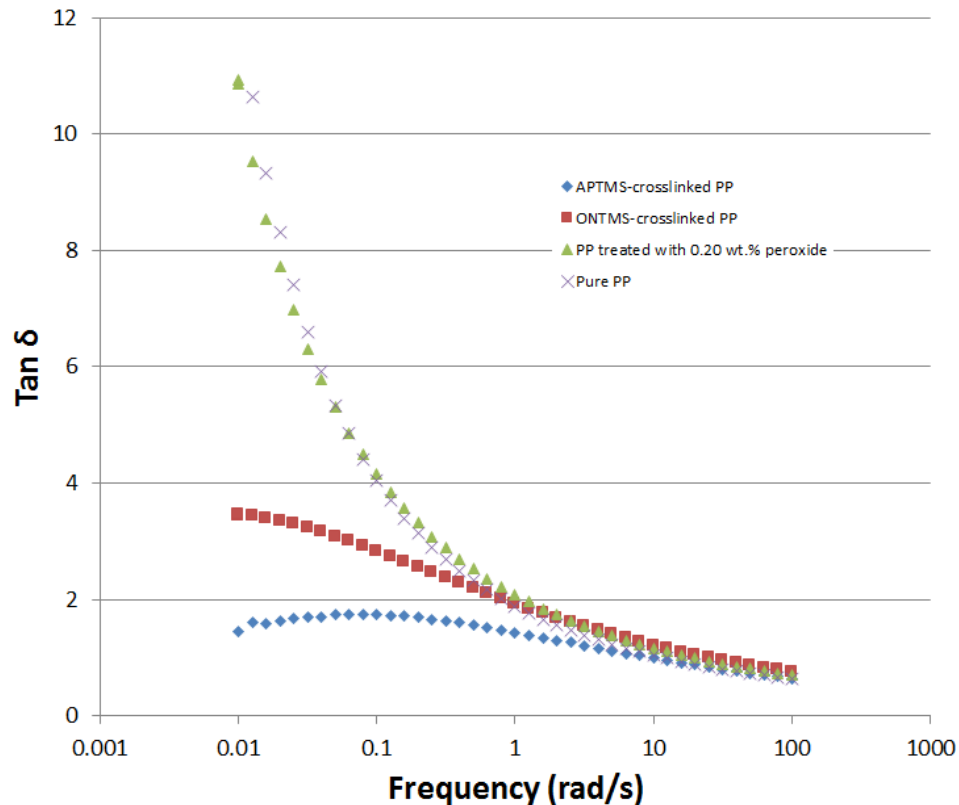


Figure 4.20 $\tan \delta$ versus angular frequency of the pure PP, PP reacted with 0.20 wt.% peroxide, ONTMS-crosslinked PP (0.20 wt.% peroxide), and APTMS-crosslinked PP (0.020 wt.% peroxide) at 180°C

Figure 4.21 presents the out of phase viscosity (η'') as a function of in phase viscosity (η') for the tested samples. This kind of plot is known as the Cole-Cole plot. The Cole-Cole plots for the pure PP and PP reacted with peroxide exhibited almost a semicircle shape reflecting their linear structure. The decrease in radius of the plot of the PP reacted with peroxide was a result of its lower molecular weight compared to the pure PP. The long relaxation mechanism caused by the presence of crosslinked materials can be seen clearly in the Cole-Cole plots of ONTMS-crosslinked PP and APTMS-crosslinked PP. These plots exhibited upturning at high viscosity which corresponds to low frequency and the effect was more obvious with APTMS-crosslinked PP. (Zhang, 2012)

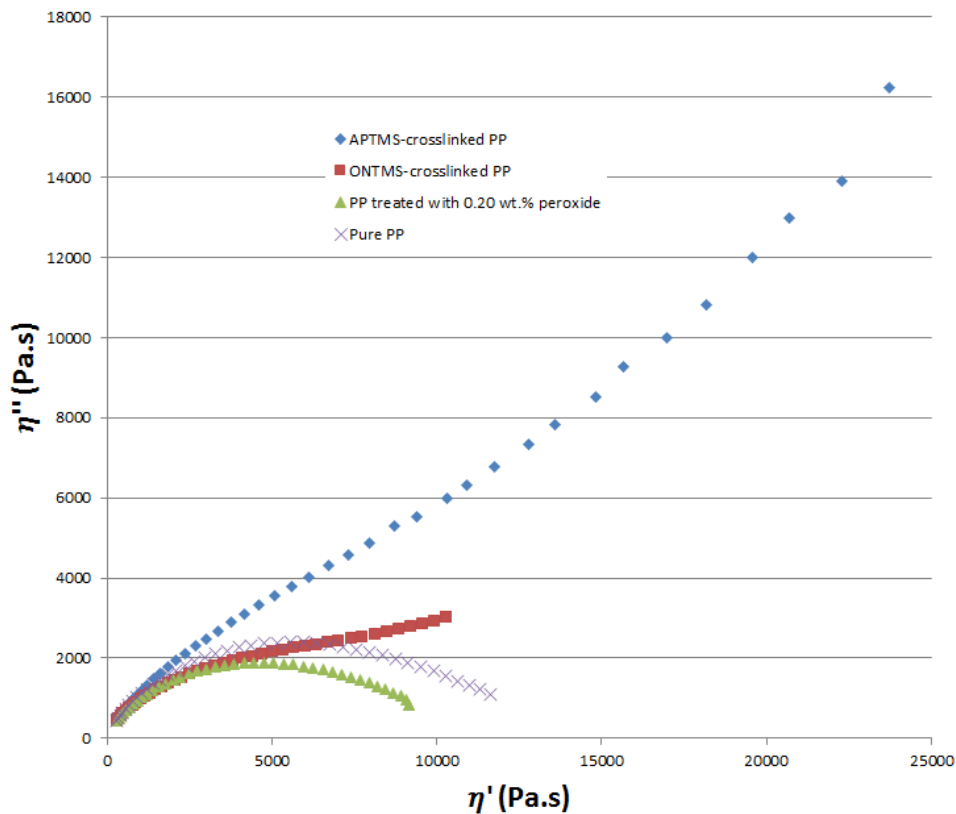


Figure 4.21 Cole-Cole plot of the pure PP, PP reacted with 0.20 wt.% peroxide, ONTMS-crosslinked PP (0.20 wt.% peroxide), and APTMS-crosslinked PP (0.020 wt.% peroxide) at 180°C

Chapter 5

Results and Discussions: Influence of PP Grafted with Silane on Mechanical Properties of Wood-fiber/PP Composites

The main objective of this chapter was to study the influence of PP grafted with silane on the mechanical properties of wood-fiber/PP composites. Two different PP-g-silane samples were selected, namely, PP-g-APTMS and PP-g-Azidosilane since they haven't been studied before and they had the highest grafting degrees as revealed by the results in Chapter 4. High concentration of grafted silane was expected to have a clear impact on the mechanical properties of the composites. Moreover, PP-g-Azidosilane was compared with PP-g-APTMS since it was expected to have more uniform distribution of silane grafts as explained previously in Chapter 4. Wood fibers were used here to evaluate its impact on the mechanical properties of PP with and without coupling agents. The mechanical properties measured in this study were tensile strength and modulus, elongation at break, flexural strength and modulus, and Izod impact strength.

5.1 Influence of PP-g-APTMS

Five different formulations were prepared and summarized in Table 5.1.

Table 5.1 Wood-fiber/PP composites prepared with different PP-g-APTMS concentrations

Sample	PP Concentration (wt.%)	Wood fiber Concentration (wt.%)	PP-g-APTMS Concentration (wt.%)
PP	100	0	0
C0	70	30	0
C1	69	30	1
C2	68	30	2
C3	65	30	5

PP-g-APTMS was added to the wood-fiber/PP composites in three different concentrations to study its influence on the mechanical properties of the composites. Table 5.2 shows the mechanical testing results obtained.

Table 5.2 Tensile strength and modulus, elongation at break, flexural strength and modulus, and IZOD impact strength of pure PP and wood-fiber/PP composites (Note: the values inside the brackets indicate the standard deviations)

Sample	Tensile Strength (MPa)	Tensile Modulus (MPa)	Elongation at Break (%)	Flexural Strength (MPa)	Flexural Modulus (MPa)	IZOD Impact Strength (J/m)
PP	40.66	172.12	263.08	50.72	1224.83	49.60
	(0.40)	(7.80)	(55.6)	(2.43)	(174.62)	(4.55)
C0	36.90	211.58	15.93	51.07	2093.83	41.54
	(0.45)	(22.88)	(1.40)	(1.51)	(105.56)	(1.45)
C1	38.26	294.11	13.44	55.23	2299.00	36.26
	(1.74)	(42.11)	(1.10)	(1.09)	(188.27)	(1.85)
C2	41.65	320.70	13.48	59.10	2256.17	33.77
	(2.95)	(31.19)	(1.50)	(1.08)	(70.90)	(2.18)
C3	46.81	344.57	14.24	69.03	2387.33	35.16
	(3.50)	(42.95)	(8.00)	(0.67)	(148.45)	(2.12)

5.1.1 Tensile Strength

The effect of PP-g-APTMS and its concentration on the tensile strength of polypropylene composites was studied and the results obtained are shown in Figure 5.1. The incorporation of wood fibers into the PP matrix without any coupling agent reduced the tensile strength from 40.66 MPa to 36.90 MPa. This behavior can be attributed to the weak interfacial adhesion and bonding strength caused by the poor compatibility between the PP matrix and the wood fibers. Wood fiber is not compatible with PP because it is hydrophilic whereas PP is a hydrophobic polymer. Gaps or micro-voids can be created by the poor adhesion and lead

to little stress transfer from the PP matrix to the wood fibers at the interface during the tensile test. As a result, it is easier for the composite to break under stress. In this case, the wood fiber did not reinforce PP but instead it behaved as a filler. The observed decrease in the tensile strength of the uncoupled wood/fiber/PP composite following the is in agreement with previous studies (Bouza, 2009; Kim, 2011)

However, the addition of 1.0 wt.% of PP-g-APTMS to the formulation increased the tensile strength to 38.26 MPa. With 2.0 wt.% of PP-g-APTMS, the tensile strength of the composite (41.65 MPa) exceeded that of the pure PP (40.66 MPa). Further increase in the concentration of PP-g-APTMS to 5.0 wt.% caused a significant increase in tensile strength up to 46.81 MPa. The improvement in tensile strength of the composite as a result of the addition of the polymeric coupling agent can be attributed to the improved chemical compatibility between the wood fibers and the PP matrix. Strong interactions are expected to be established between the wood fibers and the PP matrix. The hydroxyl groups on the surface of the wood fibers can interact chemically with the silanol groups (-Si-OH) or physically with the siloxane groups (-Si-O-Si-) in PP-g-APTMS whereas the PP chains in the PP matrix can interact with the PP chains in PP-g-APTMS. These strong interactions can therefore significantly improve the adhesion between the two components of the composite and lead to effective load transfer from the PP matrix to the wood fibers. Therefore, the fiber strength can be effectively utilized. (Xie, 2010; Natchtigall, 2007)

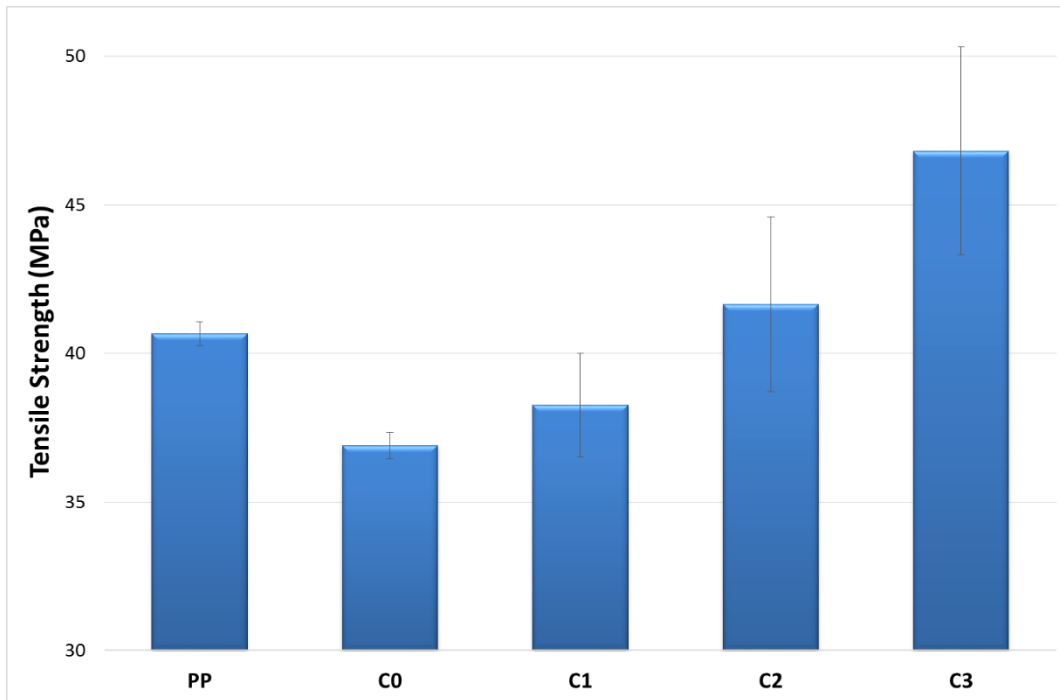


Figure 5.1 Tensile strength of PP and wood-fiber/PP composites at different PP-g-APTMS concentrations

5.1.2 Tensile Modulus

It can be seen in Figure 5.2 that all composites exhibited remarkably higher tensile moduli compared to the pure PP. It is known that filler modulus is one of the main factors that affect the modulus of the composite (Ansari, 2009; Girone`s, 2007). Thus, the higher modulus of the wood fibers compared to the pure PP can be responsible for the increase in tensile modulus after incorporating the wood fibers into PP matrix without any coupling agent. In addition, the much stiffer wood fibers have the capability to restrict the mobility of the PP matrix chains and thus impart rigidity to the composite (Arbelaiz, 2005). The improvement in tensile modulus indicates also the presence of some degree of adhesion between the wood fibers and the PP matrix. The modulus of the composite is related to its stiffness before fracture (at small deformations) and its value is obtained from the slope of the straight line in the stress-strain curve. Therefore, the adhesion, even if it is poor, can improve the stiffness and tensile modulus of the composite. However, it was seen earlier that the adhesion was not enough to improve the tensile strength. This can be explained by the fact that the tensile

strength of the composite is caused by the composite break at the weakest point of the material and this point might occur below the PP matrix strength if the adhesion between the two components fails at a lower stress. This explains why the tensile modulus increased whereas the tensile strength decreased. (Abu-Sharkh, 2004)

A further increase in the tensile modulus can be seen after the addition of PP-g-APTMS. In the case of small strains, the tensile modulus reflects the ability of the PP matrix and the wood fibers to transfer elastic deformation. In the elastic zone, the deformation capacity of the PP matrix can be restricted because of the improved adhesion with the wood fibers resulting in higher tensile modulus. (Demir, 2006) Therefore, the increase in tensile modulus in this case can be attributed to the improved adhesion between the PP matrix and the wood fiber by the chemical interactions explained above. This can be supported by the progressive increase in the tensile modulus with the increase in the concentration of PP-g-APTMS in the composites. However, the low equilibrium torque observed during the preparation of PP-g-APTMS indicates that this coupling agent had a low molecular weight. Therefore, the addition of PP-g-APTMS might help in increasing the stiffness of the composites.

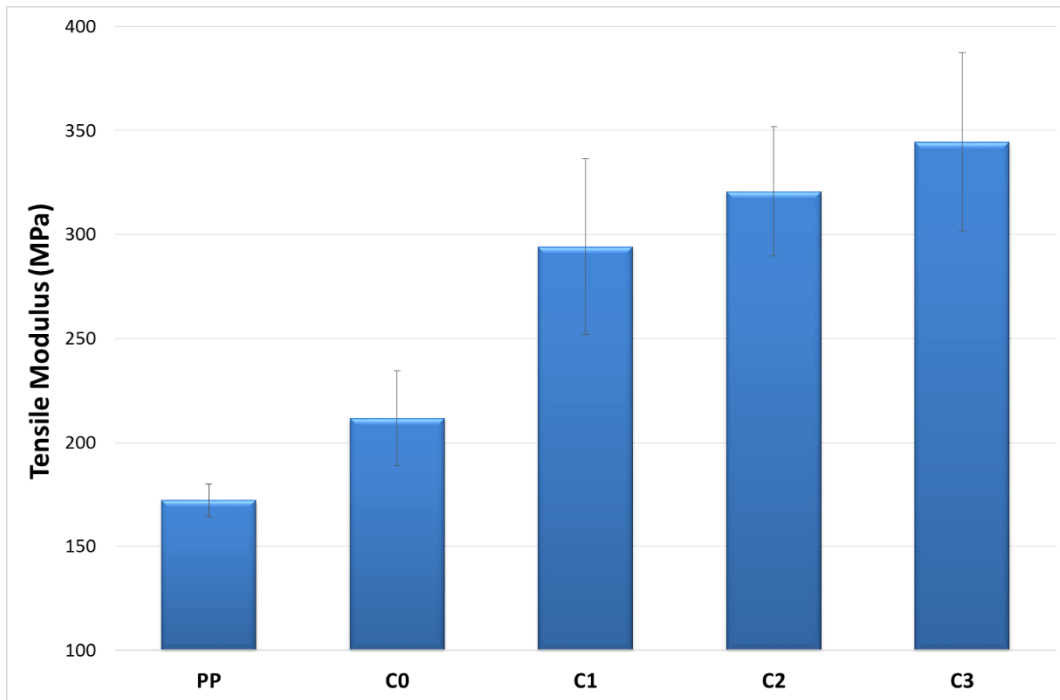


Figure 5.2 Tensile modulus of PP and wood-fiber/PP composites at different PP-g-APTMS concentrations

5.1.3 Flexural Strength

Figures 5.3 shows the effect of the wood fibers and PP-g-APTMS on the flexural strength of Wood-fiber/PP composites. The addition of only wood fibers did not significantly improve the flexural strength of the composite. The existence of a strong interface between the wood fibers and the PP matrix is required to develop flexural strength in the composite. Therefore, it can be said that the weak interfacial adhesion caused by the incompatibility between the wood fibers and the PP matrix was not sufficient to increase the flexural strength of the composite. However, the composite became less flexible and more rigid after the addition of PP-g-APTMS as indicated by the increase in flexural strength. In addition, the clear progressive improvement in the flexural strength with the increase in PP-g-APTMS indicates clearly that the addition of PP-g-APTMS improved the interaction and interfacial adhesion between the wood fibers and the PP matrix. The addition of 5 wt.% of PP-g-APTMS increased the flexural strength by 36% in comparison with the pure PP. (Kim, 2011)

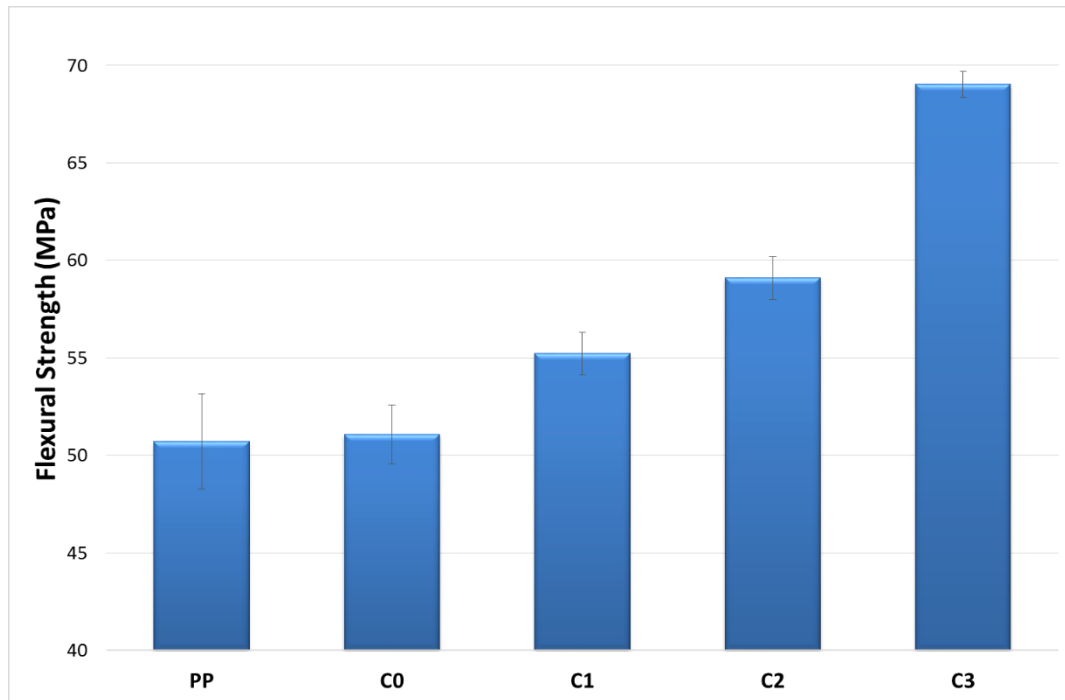


Figure 5.3 Flexural strength of PP and wood-fiber/PP composites at different PP-g-APTMS concentrations

5.1.4 Flexural Modulus

Flexural moduli of pure PP and its composites are presented in Figure 5.4. The flexural modulus of the PP composite increased considerably upon the incorporation of the wood fiber without PP-g-APTMS. It is well known that incorporation of rigid particles significantly improves the stiffness of wood-fiber/PP composites. (Abu Bakar, 2010) It can also be seen that the addition of the polymeric coupling agent PP-g-APTMS and increasing its concentration caused further improvements in the flexural modulus of the composites. The enhanced adhesion and interaction between the wood fibers and the PP matrix caused by addition of PP-g-APTMS might be the cause of the improved flexural modulus of the composites. (Ansari, 2009) However, it has been suggested that adhesion is not so influential at low strains at which flexural modulus is measured. Another factor that could improve the stiffness of the composite is the improved crystallinity that could be attained with the addition of the low molecular weight coupling agent PP-g-APTMS. (Sobczak, 2014)

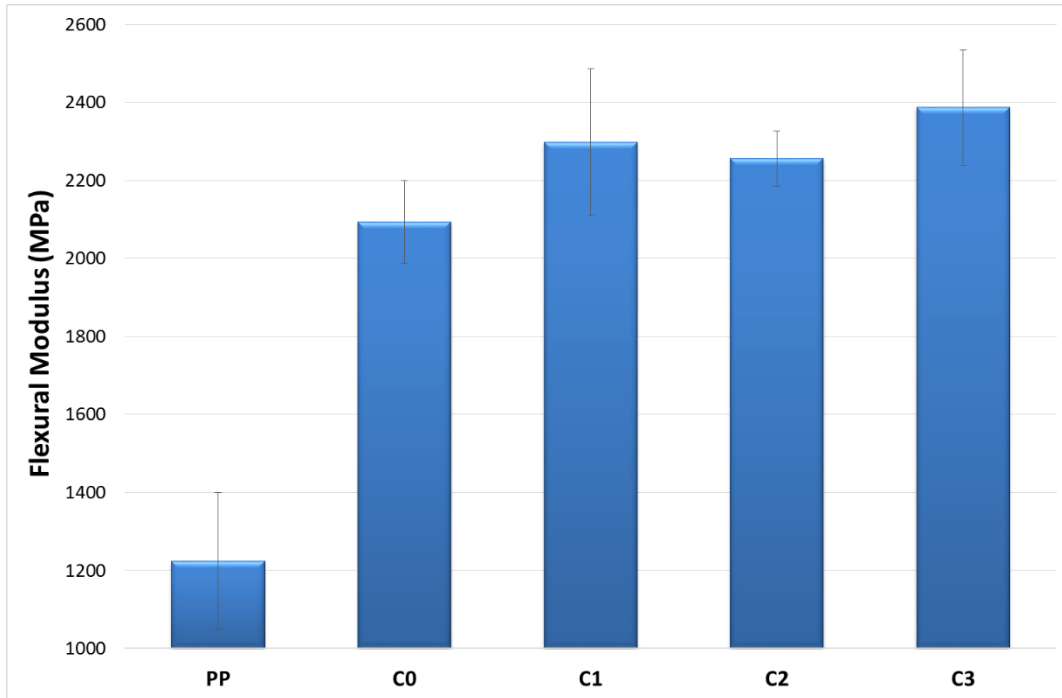


Figure 5.4 Flexural modulus of PP and wood-fiber/PP composites at different PP-g-APTMS concentrations

5.1.5 Impact Strength

Impact tests were carried out to study the mechanical behavior of the PP and its composites during a fast strike. It can be seen from Figure 5.5 that the impact strength of the PP matrix decreased significantly upon adding the wood fibers. This reduction in impact strength can be explained by the fact that the rigid wood fibers can restrict the mobility of the PP matrix chains and limit their capability to deform easily. Hence, the ability of the composite to absorb the impact energy during the crack propagation is reduced and as a result the ductility of the composite is expected to decline. In addition, the poor interfacial bonding between the wood fibers and the PP matrix may induce the formation of micro-voids and micro-cracks between the wood fibers and the PP matrix and create a micro-crack propagation during the impact test.

It can be seen from the figure that the incorporation of the polymeric coupling agent decreased the impact strength further. According to literature, an optimum bonding level between the fibers and the matrix is recommended to achieve good impact strength

(Nourbakhsh, 2008). It was also hypothesized that a slightly weaker adhesion is desirable for high impact strength. This slightly weaker adhesion results in consuming some of the impact energy to support the fiber pull-out whereas strong adhesion leads to rapid fiber fracture with less consumption of impact energy. (Karmarkar, 2007) Therefore, the bonding level in the composites coupled with PP-g-APTMS might be high enough to stiff the PP matrix chains and thus decrease the impact strength of the composites. The variations in the concentration of PP-g-APTMS did not practically affect the impact strength if the standard deviations are considered.

Another reason for the further reduction of the impact strength might be the low molecular weight of PP-g-APTMS. This might adversely affect the impact strength of the composite if PP-g-APTMS is incorporated in the composite. Ichazo et al. (2001) used two types of polymeric coupling agents (PP-g-MA) to prepare wood flour/PP composites and found that the coupling agent with low molecular weight gave a composite with a lower impact strength value. The authors attributed that to the low molecular weight of this coupling agent.

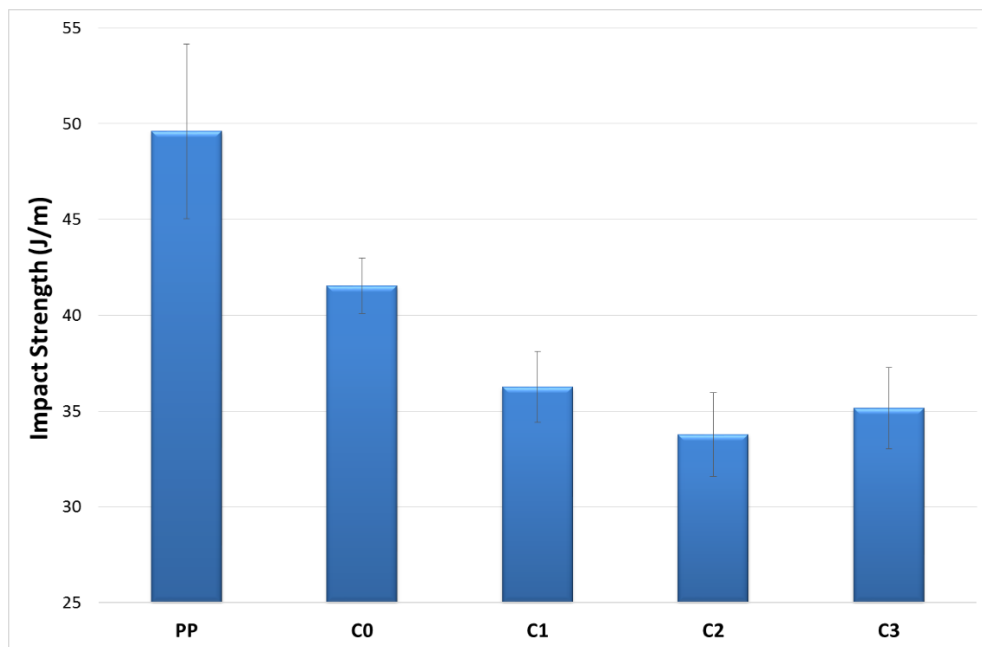


Figure 5.5 Impact strength of PP and wood-fiber/PP composites at different PP-g-APTMS concentrations

5.1.6 Elongation at break

The effect of wood fibers and APTMS-g-PP introduction into PP on elongation at break is shown in Figure 5.6. The elongation at break exhibited a sharp decrease from 263 % to almost 16 % after incorporating the wood fibers into the PP matrix. Similar behavior was observed by many researchers after the addition of natural fibers into PP (Demir, 2006; Bouza, 2009). This steep drop in elongation at break of the composite was most probably due to the less ductility and higher modulus of wood fibers which can in turn restrict the deformation of the PP matrix chains.

The figure shows also that the elongation at break of the composites decreased slightly after incorporating PP-g-APTMS. In addition, the variation of PP-g-APTMS content in the composite had no significant impact on the elongation at break. The slight drop observed with the addition of PP-g-APTMS could be ascribed to the improved stiffening and improved adhesion attained between the wood fibers and the PP matrix.

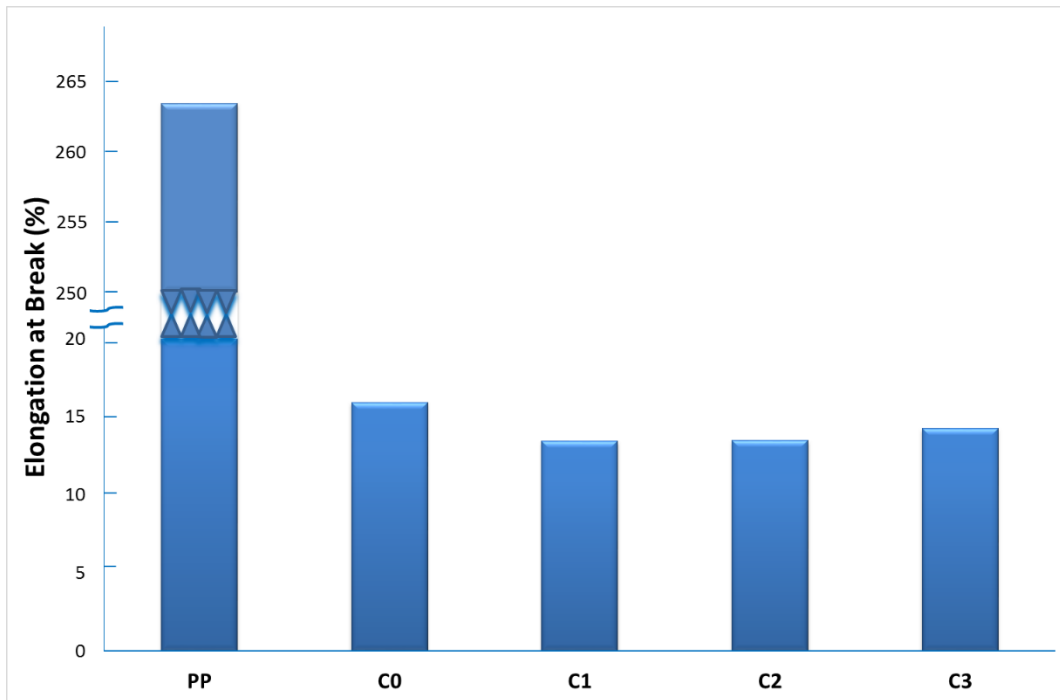


Figure 5.6 Elongation at break of PP and wood-fiber/PP composites at different PP-g-APTMS concentrations

5.2 Influence of PP-g-Azidosilane

PP-g-Azidosilane was added in one concentration to the wood-fiber/PP composite to study its effect on the mechanical properties. Its performance was also compared with PP-g-APTMS. The formulations studied here are presented in Table 5.2 and the results obtained are shown in Table 5.3 and Figures 5.7 to 5.11.

Table 5.3 Wood-fiber/PP composites prepared without coupling agent, with PP-g-Azidosilane, and with PP-g-APTMS

Sample	PP Concentration (wt.%)	Wood fiber Concentration (wt.%)	Coupling agent Concentration (wt.%)
Non-coupled Composite	70	30	0
Composite coupled with PP-g-Azidosilane	65	30	5
Composite coupled with PP-g-APTMS	65	30	5

Table 5.4 Tensile strength and modulus, flexural strength and modulus, and IZOD impact strength of different wood-fiber/PP composites (Note: the values inside the brackets indicate the standard deviations)

Sample	Tensile Strength (MPa)	Tensile Modulus (MPa)	Flexural Strength (MPa)	Flexural Modulus (MPa)	IZOD Impact Strength (J/m)
Non-coupled Composite	36.90 (0.45)	211.58 (22.88)	51.07 (1.51)	2093.83 (105.56)	41.54 (1.45)
Composite coupled with PP-g-Azidosilane	39.12 (1.24)	255.57 (21.41)	53.68 (1.49)	2280.00 (113.47)	38.59 (3.10)
Composite coupled with PP-g-APTMS	46.81 (3.50)	344.57 (42.95)	69.03 (0.67)	2387.33 (148.45)	35.16 (2.12)

The addition of 5 wt.% PP-g-Azidosilane into the composite improved the mechanical properties compared to the non-coupled wood-fiber/PP composite (except the impact

strength). However, the improvement was less in comparison with 5 wt.% PP-g-APTMS. The level of adhesion in the case of PP-g-Azidosilane seems to be not as good as in the case of PP-g-APTMS although it contained more silane grafts. It was seen earlier in Chapter 4 that PP-g-Azidosilane contained more siloxane groups (Si-O-Si) compared to PP-g-APTMS as revealed by the FT-IR analysis. Furthermore, PP-g-APTMS used in composites preparation was prepared with less amount of peroxide (0.10 wt.%) compared to the one analyzed by FT-IR. This might indicate that the concentration of the silanol groups (Si-OH) available for reaction with the fibers was less in the case of PP-g-Azidosilane compared to PP-g-APTMS since some of them were converted to siloxane groups. The siloxane groups may form hydrogen bonds with the hydroxyl groups in the wood fibers. However, the influence of these physical bonds is not as strong as the chemical covalent bonds resulting from the reaction between the silanol groups and the hydroxyl groups in the wood fibers. As a result, the adhesion is expected to be improved to less extent in this case.

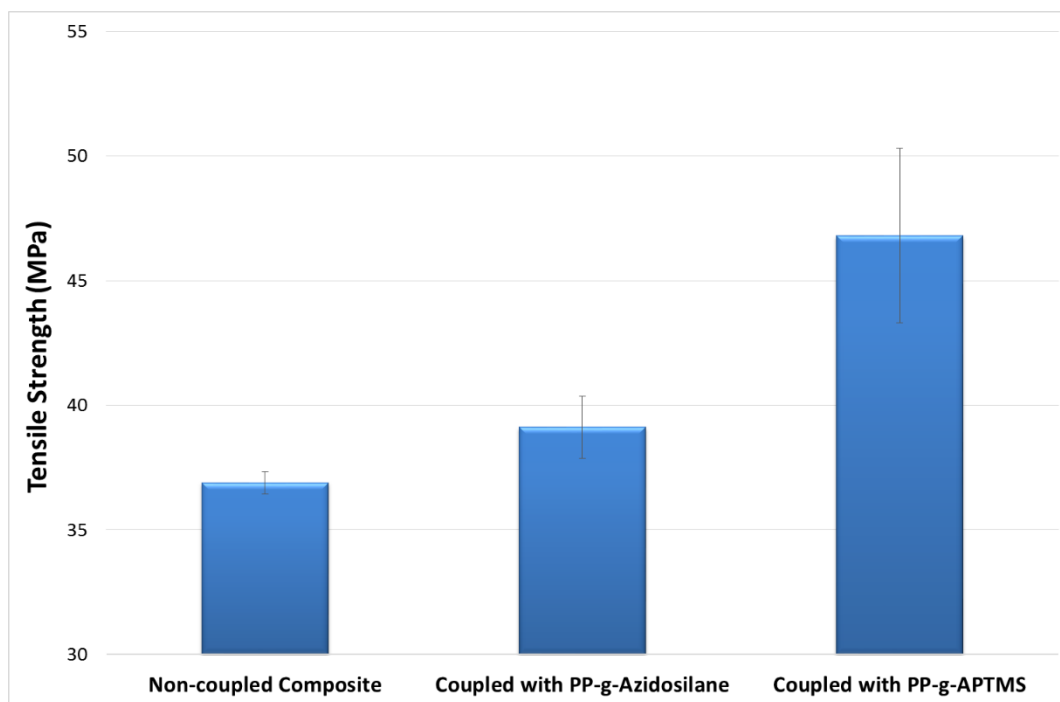


Figure 5.7 Tensile strength of the non-coupled composite, and composites coupled with PP-g-Azidosilane and PP-g-APTMS (both at 5 wt.%)

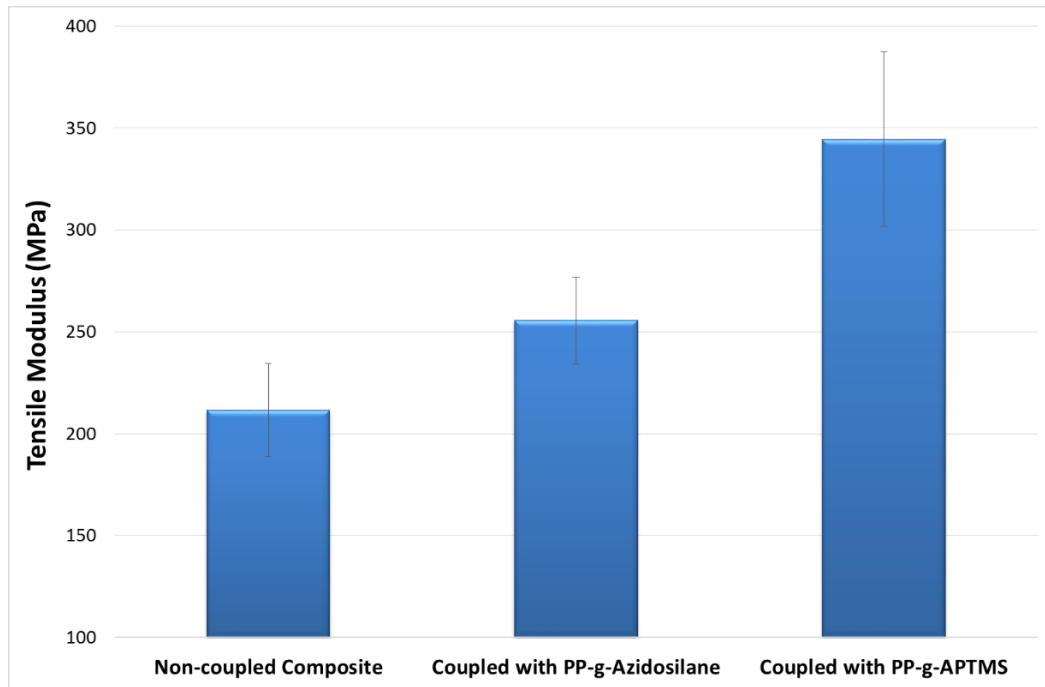


Figure 5.8 Tensile modulus of the non-coupled composite, and composites coupled with PP-g-Azidosilane and PP-g-APTMS (both at 5 wt.%)

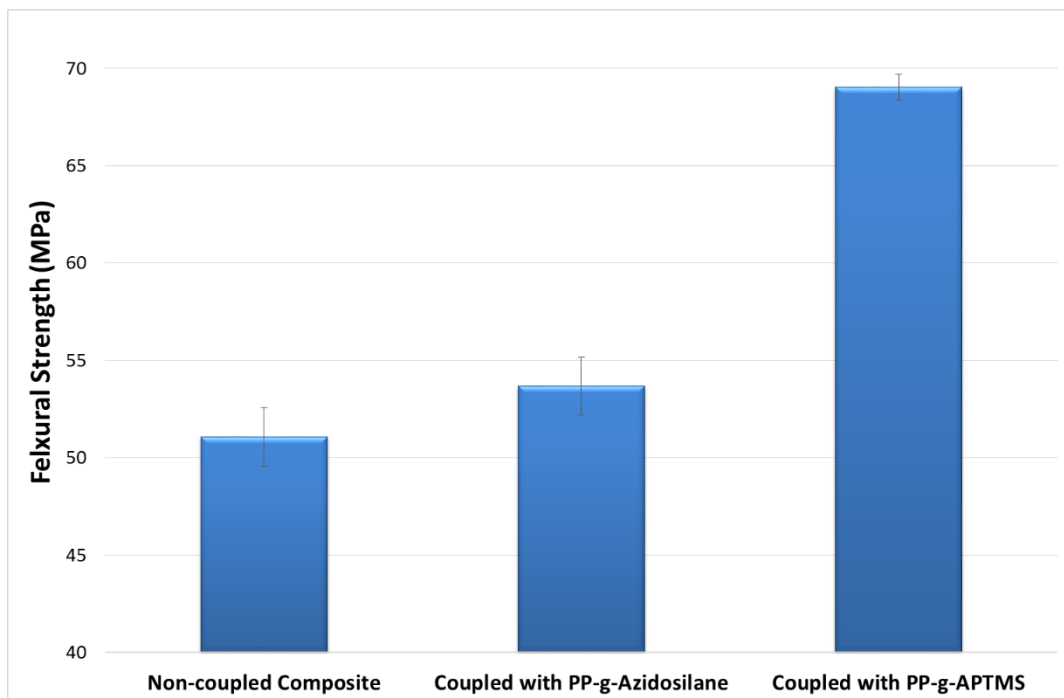


Figure 5.9 Flexural strength of the non-coupled composite, and composites coupled with PP-g-Azidosilane and PP-g-APTMS (both at 5 wt.%)

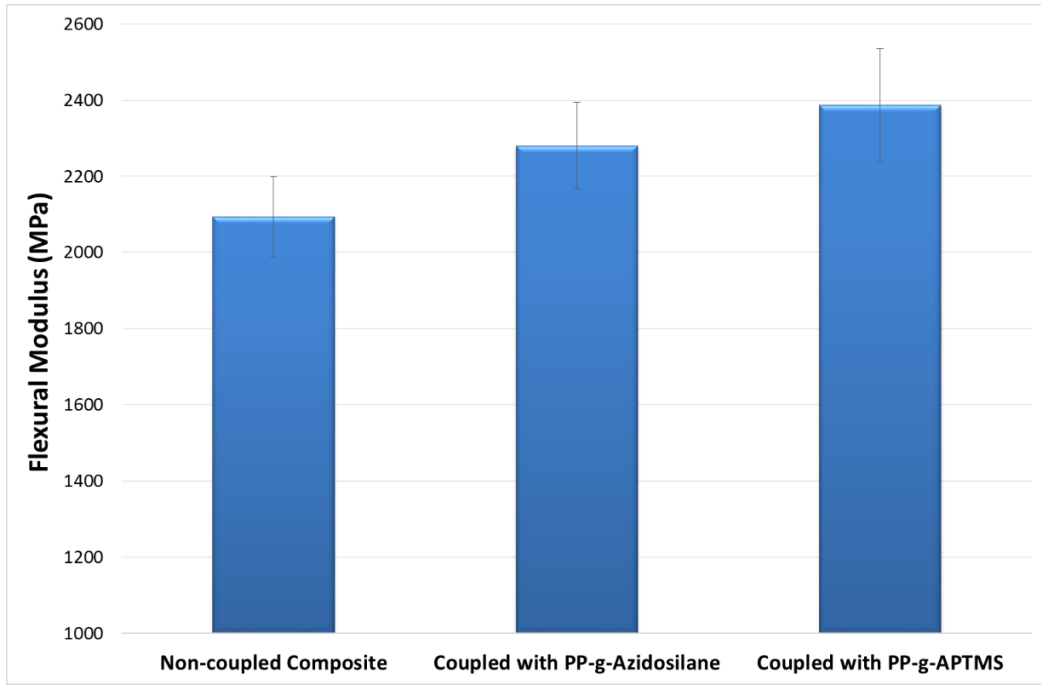


Figure 5.10 Flexural modulus of the non-coupled composite, and composites coupled with PP-g-Azidosilane and PP-g-APTMS (both at 5 wt.%)

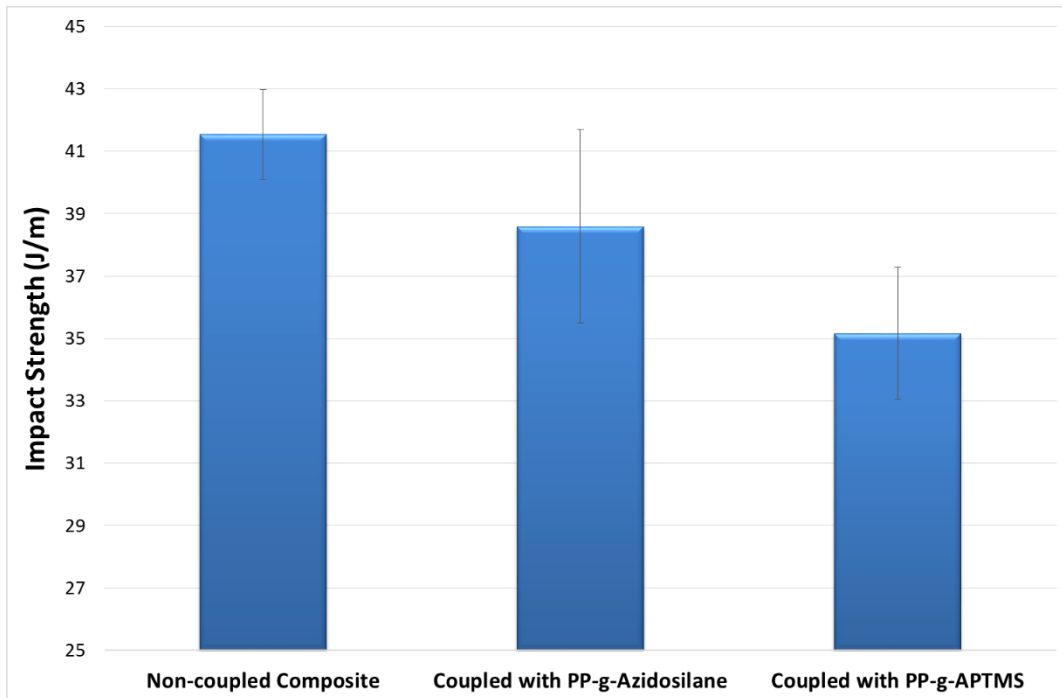


Figure 5.11 Impact strength of the non-coupled composite, and composites coupled with PP-g-Azidosilane and PP-g-APTMS (both at 5 wt.%)

Chapter 6

Conclusions and Recommendations

A polypropylene homopolymer with MFI of 3.0 g/10min. was chemically modified with nine different organo-functional silanes. Each modification (grafting) was carried out in a co-rotating twin-screw mini-extruder. Crosslinking of PP-g-silane was accomplished in a hot water bath. The work went through the following stages:

1. Identification of the grafting efficiencies of these silanes using FT-IR analysis and gel content test.
2. Study of the influence of crosslinking on the crystallization behavior of the crosslinked PP and its soluble materials using DSC.
3. Study of the influence of low crosslinking degrees (gel content ≤ 5 wt.%) on the PP melt properties (MFI and oscillatory shear rheological properties). Two silanes with different grafting efficacies were studied here.
4. Study of the influence of PP-g-silane (no crosslinking) on the mechanical properties of wood-fiber/PP composites. The two most effective silanes in terms of grafting were chosen for the study.

The obtained results are highlighted as follows:

1. The grafting efficiency was on the following order:
6-Azidosulfonylhexyltriethoxysilane (Azido-silane) > (3-acryloxypropyl)trimethoxysilane (APTMS) > 3-methacryloxypropyltrimethoxysilane (VMMS) > Vinyltrimethoxysilane (VTMS), 7-octenyltrimethoxysilane (ONTMS), Ureidopropyltrimethoxysilane (UPTMS), (3-glycidoxypropyl)trimethoxysilane

(GPTMS), 3-aminopropyltrimethoxysilane (AMPTMS), Bis(3-trimethoxysilylpropyl)amine (BTMSPA).

2. Crosslinking was found to significantly increase the crystallization peak temperature (T_c) of PP except with UPTMS, GPTMS, AMPTMS, and BTMSPA.
3. The soluble materials of highly crosslinked samples (with APTMS and VMMS) exhibited T_c close to that of the pure PP except with Azido-silane.
4. The soluble materials of lightly crosslinked samples (with VTMS and ONTMS) exhibited high T_c compared to that of the pure PP.
5. Light crosslinking (gel content ≤ 5 wt.%) was found to decrease MFI, increase complex viscosity (η^*) and storage modulus (G') at low frequency, and decrease $\tan \delta$ at low frequency. APTMS-crosslinked PP (gel content ~ 5 wt.%) had greater influence compared to ONTMS-crosslinked PP (gel content 2 wt.%).
6. In general, the addition of PP-g-APTMS and PP-g-Azidosilane (both not crosslinked) improved the mechanical properties of wood-fiber/PP composites. PP-g-APTMS had better effect compared to PP-g-Azidosilane.

To the best of the author's knowledge, a gel content of as high as 80-90 wt.% could be achieved by crosslinking PP with organo-functional silanes. The most effective silane used in previous works was APTMS. However, based on the results presented in this thesis, 6-Azidosulfonylhexyltriethoxysilane (Azido-silane) could be used to achieve higher gel contents by carefully controlling grafting and crosslinking reactions conditions. Interestingly, the degradation (decrease in molecular weight) associated usually with grafting PP with organo-functional silanes was avoided when using Azido-silane since the addition of peroxide was not required in this case.

Moreover, melt elasticity of PP with low gel content can be enhanced using low concentrations of both peroxide and highly effective silanes like APTMS or VMMS. Based on the melt properties results, melt strength and extensional viscosity are expected to improve accordingly based on the literature. Previous works aiming at improving melt

strength of PP with low gel content concentrated only on vinyl-silanes, namely, VTES and VTMS. The advantage associated with the use of APTMS and VMMS is the possible use of low concentrations of peroxide which reduces the extent of degradation.

The use of PP grafted with silanes in the preparation of natural-fiber/PP composites is rarely reported in literature. To the best of the author's knowledge, only PP-g-VMMS and PP-g-VTES were studied previously in this field and found better than PP-g-MAN which is used commercially in such application. This study reported the performance of PP-g-APTMS and PP-g-Azidosilane. Although PP-g-Azidosilane was grafted more onto PP compared to APTMS, its influence on the mechanical properties of wood-fiber/PP composites was not as expected.

Among the recommendations for future works are:

1. Crosslinking PP with 6-Azidosulfonylhexyltriethoxysilane (Azido-silane) and identifying the optimum processing conditions for grafting and crosslinking reactions in order to achieve the highest gel content (crosslinking degree). Crosslinked PP with high gel content can be used in applications that require high thermal resistance especially under mechanical stresses.
2. Preparation of lightly crosslinked PP (gel content ≤ 5 wt.%) for high melt strength applications using APTMS or VMMS and without using peroxide. PP radicals can be generated by heat. It is recommended also to study the possibility of performing crosslinking reactions before grafting reactions either in a separate step or in the first zones of the extruder. A gel-free long chain branched PP (LCB-PP) is recommended also to be prepared using the same procedure.
3. APTMS and VMMS are expected to produce bi-modal distributions of molecular weight and branching. Based on the results presented in this thesis, Azido-silane could potentially produce more uniform distributions. Therefore, it would be interested if one can prepare a gel-free LCB-PP using Azido-silane and use GPC analysis to study the resulting distributions. For this purpose, Azido-silane can be used in very low concentrations due to its high grafting efficiency. It is worth noting

that conventional procedures used to prepare commercial LCB-PP are known to generate bi-modal distributions.

4. Preparation of natural-fiber/PP composites using PP-g-Azidosilane and studying the effect of the increase in the concentration of siloxane groups (Si-O-Si) on the mechanical properties of the composites. The results might reveal the cause of the unexpected low performance of PP-g-Azidosilane compared to PP-g-APTMS although it showed a higher grafting degree.
5. Studying the effect of the amount of grafted silane in PP-g-silane on the mechanical properties of natural-fiber/PP composites by using PP-g-silane with different contents of grafted silane.
6. Preparation of natural-fiber/PP composites using Azido-silane. It is recommended here to perform the grafting reactions along with the composite compounding in one step and compare this procedure with the procedure used in this thesis. This procedure is expected to utilize most of the silanol groups (Si-OH) before being consumed in crosslinking reactions and converted into siloxane groups. It is also recommended to facilitate the crosslinking reactions after the preparation of the composites and study the effect of this facilitated crosslinking on the impact and creep resistance of the composites.

Bibliography

- Abu Bakar, M. B., Ishak, Z. A. M., Taib, R. M., Rozman, H. D., & Jani, S. M. (2010). Flammability and Mechanical Properties of Wood Flour-Filled Polypropylene Composites. *Journal of Applied Polymer Science*, *116*, 2714–2722.
- Abu-Sharkh, B. F., Kahraman, S. H., Abbasi, S. H., & Hussein, I. A. (2004). Effect of Epolene E-43 as a Compatibilizer on the Mechanical Properties of Palm Fiber–Poly(propylene) Composites. *Journal of Applied Polymer Science*, *92*, 2581–2592.
- An, Y., Zhang, Z., Bi, W., Wang, Y., & Tang, T. (2008). Characterization of High Melt Strength Polypropylene Synthesized via Silane Grafting Initiated by In Situ Heat Induction Reaction. *Journal of Applied Polymer Science*, *110*, 3727–3732.
- Ansari, M., & Ismail, H. (2009) The Effect of Silane Coupling Agent on Mechanical Properties of Feldspar Filled Polypropylene Composites. *Journal of Reinforced Plastics and Composites*, *28*, 3049-3060.
- Arbelaiz, A., Ferná ndez, B., Cantero, G., Llano-Ponte, R., Valea, A., & Mondragon, I. (2005). Mechanical properties of flax fiber/polypropylene composites. Influence of fiber/matrix modification and glass fiber hybridization. *Composites: Part A*, *36*, 1637–1644.
- ASTM International. (2010). ASTM D1708-10 Standard Test Method for Tensile Properties of Plastics by Use of Microtensile Specimens.
- ASTM International. (2010). ASTM D256-10 Standard Test Methods for Determining the IZOD Pendulum Impact Resistance of Plastics.
- ASTM International. (2010). ASTM D790-10, Standard Test Methods for Flexural Properties of Unreinforced and Reinforced Plastics and Electrical Insulating Materials.
- Backer, M., Smints, V., & Deheunynck, D. Polymers Modified by Silanes. U.S. Patent 8,476,375 B2, issued July 2, 2013.
- Beltran, M., & Mijangos, C. (2000). Silane Grafting and Moisture Crosslinking of Polypropylene. *Polymer Engineering and Science*, *40*, 1534-1541.

- Bledzki, A. K., & Gassan, J. (1999). Composites reinforced with cellulose based fibres. *Progress in Polymer Science*, 24, 221-274.
- Blonk, W. J., He, Z. A., & Picci, M. (2002). Catalysis of the Epoxy-Carboxyl Reaction. *Journal of Coatings Technology*, 74, 33-41.
- Borsig, E., van Duin, M., Gotsis, A. D., & Picchioni, F. (2008). Long Chain Branching on Linear Polypropylene by Solid State Reactions. *European Polymer Journal*, 44, 200–212.
- Bouza, R., Abad, M. J., Barral, L., & Ladra, M. (2009). Effects of Vinyltrimethoxy Silane on Mechanical Properties and Morphology of Polypropylene-Woodflour Composites. *Polymer Engineering and Science*, 49, 324–332.
- Cartier, H., & Hu, G. (1998). Styrene-Assisted Melt Free Radical Grafting of Glycidyl Methacrylate onto Polypropylene. *Journal of Polymer Science: Part A: Polymer Chemistry*, 36, 1053–1063.
- Chaudhary, B. I., Sengupta, S. S., Cogen, J. M., & Curto, M. (2011). Silane Grafting and Moisture Crosslinking of Polypropylene. *Polymer Engineering and Science*, 51, 237–246.
- Chaudhary, B. I., Parent, J. S., Finlayson, M. F., Weaver, J. D., Cong, R., & Wang, J. Silane-coupled Propylene-based Polymers and Method. U.S. Patent 2011/0009514 A1, issued January 13, 2011.
- Demir, H., Atikler, U., Balkose, D., & Tihminhoglu, F. (2006). The effect of fiber surface treatments on the tensile and water sorption properties of polypropylene–luffa fiber composites. *Composites: Part A*, 37 447–456.
- Demje´na, Z., Puka´nszky, B., & Jr, J. N. (1999). Possible coupling reactions of functional silanes and polypropylene. *Polymer*, 40, 1763–1773.
- El Mabrouk, K., Parent, J. S., Chaudhary, B. I., & Cong, R. (2009). Chemical modification of PP architecture: Strategies for introducing long-chain branching. *Polymer*, 50, 5390–5397.

- Garcia, L., Morales, G., Avalos B, F., & Acuna, P. (2013). Use of the Trifunctional Cyclic Initiator, DEKTP, as the Radical Initiator in the Modification of Poly(propylene) in the Presence of Different Branching/Crosslinking Co-Agents. *Macromolecular Symposia*, 325, 213-219.
- Girone`s, J., Me´ndez, J., Boufi, S., Vilaseca, F., Mutje´, P. (2007). Effect of Silane Coupling Agents on the Properties of Pine Fibers/Polypropylene Composites. *Journal of Applied Polymer Science*, 103, 3706–3717.
- Hu, M., Wang, Z., Qu, B., & Hu, K. (2006). Vapour phase grafting of vinyltrimethoxysilane and water crosslinking of polypropylene. *Reactive & Functional Polymers*, 66, 287–296.
- Huang, H., Lu, H. H., & Liu, N. C. (2000). Influence of Grafting Formulations and Extrusion Conditions on Properties of Silane-Grafted Polypropylenes. *Journal of Applied Polymer Science*, 78, 1233–1238.
- Ichazo, M. N., Albano, C., Gonzalez, J., Perera, R., & Candal, M. V. (2001). Polypropylene/wood flour composites: treatments and properties. *Composite Structures*, 54, 207-214.
- Jørgensen, J. K., Redford, K., Ommundsen, E., & Stori, A. (2007). Molecular Structure and Shear Rheology of Long Chain Branched Polypropylene Formed by Light Cross-Linking of a Linear Precursor with 1,3-Benzenedisulfonyl Azide. *Journal of Applied Polymer Science*, 106, 950–960.
- Karian, H. G. (Ed.). (2003). *Handbook of Polypropylene and Polypropylene Composites*. New York: Marcel Dekker Inc.
- Karmarkar, A., Chauhan, S. S., Modak, J. M., & Chanda, M. (2007). Mechanical properties of wood–fiber reinforced polypropylene composites: Effect of a novel compatibilizer with isocyanate functional group. *Composites: Part A*, 38, 227–233.
- Khanam, P. N., & AlMaadeed, M. A. (2014). Improvement of ternary recycled polymer blend reinforced with date palm fiber. *Materials and Design*, 60, 532–539.
- Kim, T., Lee, S., Chun, S., Doh, G., & Paik, K. (2011). Effect of silane coupling on the fundamental properties of wood flour reinforced polypropylene composites. *Journal of Composite Materials*, 45, 1595-1605.

- Legendijk, R. P., Hogt, A. H., Buijtenhuijs, A., & Gotsis, A. D. (2001). Peroxydicarbonate Modification of Polypropylene and Extensional Flow Properties. *Polymer*, *42*, 10035-10043.
- Launer, P. J. (2013). Infrared Analysis of Organosilicon Compounds: Spectra-structure Correlations. In B. Arkles & G. L. Larson, (Eds.), *Silicon Compounds: Silanes & Silicones* (pp. 175-178). Morrisville: Gelest, Inc.
- Li, S., Xiao, M., Wei, D., Xiao, H., Hua, F., & Zheng, A. (2009). The melt grafting preparation and rheological characterization of long chain branching polypropylene. *Polymer*, *50*, 6121–6128.
- Li, Z., Hu, G., Corriou, J., Hoppe, S., Fonteix, C., Laine, R., et. al. (2013). A Reactive Extrusion Process for the Free Radical Grafting of Silanes Onto Polypropylene: Effects of Processing Conditions and Properties of Water Cross-Linked Silane-Grafted Polypropylene. *Polymer Engineering and Science*, *53*, 1571–1581.
- Liu, N. C., Yao, G. P., & Huang, H. (2000). Influences of grafting formulations and processing conditions on properties of silane grafted moisture crosslinked polypropylenes. *Polymer*, *41*, 4537–4542.
- Maier, C., & Calafut, T. (1998). *Polypropylene, The Definitive User's Guide and Data book*. New York: Plastics Design Library.
- Malpass, D. B., & Band, E. (2012). *Introduction to industrial polypropylene: properties, catalysts, processes*. New Jersey: John Wiley & Sons.
- Moad, G. (1999). The synthesis of polyolefin graft copolymers by reactive extrusion. *Progress in Polymer Science*, *24*, 81-142.
- Munteanu, D. (1997). Moisture Crosslinkable Silane-Modified Polyolefins. In S. Al-Malaika (Ed.), *Reactive Modifiers for Polymers* (pp. 196-265). London: Blackie Academic & Professional.
- Nachtigall, S. M. B., Cerveira, G. S., & Rosa, S. M. L. (2007). New polymeric-coupling agent for polypropylene/wood-flour composites. *Polymer Testing*, *26*, 619–628.
- Nachtigall, S. M. B., Stedile, F. C., Felix, A. H. O., & Mauler, R. S. (1999). Polypropylene Functionalization with Vinyltriethoxysilane. *Journal of Applied Polymer Science*, *72*, 1313–1319.

- Nourbakhsh, A., Kokta, B. V., Ashori, A., & Jahan-Latibari, A. (2008). Effect of a Novel Coupling Agent, Polybutadiene Isocyanate, on Mechanical Properties of Wood-Fiber Polypropylene Composites. *Journal of Reinforced Plastics and Composites*, *27*, 16–17.
- Parent, J. S., Bodsworth, A., Sengupta, S. S., Kontopoulou, M., Chaudhary, B. I., Poche, D., et al. (2009). Structure–rheology relationships of long-chain branched polypropylene: Comparative analysis of acrylic and allylic coagent chemistry. *Polymer*, *50*, 85–94.
- Parent, J. S., Sengupta, S. S., Kaufman, M., & Chaudhary, B. I. (2008). Coagent-induced transformations of polypropylene microstructure: Evolution of bimodal architectures and cross-linked nano-particles. *Polymer*, *49*, 3884–3891.
- Paunikallio, T., Suvanto, M., & Pakkanen, T. T. (2008). Grafting of 3-(trimethoxysilyl)propyl methacrylate onto polypropylene and use as a coupling agent in viscose fiber/polypropylene composites. *Reactive & Functional Polymers*, *68*, 797–808.
- Rachini, A., Mougin, G., Delalande, S., Charneau, J.-Y. Barrès, C., & Fleury, E. (2012). Hemp fibers/polypropylene composites by reactive compounding: Improvement of physical properties promoted by selective coupling chemistry. *Polymer Degradation and Stability*, *97*, 1988–1995.
- Rätzsch, M. (1999). Reaction Mechanism to Long-Chain Branched PP. *Pure and Applied Chemistry A36(11)*, 1759–1769.
- Rätzsch, M., Arnold, M., Borsig, E., Bucka, H., & Reichelt, N. (2002). Radical Reactions on Polypropylene in the Solid State. *Progress in Polymer Science*, *27*, 1195–1282.
- Romani, F., Corrieri, R., Barga, V., & Ciardelli, F. (2002). Monitoring the chemical crosslinking of propylene polymers through rheology. *Polymer*, *43*, 1115–1131.
- Salimi, A., Atai, M., Mirabedini, M., & Mohseni, M. (2009). Thermo-oxidative Reactions of Polypropylene Wax in the Molten State. *Journal of Applied Polymer Science*, *111*, 2703–2710.

- Shieh, Y., Chen, J., & Lin, C. (2001). Thermal Fractionation and Crystallization Enhancement of Silane-Grafted Water-Crosslinked Low-Density Polyethylene. *Journal of Applied Polymer Science*, 81, 591–599.
- Shing, J. B. W., Baker, W. E., & Russell, K. E. (1995). Kinetics and Mechanism of the Grafting of 2-(Dimethylamino)ethyl Methacrylate onto Hydrocarbon Substrates. *Journal of Polymer Science: Part A Polymer Chemistry*, 33, 633-642.
- Sobczak, L., Welser, W., Brüggemann, O., & Haider, A. (2014). Polypropylene (PP)-based wood polymer composites: Performance of five commercial maleic anhydride grafted PP coupling agents. *Journal of Thermoplastic Composite Materials*, 27, 439–463.
- Song, G., Yang, S., Yang, C., & She, X. (2006). Foaming polypropylene prepared by a novel one-step silane-grafting and crosslinking method. *Journal of Porous Materials*, 13, 297-301.
- Stuart, B. H. (2004) *Infrared Spectroscopy: Fundamentals and Applications*. Chichester: John Wiley & Sons.
- Su, F., & Huang, H. (2010). Influence of Polyfunctional Monomer on Melt Strength and Rheology of Long-Chain Branched Polypropylene by Reactive Extrusion. *Journal of Applied Polymer Science*, 116, 2557–2565.
- Su, F., & Huang, H. (2010). Rheology and Melt Strength of Long Chain Branching Polypropylene Prepared by Reactive Extrusion with Various Peroxides. *Polymer Engineering and Science*, 50, 342–351.
- Su, F., & Huang, H. (2011). Supercritical carbon dioxide-assisted reactive extrusion for preparation long-chain branching polypropylene and its rheology. *Journal of Supercritical Fluids*, 56, 114–120.
- Tian, J., Yu, W., & Zhou, C. (2006). The Preparation and Rheology Characterization of Long Chain Branching Polypropylene. *Polymer*, 47, 7962-7969.
- Tripathi, D. (2002). *Practical Guide to Polypropylene*. Shropshire: Rapra Technology Limited.

Wang, X., Tzoganakis, C., & Rempel, G. L. (1996). Chemical Modification of Polypropylene with Peroxide/Pentaerythritol Triacrylate by Reactive Extrusion. *Journal of Applied Polymer Science*, *61*, 1395-1404.

Wang, Z., Wu, X., Gui, Z., Hu, Y., & Fan, W. (2005). Thermal and crystallization behavior of silane-crosslinked polypropylene. *Polymer International*, *54*, 442-447.

Xie, Y., Hill, C. A. S., Xiao, Z., Militz, H., & Mai, C. (2010). Silane coupling agents used for natural fiber/polymer composites: A review. *Composites: Part A*, *41*, 806-819.

Yang, S., Song, G., Zhao, Y., Yang, C., & She, X. (2007). Mechanism of a One-Step Method for Preparing Silane Grafting and Cross-linking Polypropylene. *Polymer Engineering and Science*, *47*, 1004-1008.

Zhang, Z., Wan, D., Xing, H., Zhang, Z., Tan, H., Wang, L., et. al. (2012). A new grafting monomer for synthesizing long chain branched polypropylene through melt radical reaction. *Polymer*, *53*, 121-129.

Zhao, W., Huang, Y., Liao, X., & Yang, Q. (2013). The molecular structure characteristics of long chain branched polypropylene and its effects on non-isothermal crystallization and mechanical properties. *Polymer*, *54*, 1455-1462.

Zhou, S., Hu, M., Hu, Y., & Wang, Z. (2009). Influence of Coagents on the Silane Grafting and Cross-linking of Polypropylene. *Polymer-Plastics Technology and Engineering*, *48*, 193-200.

Appendix

Differential Scanning Calorimetry (DSC) exotherms

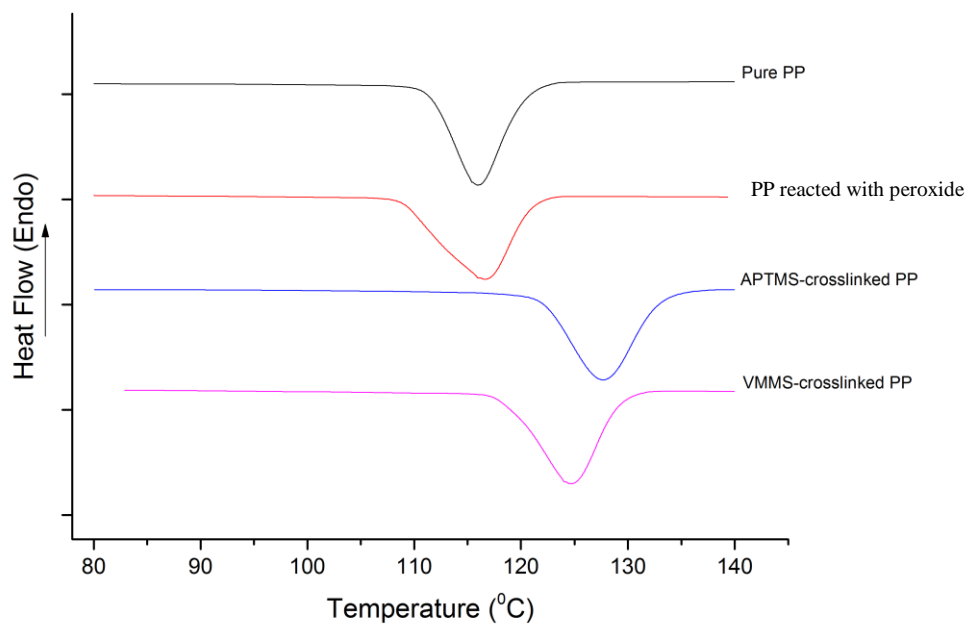


Figure A.1 The DSC exotherms under non-isothermal conditions of the pure PP, PP reacted with peroxide, APTMS-crosslinked PP, and VMMS-crosslinked PP

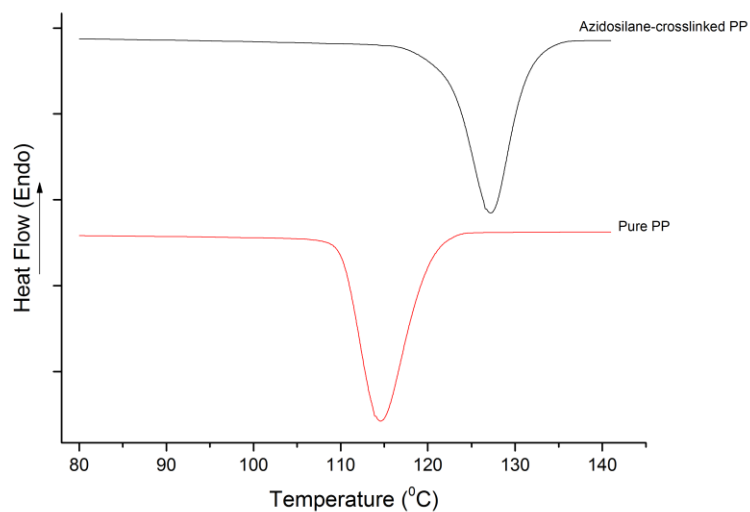


Figure A.2 The DSC exotherms under non-isothermal conditions of the pure PP, and Azidosilane-crosslinked PP

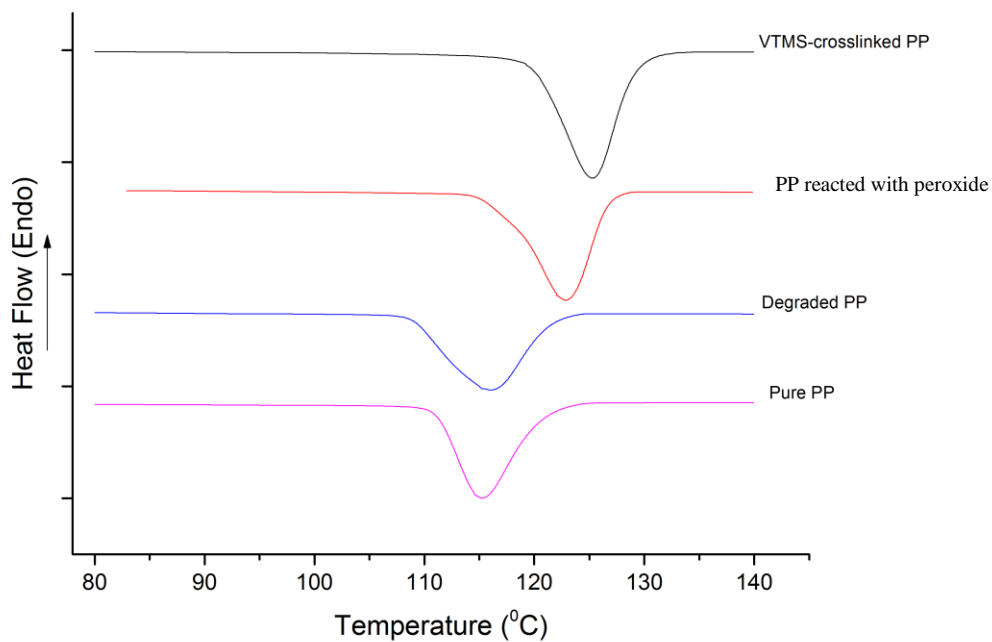


Figure A.3 The DSC exotherms under non-isothermal conditions of the pure PP, PP reacted with peroxide, ONTMS-crosslinked PP, and VTMS-crosslinked PP

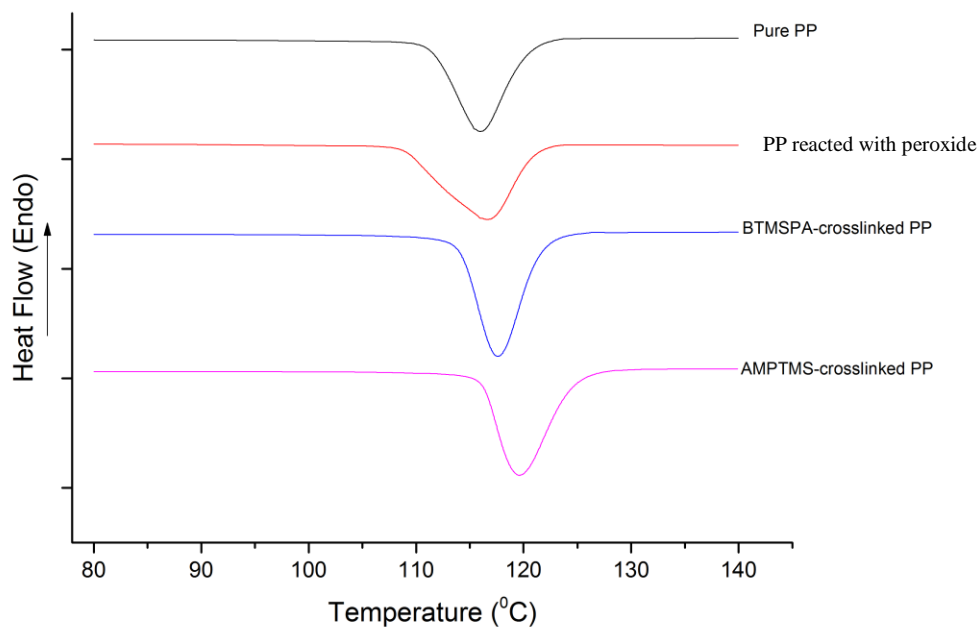


Figure A.4 The DSC exotherms under non-isothermal conditions of the pure PP, PP reacted with peroxide, BTMSPA-crosslinked PP, and AMPTMS-crosslinked PP

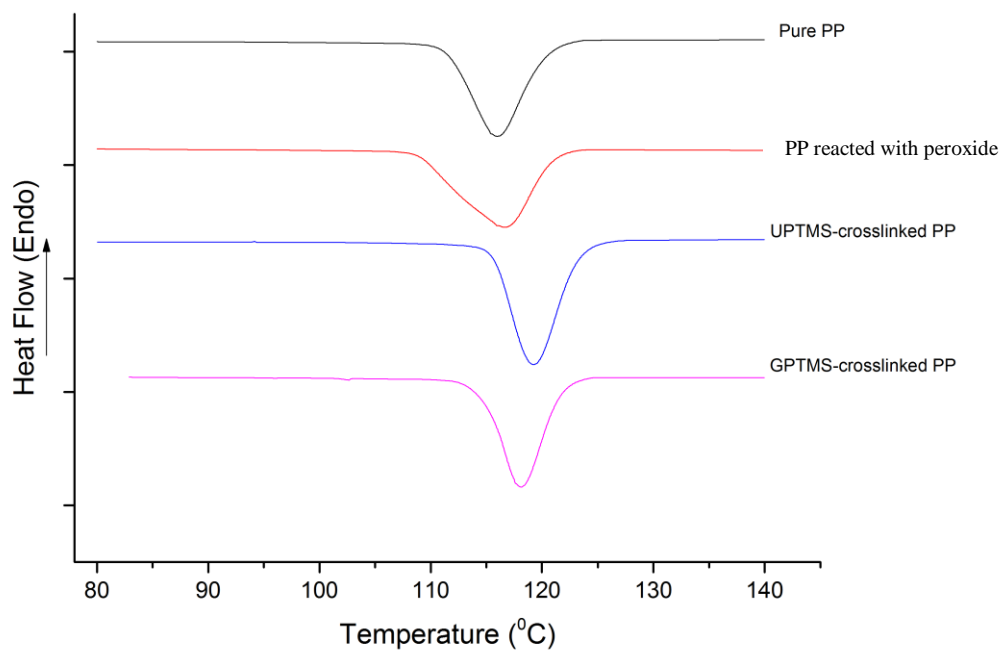


Figure A.5 The DSC exotherms under non-isothermal conditions of the pure PP, PP reacted with peroxide, UPTMS-crosslinked PP, and GPTMS-crosslinked PP

Gel Permeation Chromatography (GPC) Data

MW Averages

Mp: 176755	Mn: 72360	Mv: 225861	Mw: 259706
Mz: 609801	Mz+1: 1040783	PD: 3.5891	

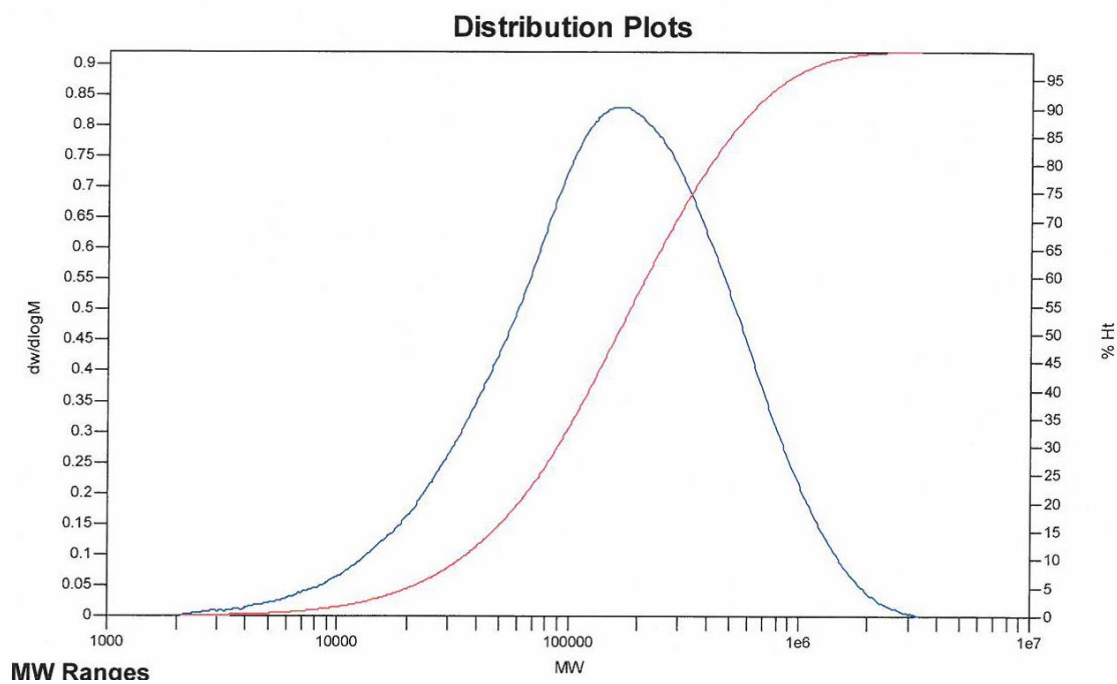


Figure A.6 GPC data for the PP reacted with peroxide (0.20 wt.%)

GPC Results

Dist Name	Mn	Mw	MP	Mz	Mz+1	Mv	Poly dispersity	MW Marker 1	MW Marker 2
1	64581	289081	175813	770013	1456980	246638	4.476250		

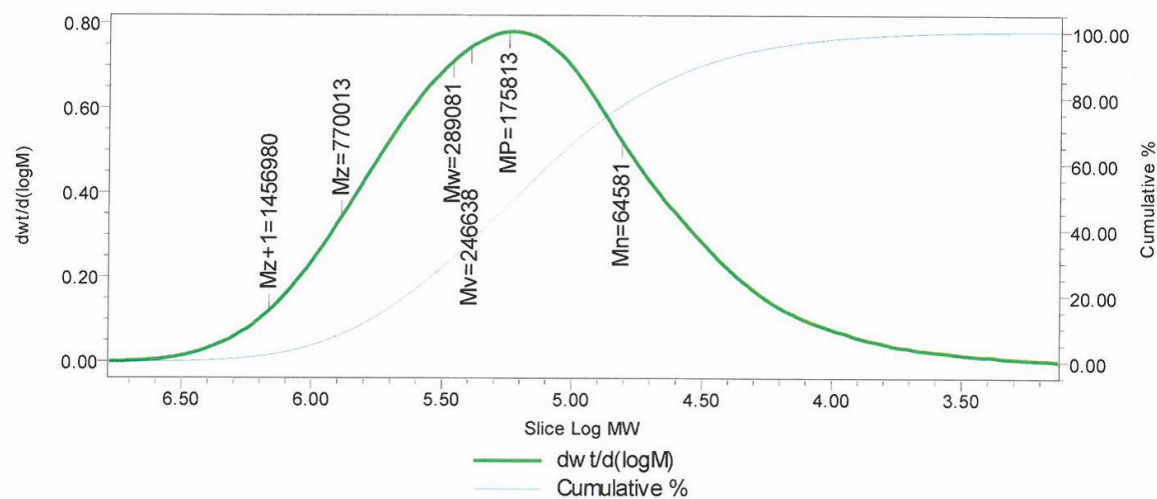


Figure A.6 GPC data for the soluble fraction of ONTMS-crosslinked PP (0.20 wt.% peroxide)